INTERMITTENCY AND ROUTE TO CHAOS IN THERMOACOUSTIC OSCILLATIONS

A THESIS

submitted by

LIPIKA KABIRAJ

for the award of the degree

of

DOCTOR OF PHILOSOPHY

DEPARTMENT OF AEROSPACE ENGINEERING
INDIAN INSTITUTE OF TECHNOLOGY MADRAS.

JULY 2012

THESIS CERTIFICATE

This is to certify that the thesis titled **INTERMITTENCY AND ROUTE TO CHAOS IN THERMOACOUSTIC OSCILLATIONS**, submitted by **Lipika Kabiraj**, to the Indian Institute of Technology, Madras, for the award of the degree of **Doctor of Philosophy**, is a bona fide record of the research work done by her under our supervision. The contents of this thesis, in full or in parts, have not been submitted to any other Institute or University for the award of any degree or diploma.

Prof. R. I. Sujith
Research Guide
Professor
Dept. of Aerospace Engineering
IIT-Madras, 600 036

Place: Chennai

Date: 12^{th} July 2012

ACKNOWLEDGEMENTS

I would like to express my sincere gratitude to Prof. R. I. Sujith for guiding my research work. He has been a mentor to me. Everything that I learned during my doctoral research, particularly in the fields of acoustics & combustion and experimental diagnostic techniques, is under his guidance. I am grateful to him for teaching me the importance of organization and self-evaluation in research and in life. I am particularly thankful to him for placing his confidence in me and for his constant encouragement towards independent thinking and research. This thesis and the development of my research career would not have been possible in the absence of his guidance and support.

I was introduced to the field of nonlinear time series analysis by Dr. P. Wahi (Indian Institute of Technology Kanpur, India). The subject has been an integral aspect of my thesis and I am immensely grateful to Dr. Wahi for discussions on this subject and his guidance on its implementation.

The Department of Aerospace Engineering has been extremely supportive and appreciative of my doctoral research. For this, I am thankful to Prof. Kurian, Prof. Sriram and Prof. Bhaskar. I also sincerely thank the Dean of Academic Research for granting financial support and permission to present my work at the prestigious ASME Gas Turbine Turbo Expo conference. This conference was the first opportunity for me to present my research work on an international platform. This work was funded by Department of Science and Technology, India, and Aeronautics Research & Development Board, India. I would like to acknowledge their support.

My technical abilities and knowledge are a result of the teachings by professors from the Department of Aerospace Engineering, Prof. S. R. Chakravarthy, emeritus Prof. E. G. Tulapurkara, Dr. T. M. Muruganandam, Dr. A. Sameen, Dr. Sunetra Sarkar, Dr. K. V. Nagendra Gopal, the Department of Physics: Prof. V. Balakrishnan, Prof. Neelime Gupte, Prof. S. Lakshmi Bala, Prof. Arul Lakshminarayan and Prof. Arun K. Tangirala at the Department of Chemistry at the Indian Institute of Technology, Madras. I take

this opportunity to express my gratitude to them. I am also very thankful to Prof. J. K. Prasad, Birla Institute of Technology, Mesra, India, who introduced me to the field of scientific research.

A part of my work has been a result of the collaboration between Prof. R. I. Sujith and TU Munich. I thank Prof. Sujith, Prof. Polifke, Dr. Hirsch and Prof. Krischer for giving me the opportunity to carry out research at TU Munich. The work itself was a result of significant contributions by Dr. Morales for which I gratefully thank him. During my stay, I received invaluable assistance from students working in the research group of Prof. Polifke, specially from Ralph, Sebastian and Tanya. I thank them for their help.

All the former and present students of the Combustion Flow Diagnostic Laboratory have extended their help selflessly and promptly whenever I was in need of advice or support. I cannot possibly thank them enough. Discussions with Tide, Rajkumar, Devendra, Kushal and Varun were always beneficial in clarification of concepts on fluid dynamics, gas dynamics, combustion, acoustics and thermoacoustics. Critical comments on my investigations were often given by Satheesh, Priya, Balaji, Koushik, Sharath, Varun, Joseph, Vikrant, Vineeth, Mr. Rana and Tarun. Discussions with Manikandan helped me to initiate design and fabrication of my setup. I received help from Aditya in learning and implementing LabVIEW and MATLAB and also in the fabrication and setting up of experiments. I learned optical diagnostic techniques and processing with help from Ramgopal. The time I spent in the laboratory would not have been successful without the support of former students and colleagues, Jayaraman, Guru, O.J. Sreenivasan Jayasurya, Shreerekha, Thomas, Nishant, Rajni, Roopa, Anshu, Avishek, Pushkarini and Ellena and present colleagues, Vivek, Rajiv, Irfan, Rajrishi, David, Rajesh, Trinath, Mr. Thampi, Vishnu, Harshini and Debolina.

I thank the office staff at the Department of Aerospace Engineering and the staff at the administrative section, IIT Madras for their assistance with official issues.

The experimental setup was fabricated by Mr. Ranganathan. I am grateful for his patient and hard work. Assistance from the department workshop, particularly Mr. Shankara Kumaraswamy and Mr. Kennedy is gratefully acknowledged.

In the end, I would like to thank my parents and my sisters. They have morally and mentally strengthened me at every step throughout my research. And I thank God for the gift of life and a right mind to take the decision of pursuing research as a career.

ABSTRACT

KEYWORDS: combustion instability; premixed flame; flame blowout; Ruelle-Takens route to chaos; frequency locking route to chaos; intermittency; nonlinear time series analysis; recurrence analysis; nonlinear coupled oscillator.

Confined combustion is known to result in spontaneously excited, self-sustained pressure oscillations, due to the establishment of a positive feedback between unsteady heat release rate and the acoustic field of the combustor. Technically referred to as thermoacoustic instability, the occurrence of such oscillations in practical combustion systems such as gas turbines, industrial burners etc., is a major engineering problem. In particular, the fact that low emission systems running on lean equivalence ratio are more susceptible to this instability makes it is a hindrance to advances in cleaner combustion technology.

In this thesis, nonlinear thermoacoustic oscillations have been investigated from the point of view of the dynamical systems theory. The focus of this work is based on the study of nonlinear transitions in a simple thermoacoustic system through an experimental bifurcation analysis. Self-excited thermoacoustic oscillations are investigated using nonlinear time series analysis. Results indicate that the dynamics of thermoacoustic oscillations are not limited to limit cycle oscillations. The limit cycle state obtained at the onset of the instability undergoes further bifurcations leading to a variety of complex nonlinear states. Bifurcation scenarios in two laboratory flame configurations, a single conical laminar flame and a multiple laminar flame configuration, confined within a duct, have been investigated.

In the case of a single flame, a ducted laminar premixed conical flame stabilized on a fully developed circular jet flow was studied. The relative flame location with respect to the duct was considered as the bifurcation parameter. According to the bifurcation

analysis, nonlinear transitions undergone by thermoacoustic oscillations follow an intermittency route to flame blowout. The primary bifurcation to limit cycle oscillations from a non-oscillatory state was observed to occur via a subcritical Hopf bifurcation. The limit cycle oscillations underwent a further bifurcation to quasi-periodic oscillations characterized by strong flame modulations featuring nonlinear effects such as lift-off, cusping, flame elongation and subsequent pinch-off. The quasi-periodic state loses stability, resulting in an intermittent state identified as type-II through recurrence analysis of phase space trajectories reconstructed from the time trace of acoustic pressure. At this state, the flame undergoes repeated lift-off and reattachment. Instantaneous flame images suggest that the intermittent flame behavior is influenced by jet flow dynamics. These experiments suggest a link between the phenomena of thermoacoustic instability and flame blowout. Intermittency occurs as a precursor to thermoacoustically induced flame blowout.

The investigation was extended to the bifurcation analysis of a ducted multiple injection burner. By implementing advanced nonlinear time series analysis on experimentally obtained pressure and intensity (CH^* chemiluminescence) time series, the dynamics of the obtained oscillatory states was characterized. By changing a control parameter, the location of the source of combustion, it was observed that the transition to self-excited, limit cycle oscillations is shown to occur via the subcritical Hopf bifurcation. Following this transition, the system enters a chaotic state through either a quasi-periodic route (the Ruelle-Takens scenario) or via frequency-locking. These two routes to chaos obtained in the investigated thermoacoustic system have also been reported in several other nonlinear systems. The route followed by the system depends on the operating parameter, particularly the equivalence ratio. In this thesis, cases corresponding two different operating condition have been presented to illustrate the two routes to chaos. The highly nonlinear interaction between the flames and the acoustic modes of the duct is clearly reflected in the high speed flame images acquired simultaneously with acoustic pressure oscillations.

With the aim of replicating the experimental results, a nonlinear model consisting of two coupled oscillators with time delay is formulated. The essential aspect, the Ruelle-Takens route to chaos observed in experiments, was captured quite well by this model.

TABLE OF CONTENTS

LIST OF TABLES

LIST OF FIGURES

ABBREVIATIONS

FTF	Flame Transfer Function
FDF	Flame Describing Function
NFDF	Nonlinear Flame Describing Function
LPG	Liquified Petroleum Gas
AMI	Average Mutual Infomation

GENERAL NOTATION

V	Volume
T	Oscillation time period
p'	Pressure fluctuations
u'	Velocity fluctuations
q'	Heat release rate fluctuations
x_f	Flame location
E	Loss in acoustic energy
$\hat{p}$	Pressure amplitude
ω	Eigenfrequency
Σ'	Flame surface area fluctuations
n	Interaction index in the n-tau model
A	System matrix
$\bar{u}$	Upstream flow velocity
$\bar{p}$	Mean pressure
$\mathbf{X}$	State variable
$\dot{\mathbf{X}}$	First order time-derivative of the state variables
$\mathbf{\Phi}$	System of equations governing a general dynamical system
μ	Parameter
λ	Eigenvalue
N	Number of points in phase space
C(r)	Correlation sum
λ_m	Maximal Lyapunov exponent
d_A	Dimension of the attractor
d_E	Embedding dimension
ϕ	Equivalence ratio
$s(n)$	Time series
τ	Time delay
$p(n)$	Pressure time series
$\mathbf{R}$	Recurrence matrix
Θ	Heaviside function
ϵ	Threshold value
$I(t)$	Intensity time series
$p(t)$	Pressure time series
V_a	Volumetric flowrate of air
V_f	Volumetric flowrate of fuel
γ	Specific heat ratio
M	Mach number
K	Dimensionless heater power
ζ_q	Damping coefficient of mode q

CHAPTER 1

INTRODUCTION

The term thermoacoustic instability refers to self-sustained oscillations in pressure and heat release rate. Such instability arises in systems involving confined combustion, when the acoustic driving due to interaction between acoustic modes of the confinement and unsteady heat release rate exceeds the acoustic losses in the system (Rayleigh, 1878). The acoustic field in a medium is the spatially and temporally alternating compression and rarefaction manifested as oscillations in local thermodynamic variables (pressure, density, temperature) and velocity oscillations. The fluctuations of unsteady heat release rate can constructively interact with the acoustic field of the confinement and lead to the onset of thermoacoustic oscillations. Illustrating with an example, an electrically heated mesh when placed in a hollow duct would produce audible sound as a result of the development of thermoacoustic instability. This is the Rijke tube, which often serves as a prototypical model for investigations of thermoacoustic instability. Industrial gas-turbines, rocket motors, furnaces and boilers and other systems involving confined combustion often face the risk of detrimental high amplitude pressure oscillations that appear due to the development of thermoacoustic instability within the system (Zinn and Lieuwen, 2005; McManus *et al.*, 1993). Hence, the subject of thermoacoustic instability is currently of a major importance.

The main problem associated with thermoacoustic instabilities is the high amplitude pressure pulsation that is detrimental to the combustion system. The self-sustained oscillations can induce structural vibrations within the combustor and other structural components of the system in general, leading to reduced life span of the combustion system, reduced efficiency and even complete system failure as in the case of rocket engines (Zinn and Lieuwen, 2005). Figure 1.1 shows parts of a gas-turbine combustor damaged due to such pressure pulsations. Another issue, not less concerning, is that the instability stands as an obstacle to the development of new generation, low emission combustion systems such as gas turbine engines, engines for aero and power generation. A shift towards cleaner system is currently the subject of a worldwide campaign

a) Transition piece b) Combustion liner

Figure 1.1: Pictures of damaged structural components of a gas turbine illustrating the consequences of high amplitude thermoacoustic oscillations. Figures are reproduced with permission from Preetham (2007).

to prevent serious damage to the environment. In combustion systems, one strategy to achieve lower emissions, particularly NOx emissions, is to operate at lean equivalence ratios. Doing so primarily lowers the flame temperature, thus lowering NOx emissions. However, lean combustion causes the system to become more susceptible to thermoacoustic instabilities. In order to achieve high efficiency with low emissions, active and passive control techniques are employed to disrupt the thermoacoustic coupling. However, the efficacy of the available control strategies is still limited and hence, research efforts to investigate the dynamics of thermoacoustic oscillations continue.

On a historical note, the issue of oscillating flames occurring simultaneously with audible sound was noticed in applications that involved combustion within confinements such as tubes or vessels more than two centuries ago. In 1777, Higgins (as reported by Plavnik, 2006) observed the phenomenon of sound generated due to confined combustion while working with slow hydrogen stream combustion in a vessel. The unexpected generation of sound was interesting and caught the attention of more investigators. In 1857, Tyndall (1857) published his report on the process of sound generation within tubes of different lengths enclosing hydrogen flames of varying sizes. He confirmed that the sound generated corresponded to the fundamental note and the octaves of the enclosing ducts. Additionally, he reported the effect of externally introduced sound on the flame: '*As the sounds of the flame and siren approached perfect unison, the flame shook, jumping up and down within the tube*'. A report by Le Conte (1858) included the observation of flames responding to music played by instrumental-

ists in a party hall. These reports incited further detailed investigations on the source of flame oscillations and the associated sound generation. The most notable work among early investigations is by Rayleigh (1878). He put forth a scientific reasoning for the phenomenon of thermoacoustic instability which is now referred to as the Rayleigh criterion, which forms the basis of investigations even now. However, Rayleigh criteria, gives only the condition necessary for the occurrence of thermoacoustic instability and cannot be used in the original form for prediction. Further, it does not reveal the mechanisms that result in the unsteady heat release rate.

1.1 Rayleigh Criteria

A sound explanation for the occurrence of thermoacoustic instability was first presented by Rayleigh (1878). The explanation was later formulated mathematically by Putnam (1971) and is now popularly referred to as the Rayleigh criterion. The criterion states that during the occurrence of thermoacoustic instability, unsteady heat release rate and acoustic pressure oscillations are in phase. When in phase, the interaction between the two contributes to the acoustic energy within the system or in other words, acts as acoustic driving. A simple mathematical representation of the criterion is as follows

$$\int_V \int_0^T p'(\vec{x_f}, t)\, q'(\vec{x_f}, t)\, dt > \int_V \int_0^T \sum_i E_i(\vec{x_f}, t) dt dV \tag{1.1}$$

The equation gives a necessary condition for thermoacoustic instability, in terms of acoustic driving and damping. Here, V is the volume of the system over which the integration is performed, T is the time period of one oscillation. $p'(\vec{x_f}, t)$ is the pressure fluctuation at the flame location x_f, at time t. $q'(\vec{x_f}, t)$ is the unsteady heat release rate at time t at flame location, x_f. $E_i(\vec{x_f}, t)$ represents acoustic energy losses due to different mechanisms such as viscous dissipation and loss of acoustic energy at system boundaries. The correlation between $p'(\vec{x_f}, t)$ and $q'(\vec{x_f}, t)$ given on the left hand side of Eqn. (1.1) is the acoustic driving due to flame-acoustic coupling. When acoustic driving due to this correlation is greater than acoustic losses in the system, oscillations in the system grow leading to thermoacoustic instability.

These basic feedback mechanisms that lead to thermoacoustic instability incorporates complexities that are yet to be completely understood. Among the physical processes involved with thermoacoustic oscillations, acoustic wave propagation is fairly well-understood. However, evaluating the interaction of unsteady heat release rate with acoustic field is quite complex. In thermoacoustic systems, the mentioned coupling is often affected significantly by additional factors such as hydrodynamics. The unsteady heat release rate is also a strong function of the amplitude and frequency of acoustic oscillations. In the simplest thermoacoustic system, the Rijke tube, local heat release rate from the surface of individual wires is governed by convective heat transfer to the mean flow. This process is coupled to the dynamics of the hydrodynamic zone that envelopes the wire mesh. The onset of thermoacoustic instability causes fluctuations in the mean flow velocity, which in turn affects the heat transfer. Thus, we can see that the physics of thermoacoustic instability in a Rijke tube is dependent not only on the coupling between acoustic pressure oscillation and unsteady heat release rate but also on the hydrodynamics in the near field of the wire mesh (Mariappan and Sujith, 2011). In practical systems, the source of heat release is often turbulent flame stabilized over a complex flow field. The phenomenon of thermoacoustic instability within such systems is a result of an interplay between several physical processes and therefore, requires a more detailed treatment. Additionally, evaluating the acoustic energy losses term on the right hand side of Eqn. (1.1) is difficult and quite often simplified models or approximations are employed.

Adding to the complexities described in the previous paragraph, is the inherent nonlinear nature of thermoacoustic instability. The exponential growth of thermoacoustic oscillations is arrested by nonlinear mechanisms in the system. The asymptotic state of the instability is then governed by the nonlinear dynamics of the thermoacoustic system. Such considerations inspire investigations on thermoacoustic instability beyond the Rayleigh criterion, and form the subject of many current investigations.

Figure 1.2 is a schematic sketch to explain the existence of positive feedback mechanism between the acoustic field in the combustor and the unsteady heat release rate. The two sketches at the bottom demonstrate the standing waves that will be established in the combustor chamber, depending on the boundary condition, if the acoustic energy

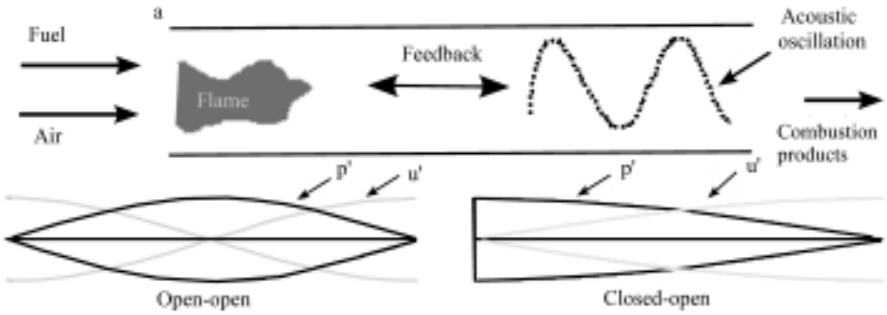

Figure 1.2: The above figure is a schematic representation of thermoacoustic system. It demonstrates how flame-acoustic coupling lead to self-sustained oscillation. The two plots in the bottom row represent the acoustic modes of the system for open-open and closed-open boundaries respectively. In the case of closed boundary p' is maximum whereas velocity fluctuation u' is minimum. For open boundary condition p' is minimum and velocity fluctuation u' is maximum.

generated by the combustion-acoustic interaction is greater than the amount of acoustic energy losses in the system. The acoustic field of the combustion chamber causes modulation in the flame shape, Fig. 1.3 shows the image of steady flame (a) and wrinkled flame (b and c). This flame area modulation modifies the unsteady heat release rate which further modifies the acoustic energy of the system.The physical insight gained from the rationale suggested by Rayleigh (1878) is that for instability to occur, a feedback interaction between unsteady heat release rate and acoustic pressure oscillations is a necessary. There are several mechanisms that cause unsteady heat release rate in combustors, for instance, flame surface area modulations, effect of coherent structures in the flow, inherent flame instabilities, flame kinematics including stretch/strain effects and chemical kinetics. In laminar premixed-flame systems, the effect of acoustic field on flame stabilization plays a dominant role (Schuller *et al.*, 2003; Ducruix *et al.*, 2005). In industrial combustion systems such as in dump combustors or in swirl combustors, the effect of coherent hydrodynamic structures associated with vortex shedding (Schadow and Gutmark, 1992) or vortex breakdown (Paschereit and Polifke, 1998) becomes dominant. Apart from these, factors such as fluctuations in local equivalence ratio or flow rate (Zinn and Lieuwen, 2005) or swirl number fluctuations (Almela *et al.*, 2010; Palies *et al.*, 2011) also play an important role.

The critical parameters that determine if a system is susceptible to instabilities are the time scales associated with the mechanisms generating unsteady heat release: con-

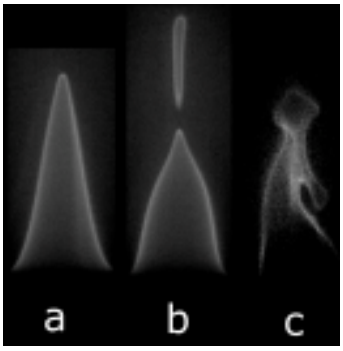

Figure 1.3: Instantaneous images of a laminar conical flame are shown here. The images illustrate flame wrinkling during the occurrence of thermoacoustic instability. Image a is a steady flame image acquired in the absence of flame-acoustic interaction. Images b and c show oscillatory flame behavior, acquired during self-sustained oscillations in the system.

vective time scales of the flame surface area fluctuations, vortex shedding frequency and convection time for equivalence ratio fluctuations. If these time scales match with the time scale of acoustic modes of the combustor, instability appears in the system. An in-phase relationship between unsteady heat release rate and pressure oscillations then ensures that energy from combustion is transferred to acoustic energy resulting in self-sustained oscillations.

Flame surface area modulation forms the dominant source of unsteady heat release rate in gas turbine combustors, particularly systems running on premixed combustion. Further, flame surface area fluctuations are a result of different mechanisms, each of which can play a governing role in the occurrence of thermoacoustic instability, depending on the system under consideration. Listed below are physical mechanisms that directly or indirectly (via flame surface area modulation) cause unsteady heat release rate oscillations in premixed flame systems.

1.2 Sources of Unsteady Heat Release Rate in Premixed Systems

1.2.1 Acoustic Disturbances

An illustration of the effect of acoustic oscillations on a laminar premixed conical flame is shown in Fig. 1.4. Acoustic oscillations result in disturbances in the flame that originate at the flame base. These disturbances are then convected along the flame leading to flame surface wrinkling (Candel, 2002). As a result, the effective surface area of the flame is modulated as seen in Fig. 1.4. In premixed flames, heat release rate fluctuations (q') due to combustion is proportional to oscillations in the total surface area of the flame (Σ') i.e. $q' \propto \Sigma'$. During self-excited instability, unsteady heat release rate via this mechanism is coupled to acoustic modes of the system. Flame-acoustic coupling based on flame surface area modulations has been extensively investigated previously (Candel, 2002; Lieuwen, 2003; Karimi *et al.*, 2009), particularly through flame transfer function studies. These studies are discussed in more detail in Chapter 2.

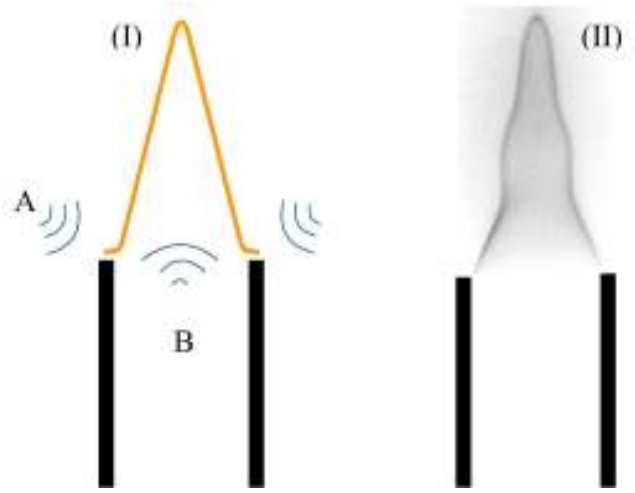

Figure 1.4: Flame wrinkling caused by acoustic oscillations (II). In the case of self-excited instability in a confined flame system, downstream acoustics (A) cause modulations of the flame surface. Flame wrinkling can also be caused by upstream acoustics (B) when coupling is established between the flame and burner tube acoustics or in the presence of upstream forcing.

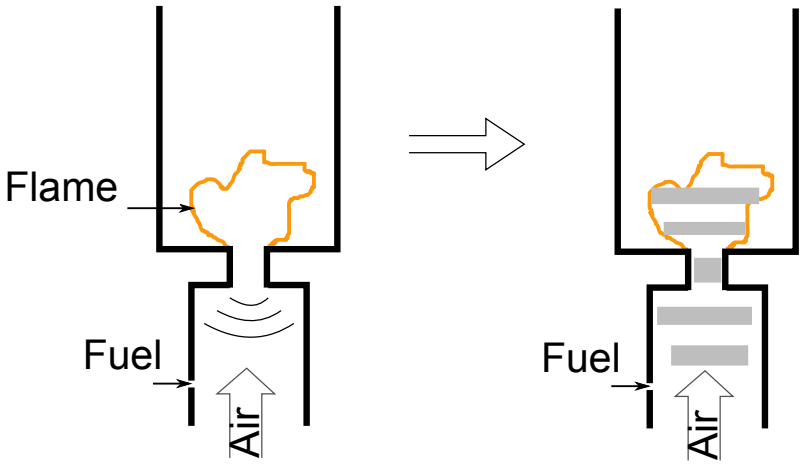

Figure 1.5: In a typical combustion chamber, acoustic perturbations move upstream of the burner into the gas and air supply lines and lead to oscillations primarily in the air supplied to the burner. This results in an oscillating fuel-air equivalence ratio within the flame. Equivalence ratios fluctuations leads to heat release rate fluctuations from the flame which could couple with combustor acoustics causing thermoacoustic oscillations.

1.2.2 Equivalence Ratio Fluctuations

Equivalence ratio fluctuations actively contribute towards thermoacoustic instability in combustion systems running on partially premixed gaseous mixtures, in systems where the air or fuel supply lines are susceptible to downstream pressure fluctuations. As seen in the schematic in Fig. 1.5, acoustic fluctuations propagate upstream of the burner and cause oscillations in the fuel/air supply, thus generating inhomogeneities in the fuel-air mixture. These inhomogeneities in the fuel-air mixture are convected till the flame by the mean flow; at the flame they cause heat release rate oscillations (Ducruix *et al.*, 2005). Lieuwen *et al.* (1998, 2001) have shown that lean premixed combustion is highly sensitive to equivalence ratio fluctuations. Additionally, they have shown that the convection time scale associated with the convection of equivalence ratio fluctuations from the fuel inlet till the flame is one of the parameters governing thermoacoustic instability. This was further confirmed by Richards and Janus (1998) who reported shifts in stability characteristics with variation in the length of the fuel nozzle. They also successfully demonstrated that effect of equivalence ratio fluctuations is strong enough to be used for controlling oscillations (Richards *et al.*, 1999).

Fluctuations in the equivalence ratio cause unsteady heat release rate directly via

Figure 1.6: A schematic representation of periodic vortex shedding in dump combustor. Often this periodic shedding couples to system acoustics causing generation of thermoacoustic oscillations in the system.

fluctuations in the local flame speed and heat of reaction. Oscillations in the local flame speed in turn lead to flame surface area oscillations, thus causing unsteady heat release rate indirectly, in addition to its direct influence. Cho (2005) presented a detailed discussion on the role of the mentioned mechanisms in the flame response of laminar flames to equivalence ratio oscillations. Their analysis indicated that flame response depends critically on the Strouhal number.

1.2.3 Coherent Structures in the Flow

Flame stabilization in most engineering flows is based on shear layer formation, for instance in dump combustors and combustion systems based on bluff-body stabilized or swirl-stabilized flames. Shear layers are associated with the development of Kelvin-Helmholtz instability that grow into coherent flow structures. Periodic vortex shedding in such systems is primarily responsible for oscillatory heat release rate. Figure 1.6 illustrates the phenomenon of vortex shedding in a dump combustor. Such vortex shedding was clearly observed through schlieren visualization during combustion instability in a dump combustor by Schadow and Gutmark (1992). Venkataraman (2000) showed that this flame-vortex interaction is the dominant mechanism for combustion instability in lean premixed dump combustors. During the occurrence of instability, a feedback loop is formed where the vortex shedding frequency matches with the frequency of acoustic oscillations in the system. Helical instabilities in swirl flows have also been identified to participate in thermoacoustic instability by Paschereit *et al.* (1998).

On the basis of these known mechanisms, both linear and nonlinear approaches have been developed for explaining the occurrence and characteristics of thermoacoustic oscillations. Linear analysis is based on the description of combustion-acoustic interac-

tions in the limit of small amplitude perturbations. The applicability of such methods is limited to simple systems and its prediction capabilities are limited to only the basic features of the instability. This is primarily due to the strong inherent nonlinear nature of thermoacoustic instability.

1.3 Nonlinear Aspect: An Outstanding Issue

It has been shown before in a number of investigations (Peracchio and Proscia, 1999; Dowling, 1999) that the nonlinear response of flame to acoustics oscillations is the reason for the nonlinear behavior of thermoacoustic instability. These studies concentrate on measuring the nonlinear flame describing functions that characterize the forced nonlinear response of flame to acoustic perturbations. Such approaches have been successful in predicting several nonlinear features of thermoacoustic instability such as limit cycle and triggering (Noiray *et al.*, 2008). However, complex flame dynamics, which cannot be characterized by describing functions, are involved in the phenomenon of self-excited thermoacoustic instabilities. These complex flame dynamics may lead to more complex states such as intermittency, quasi-periodicity and chaos. Hence, flame-response based approaches do not provide a complete description of thermoacoustic oscillations. The gap in our understanding of self-excited thermoacoustic instabilities needs to be covered in order to be able to efficiently suppress the problem of thermoacoustic instabilities in real systems.

In the quest towards the ultimate goal of having a complete control of the complex phenomenon of thermoacoustic instability in practical systems, it is quite important to first establish a thorough physical understanding of the instability in simpler configurations such as the Rijke tube (driven by electric heater or flames). This approach has previously resulted in fundamental results on the phenomenon of thermoacoustic instability. Building on the existing knowledge, understanding the nonlinear dynamics of thermoacoustic instability in a laminar premixed flame driven Rijke-type model thermoacoustic setup forms the basis of this thesis.

1.4 Motivation

Understanding the nonlinear aspects of thermoacoustic instability is extremely crucial to deal with the problem in real systems. Studies on nonlinear systems have shown that several physical systems with inherent nonlinearities exhibit complex nonlinear oscillations and follow well-defined routes to deterministic chaos. Thermoacoustic systems also have been previously reported to exhibit nonlinear behavior such as quasi-periodicity and chaotic oscillations. However, detailed investigations focused on this facet of thermoacoustic instability are lacking. As a consequence, currently it is often implicitly assumed that thermoacoustic oscillations appear in the form of limit cycle oscillations (Zinn and Lieuwen, 2005). From an industrial point of view, the major drawback of this assumption is that the assessment of the impact of self-excited instability is underestimated. The extent of potential damage that can be caused by complex oscillation states when compared to limit cycle oscillations will be higher. This is attributed to the presence of several frequencies and significant cycle-to-cycle amplitude variations in the pressure oscillations, for instance in quasi-periodic and chaotic oscillations. Such oscillations can result in an augmented cyclic fatigue, crack formation and crack propagation within structural components of the combustor (Suresh, 1998; Kurz and Brun, 2007). Clearly, control techniques tailored for limit cycle oscillations will fail in the presence of other nonlinear states. As a result, the main objective of running combustion systems with lower maintenance costs and longer life spans is hampered.

A complete description of thermoacoustic instabilities would involve characterizing and explaining the occurrence of complex nonlinear behavior in addition to limit cycle oscillations. Hence, it is required to particularly investigate the self-excited state of thermoacoustic instability in the framework of nonlinear dynamical systems theory (Strogatz, 1994). Such an approach will provide insight into the fundamental nonlinear mechanisms associated with thermoacoustic instability and will assist in exposing and resolving the shortcomings of currently employed nonlinear approaches to predict the characteristics of thermoacoustic oscillations. The work presented in this thesis is motivated by the need to understand the dynamical nature of self-excited thermoacoustic instability.

1.5 Objective of the Present Work

The objective of this investigation is to study self-excited thermoacoustic oscillations in a simple laboratory setup through a detailed experimental bifurcation analysis (Strogatz, 1994). The oscillations will be investigated through nonlinear time series analysis of experimentally acquired data. The study will include both qualitative and quantitative analysis. In particular, identifying the route followed by the system from a steady state to aperiodic oscillations through periodic limit cycle oscillations will be emphasized.

To investigate these fundamental nonlinear aspects of thermoacoustic instability, a prototypical Rijke tube system using laminar flame configuration as the source of combustion will be studied. Two flame configurations, a single conical flame and a multiple injection flame configuration will be investigated. Both these configurations have been used in several previous investigations, as the flame dynamics in these configuration can be clearly studied and modeled. Hence, the two configurations are of particular research interest and will be employed in this study. The acoustic pressure in the system, instantaneous flame images and *CH** chemiluminescence will be acquired, characterized and compared simultaneously, in an attempt to understand the flame-acoustic interaction during the appearance of nonlinear self-excited thermoacoustic oscillations.

1.6 Overview of the Thesis

This thesis is primarily aimed at investigating the nonlinear asymptotic states of thermoacoustic oscillations. In order to understand the underlying physics behind the occurrence of thermoacoustic instabilities and to accelerate the efforts in developing effective control strategies, careful experiments are required to investigate the nonlinear dynamics of thermoacoustic systems. The approach currently being adopted to deal with these instabilities is to avoid them by defining safe operating regions of combustion systems in terms of their operating parameter. It is believed that as a sensitive operating parameter is changed, thermoacoustic instability appear in the form of limit cycle oscillations, when the driving and damping processes in the system achieve a balance (Zinn and Lieuwen, 2005). In the process of understanding the instability, a natural question that

arises is whether these oscillations remain in this limit cycle behavior as the operating parameter is further changed. The current study is aimed at providing an answer to this question. In particular, the present work is based on the application of nonlinear time series analysis to experimentally obtained results from a simple laboratory combustion system.

The rest of the thesis is divided into the following chapters:

A survey of significant contributions in the field of thermoacoustic instability and investigations related directly to the present investigation is presented in **Chapter 2**. Focus has been placed on premixed flame systems. Fundamental investigations based on linear and nonlinear approaches including recent developments have been discussed. The section closes with a review of literature on the investigation of thermoacoustic instability from a dynamical systems perspective.

The details of the experimental setups studied are described in **Chapter 3**. The setups are similar to Rijke-burners driven by premixed flame. Two flame configuration are studied, a single laminar premixed flame and multiple premixed flames. The setups are designed in such a way so that bifurcation analysis can be performed by changing the location of the flame relative to combustion chamber. The instrumentation and measurement techniques used have also been discussed.

Chapter 4 elaborates the details of the analysis techniques implemented on experimentally acquired data. Discussions, relevant concepts and terminologies from dynamical system theory are explained. Fundamentals of the embedding theorem and phase space reconstruction have also been discussed.

Chapter 5 presents the result and discussions on the sequence of bifurcation present prior to thermoacoustically induced lean flame blowout. The results presented are based on the experimentally obtained pressure time series. On implementing the nonlinear time series analysis on the pressure time series, the rich dynamical nature of thermoacoustic oscillations are shown. Further, the nonlinear interaction between the flames and the acoustic modes of the duct is also reflected in the high speed flame images acquired simultaneously with pressure and flame intensity measurements.

Chapter 6 presents the result and discussions based on the experiments performed

on Rijke tube driven by multiple premixed flame. Through nonlinear time series analysis, possible routes to chaos has been established for this configuration.

A simple phenomenological formulation of the thermoacoustic system in terms of nonlinear coupled oscillator is presented in **Chapter 7**. The main objective of the formulation is to capture the route to chaos (Ruelle-Takens scenario) reported in **Chapter 6**. The thesis ends with conclusions in **Chapter 8** and an outlook for future investigations in **Chapter 9**.

CHAPTER 2

LITERATURE SURVEY

Intensive research has been conducted on the subject of thermoacoustic instability in combustion systems over the last 50-60 years. From studies on instability in solid and liquid rocket propulsion systems in the 60's (Crocco and Mitchell, 1969; Crocco and Cheng, 1956), to the present-day investigations focussed on instability in gas-turbine combustors, an immense amount of research has been performed in this field. The focus of this research has been on the fundamental mechanisms responsible for self-sustained combustion instability. Through experiments, numerical simulations and theory, the impact of pressure and velocity coupling (Culick, 1970; Ananthkrishnan *et al.*, 2005), flame-hydrodynamic interactions (Schadow and Gutmark, 1992; Poinsot and Veynante, 2005), coupling to equivalence ratio fluctuations (Zinn and Lieuwen, 2005) , entropy waves (Nicoud and Poinsot, 2005; George and Sujith, 2011) and inherent nonlinear dynamics (Jahnke and Culick, 1994; Subramanian *et al.*, 2010) were identified. In addition to fundamental research, more applied investigations were also performed in the development of low-order models (Merk, 1956; Schuermans *et al.*, 2000). These models helped in understanding the dynamics of flame-acoustic interaction which helped to adapt better control strategies (for reviews on active control see McManus *et al.*, 1993; Dowling and Morgans, 2005) and for suppressing the instability in practical systems.

Prior to being a concerning issue in gas-turbines, thermoacoustic instabilities were a major problem in solid and liquid rocket propulsion systems around the 60's (Crocco and Cheng, 1956; Crocco and Mitchell, 1969). Consequently, a large part of the theory of thermoacoustic oscillations was conceived in the following decades. In particular, the Galerkin approach and its extension to include nonlinear effects was developed by Zinn and co-workers (Powell and Zinn, 1969) and Culick and co-workers (Culick, 2006). Triggering instability and hysteresis in thermoacoustic systems was first identified and investigated in the content of instability in rocket motors (Levine and Baum, 1983; Blomshield *et al.*, 1997; Knoop *et al.*, 1997). Models based on the assumption of

nonlinear gas dynamics was proposed (Culick, 1990). Later, it was identified that combustion response and not nonlinear gas dynamics plays a significant role in triggering. More recently Ananthkrishnan *et al.* (2005) confirmed that nonlinearity in combustion response (velocity coupling) is responsible for nonlinear phenomenon triggering instability in thermoacoustic systems. Mariappan and Sujith (2010) have recently shown incorporation of pressure coupling and non-modal effects can explain transient dynamics and triggering instability in solid rocket motors.

From investigations, it is clear that in industrial premixed gas turbine combustors, where reported acoustic pressure amplitudes are of the order of $p'/\bar{p} \sim 1-5\%$ (Dowling, 1997; Peracchio and Proscia, 1999; Lieuwen, 2002), the source of nonlinearity is the flame's response to acoustic field not the nonlinear gas dynamical processes. Therefore, it is essential to include nonlinear dynamics of combustion-acoustic interaction into analytical/numerical modeling and prediction approaches.

In the subsequent sections is given, a brief overview of linear and certain nonlinear approaches is presented. This is followed by an overview of the investigations on the dynamics of self-excited thermoacoustic oscillations, a subject most pertaining to the investigation presented in this thesis.

2.1 Linear Stability Analysis

In the prediction of thermoacoustic characteristics of combustors, linear stability analysis plays a significant role. It is simple in formulation and is easy to handle computationally or numerically. Hence, it is an essential tool to predict the stability of thermoacoustic systems at the design phase. Moreover, parametric analysis of the systems through linear modeling is useful not only for predicting basic characteristics of thermoacoustic instability but also for gaining insight into the physical mechanisms involved in the phenomenon.

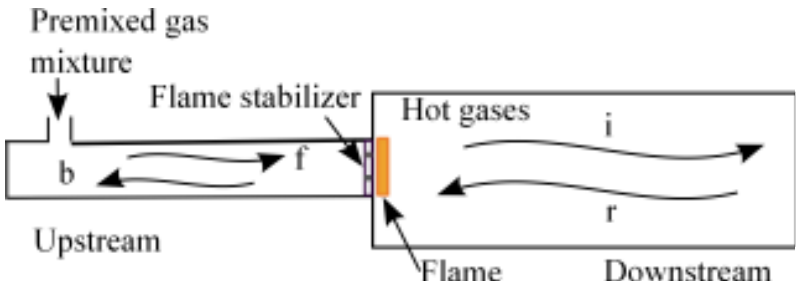

Figure 2.1: A one-dimensional model for a combustor. Geometry consists of an upstream section filled with cold reactive mixture and a downstream section with hot products from combustion. Planar acoustic waves in each section can be decomposed into forward traveling (f, i) and backward traveling waves (b, r). The flame and the area change at the flame are treated as discontinuities.

2.1.1 Helmholtz Equation

The basis of linear stability analysis is the linearisation of the conservation equations about a steady state. In the absence of discontinuities such as shocks and flames, the system acoustics is well represented by the resulting wave equation (Dowling and Williams, 1983; Rienstra and Hirschberg, 2004). Solutions of the wave equation are obtained by representing the acoustic oscillations in the chamber as a sinusoidal variation of acoustic variables in time; i.e. $p' = Re(\hat{p}(\mathbf{X})e^{i\omega t})$ and $u' = Re(\hat{u}(\mathbf{X})e^{i\omega t})$. Substituting these representations for acoustic pressure and velocity into the wave equation results in the Helmholtz equation for $\hat{p}$. Acoustic mode shapes that satisfy the boundary conditions and the corresponding eigenfrequencies can then be obtained by solving the Helmholtz equation. Since this is a linear formulation, the final solution is a linear combination of all possible solutions.

Complexities in geometry such as area changes, which exist for instance at the dump plane of a combustor, are resolved by considering the integral of linearized governing differential equations across the area change to obtain conditions relating acoustic quantities upstream and downstream. The flame is treated as a discontinuity and the jump in the acoustic variables across the flame are retrieved by the linearized Rankine-Hugoniot relations (Poinsot and Veynante, 2005). Figure 2.1 illustrates a simplified one-dimensional realization where acoustics upstream and downstream are treated as planar waves and downstream acoustics is related to upstream acoustic by the jump conditions.

The eigenfrequencies (ω) are in general complex numbers. Real part of the eigenfrequencies gives the frequency of acoustic oscillations. The imaginary part determines whether the particular mode corresponding to this frequency will grow or decay in time. For an acoustic system with no source or sink of acoustic energy, the imaginary part is zero. This is the case for duct acoustics in the absence of fluctuating acoustic energy source and/or acoustic damping mechanisms. However, in the presence of a flame, which acts as a source of acoustic energy, certain eigenfrequencies, depending on the system configuration, will have a negative imaginary part indicating an exponential growth in acoustic oscillations corresponding to the frequency given by the real part of ω. Hence, through a linear treatment of a thermoacoustic system, it becomes possible to obtain the operating conditions at which a particular mode will become unstable causing instability to set-in and the corresponding mode shape.

2.1.2 The n-tau Model

The most crucial aspect of modeling thermoacoustic instability is to model the coupling of unsteady heat release rate to the acoustic field. Such a model is the key to providing closure to the linear system of equations. The n-tau model first presented by Crocco and Cheng (1956) provides such a closure for a thermoacoustic system. A simplified expression for the n-tau model is:

$$q' \propto u'(x_f, t - \text{tau}) \tag{2.1}$$

The model states that unsteady heat release rate, q' is proportional to velocity fluctuations u' at the flame location delayed by a time-delay tau, with an acoustic amplification, n. Adaptations of this model to engineering system lead to good comparisons between predictions and experiments, primarily because mechanisms contributing to thermoacoustic instability involve inherent time-delays that play a key role in determining the onset of thermoacoustic instability (Dowling and Stow, 2003).

Predicting the frequency of the instability and the corresponding mode shapes are essential for obtaining the stability boundaries of a system and can be found through linear stability analysis. Additionally, the results can also be employed in active/passive

control strategies. Hence, the linear approach was found to be an effective analysis techniques for prediction of thermoacoustic instability. Several notable investigations were based on this approach. Though this linear model of thermoacoustic instability had its own limitations, it is effective for preliminary analysis. The n-tau model given by Crocco and Cheng (1956) was extensively implemented in several industrial and academic investigations in the field of combustion instability, some of which are described below. Although simple in its formulation, the model yielded effective prediction. This model has been verified on various types of combustion systems in its basic form or with logical extensions in order to establish the relation between the unsteady heat release rate and the flow velocity.

Bloxsidge *et al.* (1988) experimentally determined the frequency of instability associated with reheat buzz in an afterburner model. They proposed an empirical time-delayed heat release rate response to velocity fluctuations at the flame stabilization. The model incorporated two time delays associated with the convection of heat release rate oscillations with the mean flow and the inherent delay in flame response to velocity fluctuations. On similar lines, (Macquisten, 1995) investigated instability in a twin-stream afterburner with a V shaped flame holder, both experimentally and theoretically. He showed that disturbances generated in the flow velocity have an impact on the heat release rate fluctuations. The oscillations convect till the flame and produce acoustic disturbances in the flame, justifying the use of a time-delay based model. The theoretical predicted frequency of oscillations were found to compare well with those observed in experiments.

Dowling (1997) presented a time-domain simulation of combustion instability based on the empirical time-delay model developed by Bloxsidge *et al.* (1988) for heat release rate response. Based on experimental results where low frequency oscillations were observed, she modified the time-delay model for heat release rate response to acoustic oscillations to suppress the overestimated amplification at high frequencies. Furthermore, the model was extended to include a saturation of heat release rate in response to velocity fluctuations. With this type of saturation nonlinearity, the time-domain model was able to account for the observation of limit cycles and changes in the oscillation frequency with variations in the equivalence ratio. Results of linear analysis incorporating

nonlinear combustion response were found to correspond reasonably with experiments by Langhorne (1988).

Dowling (1999) modeled the flame dynamics for a bluff body stabilized flame via a linear approach extended to incorporate nonlinear effects associated with flow reversal. The flame response to fluctuations was derived from the G-equation. The results of linear flame response modeling were found to correspond to empirical time-lag formulations by Bloxsidge *et al.* (1988). Nonlinear flame response was introduced by employing a nonlinear boundary condition at the flame anchoring point. Based on visual observations, when total gas velocity exceeded flame speed, flame was assumed to be attached to the anchor. When flame speed exceeded the gas velocity, the flame was considered to propagate upstream. Modeling self-excited instabilities with the derived flame response model in a time-domain analysis was found to predict limit cycle behavior. Further, a methodology of implementation of a describing function approach to obtain limit cycle amplitudes and frequencies was suggested. A describing function evaluates the flame response not only at different frequencies but also at different forcing amplitudes.

The amplification (n) and delay (tau) in the n-tau formulation for laminar premixed flames can be derived analytically from the G-equation. This has been shown previously by Lieuwen (2003); Ducruix *et al.* (2005). However, the n-tau model in its fundamental form is insufficient to model complex flame behavior as observed in practical systems. Accordingly, extensions of the n-tau model have been developed to incorporate detailed physics of flame response. The basic n-tau model, Eqn. (2.1) assumes localized fuel injection, compact combustion and no dispersion (Lieuwen, 2003; Schuermans *et al.*, 2004). Schuermans *et al.* (2004) proposed a distributed time-lag model to be employed for turbulent swirl flames, where the mentioned assumptions clearly do not hold true.

Equivalence ratio fluctuations which form a dominant source of unsteady heat release rate also cannot be directly modeled using the basic n-tau model as pointed out by Lieuwen (2003). An extension of the n-tau formulation to include equivalence ratio oscillations was proposed in this review. According to the proposed formulation, unsteady heat release rate in response to equivalence ratio fluctuations is a result of temporal change of flame speed perturbations in addition to convection time-delay, re-

quired for mean flow to convect till the effective flame location. Detailed implications of nonlinear flame dynamics, including the effects of nonuniformities in the flow disturbances, boundary conditions and flame aspect ratio on flame response have been discussed in Preetham *et al.* (2008).

2.1.3 Forced Flame Dynamics

Thermoacoustic instability is an interplay of several physical processes, and understanding the interaction amongst these contributing processes is critical. Analytical thermoacoustic models applied currently for understanding these interactions are based on simplifications, primarily of the flame response to acoustic fluctuations. These models can predict only the linear stability of the system. It is required to consider models which take into account system dynamics which is inherently a result of nonlinear interactions, based on a detailed physical understanding. By studying the features of oscillations excited due to flame-acoustic coupling, one can expect to learn about the important effects which need to be incorporated into a thermoacoustic model. For this purpose, simple systems such as confined or unconfined laminar Bunsen-type conical premixed flames are an ideal configuration. Owing to the simplicity, they can be easily realized in experiments and in models. The basic flame-acoustic interaction is still preserved. Therefore, numerous investigations have been conducted on such systems and the results have provided significant insight. In particular, forced flame response has been extensively investigated. The flame transfer functions, FTF obtained from such investigations are employed in network models (see Candel, 2002) to describe flame-acoustic coupling and subsequently obtain stability characteristics of a system.

Perry and Blackshear (1993) developed an one-dimensional framework on the interaction of flame with acoustic waves. They concluded that flame surface area perturbations cause amplification or damping of acoustic waves passing the flame. Amplification or damping is determined by the lag between velocity perturbations and flame area perturbations. Subsequently, in the same investigation, experiments on self-excited instability in ducted laminar single and multiple flames was studied and the one-dimensional model was found to adequately explain experiments.

Boyer and Quinard (1990) studied the response of anchored premixed V-flame to homogeneous flow oscillations and modulation of the flame by Von Karman street. Analytical modeling of fluctuations was also conducted in the limit of small flame wrinkling and compared to experiments. They found that linear kinematic models could explain flame dynamics only in the regime of weak perturbations. Nonlinear features such as cusp formation could not be explained.

Fleifil *et al.* (1996) conducted a time domain and frequency domain simulation of forced flame dynamics for a laminar premixed flame stabilized on a pipe flow velocity profile. The flame response to inlet velocity fluctuations was modeled by an n-tau model similar to that used by Bloxsidge *et al.* (1988). Instead of two time-delays used by Bloxsidge *et al.* (1988) to account for convection of perturbations on the flame surface and resulting unsteady heat release rate, a single time-delay was employed. A low-pass nature of the flame was identified. The flame surface area oscillations were found in good agreement to those reported in experiments by Perry and Blackshear (1993).

Schuller *et al.* (2002), conducted a detailed investigation of the effect of upstream acoustic perturbations on the flame. Experiments were compared to numerical modeling based on the G-equation. The model could additionally account for flame cusping. The basic formulation of the G-equation can be found in the works of Williams (1985) and Kerstein *et al.* (1988). A revised formulation of inlet velocity perturbations on the flame in Schuller *et al.* (2003) was found to explain flame response in a wide range of frequencies. Specifically, deviation of flame response models to observations regarding flame behavior at high frequencies could be resolved.

A significant amount of work has been performed on the evaluation of transfer functions of laminar premixed flames through flame response studies through both experiments (Boyer and Quinard, 1990; Baillot *et al.*, 1992; Birbaud *et al.*, 2006) and modeling (Candel, 2002; Lieuwen, 2003; Karimi *et al.*, 2009). It was found that the flame has a low-pass nature, implying that amplification of acoustic waves incident on the flame occurs strongly only at low Strouhal number. The mechanism of amplification for perfectly premixed flames was identified as the wrinkling of the flame surface as a result of fluctuations that originate at flame anchoring position and convect along the flame

surface. For industrial premixed flames, the mechanism includes effects of equivalence ratio fluctuations upstream.

Forced flame dynamics and by extension, self-excited thermoacoustic instability is also affected by factors such as chemical kinetics, transport phenomena, flame stretch effects. As such, it is also important to investigate these phenomena. Clavin (1985) has reviewed the effect of chemical kinetics and transport processes for wrinkled premixed flames. Stretch effects have been recently investigated by Wang *et al.* (2009). Detailed reviews of flame-acoustic interactions have been given by Lieuwen (2003). Candel (2002) presented an extensive discussion on the role of different mechanisms in thermoacoustic instability, with focus on flame-acoustic interaction and current active and passive control techniques in his review. A report on current understanding and important investigations on flame transfer functions has been given by Ducruix *et al.* (2005) and Schuller *et al.* (2003). Hemchandra (2010) has summarized the recent developments in the modeling of flame-acoustic interaction. He explained the effect of small amplitude disturbance on both rich and lean premixed flame; the results reveal that both flames behaves differently. He further concluded that the difference is due to the dependence of equivalence ratio on flame speed and heat of reaction rate.

Investigation of flame response to equivalence ratio forcing was conducted by Sreekrishna *et al.* (2010) based on a reduced order modeling approach. The analysis was performed taking into account that equivalence ratio oscillations cause unsteady heat release rate via local fluctuations in the flame speed and heat of reaction. They concluded that due to the difference in flame speed sensitivity to equivalence ratio oscillations between lean and rich flames, the flame response is fundamentally different. Flame stretch effects were found to play a non-trivial role at high Strouhal numbers. Nonlinear flame response was also investigated. However, results at high frequencies and high amplitudes were found to deviate from the DNS of the flame response to equivalence ratio fluctuations (Santosh, 2011). The cause for this deviation, as reported in Santosh (2011), was attributed to an increased influence of hydrodynamic coupling and increased damping of equivalence ratio fluctuations at high amplitudes and high frequencies.

2.1.4 Network Model: A Linear Approach

The importance of studies on forced flame dynamics lies not only in its capability of providing an insight into flame-acoustic interaction, but also its application in stability analysis of complex systems. The network modeling approach adopted from control theory can be used for fast and efficient implementation of the classical linear analysis of thermoacoustic instabilities in the frequency domain. Each element of a combustion system, fuel/air supply ducts, combustion chamber, boundaries and the burner geometry is described by its own transfer matrix relating the upstream acoustic field to the downstream acoustic field. The transfer functions of every element, including the transfer matrix of the flame, can be combined into a system of linear equations of the form $Ax = b$. Eigenvalues of the system matrix A determine the stability of the system and the corresponding eigenfunctions describe the acoustic mode shape. The network modeling approach has been implemented on practical systems and has met with significant success in predicting instabilities.

Extensive work has been performed on the subject of network modeling by Paschereit and co-workers (Paschereit *et al.*, 1999; Paschereit and Polifke, 1998; Schuermans *et al.*, 2000) and Polifke and co-workers (Polifke *et al.*, 2001). Further, it has also been implemented in industrial systems such as annular combustors by Krebs *et al.* (1999); Pankiewitz and Sattelmayer (2003). Experimental determination of transfer matrix of a swirl flame have been presented by Paschereit *et al.* (1999) and Paschereit and Polifke (1998). By introduction of two sets of acoustic excitation, once from the upstream and then from the downstream (or equivalently simultaneous excitation from the upstream and downstream), two independent test conditions can be created and used to obtain the elements of the transfer matrix. On incorporating the transfer matrix in a network analysis, a good comparison was found between the predicted and measured frequency spectrum of pressure oscillations. The low-pass nature of the flame was also identified. Recently, André *et al.* (2009) has developed a network model to predict the combustion instability for lean premixed EV burner (Alstom). This kind of approach is helpful in understanding the system response to an extent such that implementation of active control in suppressing instability in the system becomes easy. A review of network modeling techniques, flame transfer function measurements in industrial systems

and implementation of network analysis has been presented by Paschereit *et al.* (2005). However, being linear in formulation, the network analysis cannot predict nonlinear behavior.

2.2 Nonlinear Flame Describing Function Approach

In order to explain nonlinearities in forced flame response and to infer about nonlinear dynamics of self-excited oscillations from flame response studies, the linear flame transfer function had to be extended to incorporate nonlinear dynamics. In particular, the describing function approach suggested by Dowling (1997) leads to a promising approach.

The nonlinear flame transfer function was first obtained experimentally by Durox *et al.* (1997) for a V-flame configuration. Noiray *et al.* (2008) obtained the nonlinear flame describing function for multiple premixed flames experimentally for variable burner length. The important distinction between a nonlinear describing function NDF and a linear flame transfer function FTF is that NDF is evaluated for all relevant frequencies at different amplitudes of input perturbations while FTF is evaluated for a single small amplitude, small enough to be considered a linear perturbation. Linear and nonlinear flame response has been shown via flame imaging by Karimi *et al.* (2009) for different equivalence ratios. Fluctuations in upstream flow velocity with forcing amplitudes till $u'/\bar{u}(\omega)$ of 0.9 were investigated for a single laminar conical flame. In recent developments, the nonlinear describing function approach has been shown to predict nonlinear phenomenon such as triggering and hysteresis in addition to limit cycle frequency and amplitude (Lieuwen and Neumeier, 2002; Noiray *et al.*, 2008). Moeck and Paschereit (2012) developed a multi-input describing function approach where they have considered two linearly unstable mode of the system to present the dynamical nature of the thermoacoustic oscillations.

A study of the response of heat release rate to pressure oscillations in experiments for a lean premixed flame gas turbine was conducted by Lieuwen and Neumeier (2002) by forcing at discrete frequencies and measuring pressure and *CH** radical chemilumi-

nescence oscillations. Saturation of the heat release rate response at large amplitudes was identified. Further, they studied the nonlinear interaction between forced and natural modes of the combustor that lead to frequency-locking.

The current trend of investigations on thermoacoustic instability is towards achieving a firm understanding of the nonlinear mechanisms that contribute to the phenomenon. In particular, it is essential to understand the self-excited nature of these combustion-driven oscillations. It is not surprising that several investigations have been performed previously in this area as well. In the following section we will discuss the dynamics of self-excited thermoacoustic instability.

2.3 Dynamics of Thermoacoustic Instability

A systematic approach of investigating thermoacoustic instability is to conduct numerical or laboratory experiments on the effect of system parameter changes on system dynamics. Such an investigation facilitates the evaluation of the effect of individual parameters on system stability (stability maps) and dynamics of the unstable system. Technically referred to as bifurcation analysis (Strogatz, 1994), such investigations have previously been performed on academically relevant thermoacoustic systems such as an electrically driven Rijke tube (Matveev, 2003; Subramanian *et al.*, 2010; Juniper, 2010) system and on industrially relevant, combustion driven systems (Knoop *et al.*, 1997; Lieuwen, 2002). These investigations primarily focus on the transition of the system from a steady state to instability which is typically reported to occur in the form of limit cycle oscillations. The studies have shown the existence of subcritical and supercritical Hopf bifurcation scenarios in thermoacoustic systems. Hence, it is well-established that in thermoacoustic systems, transition to instability occurs through a Hopf bifurcation, often through a subcritical Hopf bifurcation. The subcritical nature of transition results in interesting nonlinear phenomena such as triggering and hysteresis, observed in the subcritical zone of instability (Matveev, 2003; Balasubramanian and Sujith, 2008; Mariappan *et al.*, 2010; Juniper, 2010). Such dynamical behavior is particularly undesirable in practical combustion systems.

2.3.1 Triggering Instability

Linear theories and their predictive capabilities, in addition to flame response studies form a firm ground for the analysis of thermoacoustic instabilities. The insight provided by these approaches cannot be denied. However, inherent nonlinearities involved in the phenomenon of thermoacoustic instability lead to a much more variant dynamics, in addition to exponential growth and saturation to limit cycles (Dowling, 1997). In the following paragraphs, the nonlinear aspects of thermoacoustic oscillations and their analysis from a dynamical systems theory perspective is discussed.

One of the most interesting nonlinear behavior of thermoacoustic systems, identified in early investigations was the phenomenon of triggering instability. Technically, the appearance of instability in a linearly stable system on the introduction of finite amplitude disturbances is termed as triggering instability. A popular approach in the 60's to assess the stability of combustion system, particularly in liquid and solid propellant rocket systems, was to introduce pulses within the system via explosions and study the system response. This approach led to the diagnosis of pulse-triggered or triggering instability in thermoacoustic systems. In a linearly stable system, instability would arise due to the introduction of finite amplitude disturbances. This finding prompted a train of investigations.

At first, studies on obtaining triggering instability in models of thermoacoustic instability met with very little success primarily because a nonlinear treatment of combustion was still not accounted for. Further, in the 60's, the subject of nonlinear dynamics was in its infancy.

A major contribution to the analysis of bifurcation dynamics of thermoacoustic instability with focus on triggering instability was made by Jahnke and Culick (1994). Through a numerical continuation approach, they were able to obtain qualitative features of the bifurcation scenario. They obtained the stability of the steady state and the limit cycle states. Towards the end of the analysis, results also indicated the presence of quasi-periodic oscillations in a six-mode approximation of the formulation. However, triggering was not observed. Later on the basis of experiments, Ma *et al.* (1991) pointed out that the inclusion of a threshold nature of the velocity coupling was impor-

tant along with a nonlinear combustion model to model triggering instability. Ad hoc velocity coupling models in addition to nonlinear combustion response implemented in a numerical investigation by Levine and Baum (1983) and Wicker *et al.* (1996) showed the presence of triggering instability. Later, by inclusion of a threshold velocity coupling (Burnley and Culick, 2000) could obtain a bifurcation diagram which included triggering instability.

In addition to triggering, the issue of hysteresis is also an undesirable and a critical issue for combustion systems. Hysteresis occurs in systems that undergo a subcritical Hopf bifurcation. Due to hysteresis, stability in a thermoacoustically unstable system cannot be ensured by changing the operating parameters to parameters at which the system was previously observed as stable, unless the hysteresis region is completely escaped. As subcritical bifurcation is often observed in combustion systems, several reports on the observation of hysteresis can be found (Knoop *et al.*, 1997; Matveev, 2003; Mariappan *et al.*, 2010). A detailed study of hysteresis for instance, was conducted by Matveev (2003) on an electrically heated horizontal Rijke tube system. Hysteresis with respect to changes in heater power for a few mass flow rate of air through the electric heater was reported.

It is important to know the threshold amplitude required for triggering instability in systems in order to predict and control triggering instability. In this area, the most encouraging results are from the recent investigations by Noiray *et al.* (2008) and Boudy *et al.* (2011) considering single acoustic mode of the system. They reported, both experimentally and theoretically that using the nonlinear describing function approach, that it is possible to predict various nonlinear characteristics of thermoacoustic systems including triggering instability, mode switching and hysteresis. A flame transfer function based interpretation of triggering instability was also recently presented by Kim and Hochgreb (2012).

Lieuwen (2002) has shown for a lean premixed combustor that, in the subcritical zone, system can get triggered not only with the disturbance provided to the system externally but even from the background noise (Lieuwen and Banaszuk, 2005), if the noise level is sufficient enough. The susceptibility of a premixed combustor with a swirl stabilized flame to acoustic disturbances has been investigated by Moeck *et al.* (2008)

experimentally. They were also able to reproduce the experimental results on triggering and hysteresis through simulations incorporating linear acoustics and a nonlinear response of the flame to upstream air flow rate fluctuations. Jegadeesan and Sujith (2012) have studied noise-induced transition to instability in the subcritical zone through experiments on a ducted diffusion flame system. The dynamics of thermoacoustic systems is also sensitive to parametric uncertainties, which is difficult to quantify even for simple systems. Nair *et al.* (2010) and Waugh and Juniper (2011) have recently presented an approach which could be used as an effective alternative to conventional uncertainty quantification techniques for real systems.

In recent developments, it was pointed out by Balasubramanian and Sujith (2008) that the concept of non-normality also has a significant role in thermoacoustic systems. Non-normality results in transient growth of infinitesimal disturbances in a linearly stable system. In the subcritical zone, triggering can occur if this transient amplification of disturbances crosses the threshold amplitude required for triggering. Balasubramanian and Sujith (2008) have shown that thermoacoustic interactions in a confined diffusion flame system are non-normal. Subramanian and Sujith (2011) found that ducted premixed flames were also exhibit transient growth due to non-normality in the system. For a horizontal Rijke tube Juniper (2010) has shown that due to the non-normal nature of governing equations, the triggering amplitude required by the system for transition to instability is lower than the amplitude of unstable limit cycle oscillation. Applying dynamic mode decomposition on experimentally acquired data, Mariappan *et al.* (2011) have shown that the system eigen-vectors for a horizontal, electrically-driven Rijke tube system are non-orthogonal, indicating the presence of non-normality in the system. In addition to the effects of non-normality and nonlinearity in the subcritical zone, Juniper (2010), based on a dynamical systems approach, gives an analogy between triggering in thermoacoustic systems and bypass transition in fluids (Drazin, 1992). These investigations reveal that parallels can be drawn between transition of laminar fluid flows to turbulence and triggering of thermoacoustic systems.

The dynamical nature of nonlinear systems is characterized by oscillation states and bifurcations. These nonlinear characteristics are found to be strikingly similar in different physical systems. The application of dynamical systems theory has been found

to be instrumental in identifying the nonlinear characteristics of systems and categorizing them according to the bifurcation scenarios and oscillation states observed. The following sections illustrate this point. Subsequently, previous investigations focusing on analysis of thermoacoustic instability through the application of dynamical systems theory have been discussed.

2.3.2 A Few Examples of Nonlinear Systems in Nature

In the 70's and the 80's, significant advances were made in the theory of nonlinear systems with findings of low dimensional chaos and strange attractors in physical systems such as in turbulent flows Ruelle and Takens (1971), the Taylor-Couette flow (Swinney, 1983), Rayleigh-Bénard convection cells (Brandstäter *et al.*, 1983) and in chemical reactions (Roux *et al.*, 1981). Furthermore, simultaneous developments of the geometrical analysis of the phase space (Packard *et al.*, 1980; Broomhead and King, 1986) facilitated the analysis of experimentally acquired data and the identification of well-defined routes to chaos which forms an integral part of the characteristics of a nonlinear system.

Simultaneously, propelled by the new findings of the nonlinear systems theory, similar developments were being made in the investigations on acoustics, combustion and thermoacoustic instability. Kitano *et al.* (1983) reported chaos through a period-doubling route in a simple acoustic system composed of microphone, speaker, amplifier setup with a nonlinear circuit. The time-delay between speaker output detected by the microphone positioned at a distance from the speaker was a critical in the delay-induced instability.

2.3.3 Periodic and Aperiodic Nature of Thermoacoustic Oscillations

A subcritical Hopf bifurcation causes transition from a steady state to self-excited limit cycle oscillations in acoustic variables and the unsteady heat release rate from combustion. Subsequent to the Hopf bifurcation, there always exists a possibility for further bifurcations of the limit cycle. Nonlinear bifurcations and complex dynamical states such as quasi-periodic behavior of thermoacoustic oscillations was first reported in a

numerical investigation on a combustor model by Jahnke and Culick (1994).

Yazaki *et al.* (1987) identified route to chaos for a gas column system driven by temperature gradients. The setup studied was a standard configuration to realize Taconis oscillations. During the instability, two natural modes were simultaneously excited at certain operating conditions. Based on this observation, they concluded that the quasi-periodic route to chaos observed appears due to a competition between the natural instability modes of the systems.

In combustion driven thermoacoustic systems, Keanini *et al.* (1989) reported the presence of low dimensional chaos in ramjet combustion. The explanation for the observation of low dimensional chaos postulated was that the original high dimensional behavior of turbulence in the system transforms to a low dimensional chaos when order is brought about within the system due to the coupling of flame dynamics with system acoustics.

Sterling and Zukoski (1991) investigated thermoacoustic instabilities in a dump combustor characterized by vortex shedding associated with combustor acoustics. Nonlinear analysis of self-excited oscillations revealed that the stable attractor occupies a dimension greater than one which indicated the presence of a quasi-periodic-like attractor rather than a limit cycle. They reasoned that the high driving of the systems due to the Rayleigh mechanism causes cycle to cycle variations leading to deviation from a limit cycle state. It was concluded that the inherent time-delays associated with mixing, reaction rates and response of vortical structure to acoustic oscillations that can be modeled only by delay-differential equation causes the system to evolve on a high dimensional attractor and thus, transition to chaos is a possibility. Later Sterling (1993) confirmed the presence of quasi-periodicity in the system. Additionally, through simple modeling with two different types of nonlinear combustion models, he obtained a period-doubling route to chaos.

Based on the work by Sterling (1993), Lei and Turan (2009) also reported a period-doubling route to chaos in a numerical investigation with a discrete-dynamic model of the system including vaporization process in addition to delayed combustion response. In another analysis with a one-mode dynamic model, a period-3 solution was obtained

in addition to period-doubling during transitions to chaos. Dynamics of self-excited states were also investigated and it was found that changes in system parameters cause changes the periodicity of self-excited oscillations. Period doubling route to chaos was also shown recently by Subramanian *et al.* (2010) for a model electrically powered horizontal Rijke tube. Through numerical bifurcation analysis and on implementing nonlinear time series analysis the route to chaos was identified for the Rijke tube thermoacoustic system.

Very recently in experiments, Gotoda *et al.* (2011) through nonlinear analysis of combustion induced self-excited oscillations in a gas-turbine combustor reported the transition of stochastic fluctuations in the system to low dimensional chaos via periodic oscillations.

According to numerical investigations till date, period-doubling to chaos is a recurrent theme. In contrast, dynamics associated with thermoacoustic oscillations observed in experiments indicate the presence of quasi-periodicity. It is clear that further investigation is required in order to establish a complete description of thermoacoustic instability, including nonlinear dynamics. A specific aspect that forms a focal point of this investigation is that, although it has been shown that complex oscillations and chaos exists in thermoacoustic systems, a complete route to chaos has not been established from experiments. Such an investigation is needed to validate numerical results and to provide a unified explanation of the few reported observations of dynamics such as quasi-periodicity and chaos in thermoacoustic systems.

2.4 The Present Investigation

Several questions appear on the basis of previous investigations. It is clear that features such as quasi-periodicity and chaos exist in practical thermoacoustic systems and limit cycle is not the only possible asymptotic state attained by a thermoacoustic system. It needs to be clarified whether such nonlinear features are a manifestation of turbulence in the system or a competition between acoustic modes that are interacting with the flame. A complete route to chaos has been established numerically; however, it has not

been experimentally established till date. Furthermore, the period-doubling route found in numerical bifurcation analysis is in contrast to several reports on the observation of quasi-periodicity.

In the present investigation, through an experimental bifurcations analysis, we study the transition of steady state to aperiodic oscillations via periodic states in a ducted laminar premixed flame configuration. A relatively simple Rijke-tube type thermoacoustic system is investigated. Two laminar flame configurations have been studied: a single conical flame and a multiple injection configuration. These configurations have the advantage that the properties of combustion instability can be studied without significant interference from turbulence and complexities of geometry found in industrial systems. In addition, the dynamics of laminar flames similar to what is chosen for the present study, has been extensively studied before via forced flame response studies, experimentally (Matsui, 1981; Candel, 2002). This makes the configuration well-suited for fundamental studies on self-excited combustion instability.

Study of the dynamics of self-excited thermoacoustic oscillations through the analysis of the topological characteristics of phase space trajectories reconstructed from time series data of acoustic oscillations is at the heart of this study. The implementation of advanced nonlinear time series analysis techniques (Kantz and Schreiber, 2003) on experimentally acquired acoustic pressure data and CH^* chemiluminescence and simultaneous analysis of high speed flame images yields new insight into the dynamics of self-excited thermoacoustic oscillations. Since, lean operating conditions are of particular importance to the thermoacoustic community, experiments here are performed for lean equivalence ratios. Obtained results show the presence of many complex dynamical states including chaos in a laminar premixed flame driven thermoacoustic system.

CHAPTER 3

EXPERIMENTAL SETUP

In this chapter, we discuss the details of the experimental the setup and the measurement techniques used in this study. The characteristics of thermoacoustic instability depend critically on the flame configuration and on the geometry of the combustor. For a fundamental study on self-excited thermoacoustic instability, a representative system that preserves basic thermoacoustic interactions is required. Towards a complete understanding and control of the occurrence of thermoacoustic instabilities, it is essential to first identify the physical mechanisms and their role in the phenomenon in simple configurations. Complexities can then be systematically incorporated to generalize the information gained. Simplicity in the experimental configuration is also important to accelerate numerical and analytical investigations.

Based on these points, a Rijke-tube system is chosen for studies. However, instead of using an electrically heated mesh used as the heat source in conventional Rijke tubes, the more interesting case of a confined laminar premixed flame system is employed here. As mentioned already, dynamics of unconfined laminar flames has been extensively studied before, particularly in flame response studies and has been found to display a rich nonlinear behavior such as flame cusping and flame lift-off (Bourehla and Baillot, 1998).

3.1 Setup

Two flame configurations were studied: (1) a single laminar conical premixed flame and (2) multiple laminar conical premixed flames stabilized on a perforated block. The two flame configurations are presented in Fig. 3.1. The unconfined single flame configuration has been extensively studied in previous investigations (for example Durox *et al.*, 1997; Bourehla and Baillot, 1998; Lieuwen, 2002; Schuller *et al.*, 2003; Karimi

et al., 2009). As we will find in Chapter 6, the multiple injection configuration allows for more dynamics in the system. Such a configuration has been studied previously by many researchers including Matsui (1981), Noiray *et al.* (2008) and Boudy *et al.* (2011) in flame response investigations. A cylindrical borosilicate glass duct was used as the confinement in order to have optical access for investigating flame dynamics. A closed-open boundary condition for the confining glass duct was maintained via a base plate as shown in Fig. 3.1 for both cases. The advantage of having a closed bottom end is that the flame will not be affected by the air entrainment. Entrainment can cause local equivalence ratio fluctuations in the flame. To avoid such equivalence ratio fluctuations from contributing to the dynamics of thermoacoustic instability, a closed-open configuration was necessary. In addition, the quality of chemiluminescence measurements (*CH**) is also affected due to entrainment. During the occurrence of self-excited instability, the quarter-wave duct acoustic mode and its harmonics interact with the flame.

In the single flame configuration, the setup consists mainly of a single conical flame burner confined within a closed-open glass duct, $860\ mm$ in length. The burner tube is a cylindrical brass duct, $800\ mm$ in length with an inner diameter of $10\ mm$ and a wall thickness of $0.5\ mm$. The long burner tube length results in a fully developed circular jet flow profile. Liquefied petroleum gas (LPG) is used as the fuel for combustion. A lean equivalence ratio (ϕ = 0.51) was maintained for the results reported, by fixing the volumetric fuel flow rate and air flow rate at $124\ ccm$ and $7.2\ lpm$ respectively.

For the multiple flame configuration, multiple conical flames were stabilized on a circular, perforated copper block. A mild steel tube of inner diameter $16\ mm$, thickness $1.5\ mm$ and length $800\ mm$ was used as the burner tube. The glass duct in this configuration was of length $800\ mm$ with a diameter $56.5\ mm$. The perforated copper block, $18\ mm$ in thickness, with seven holes of diameter $2\ mm$ was mounted on the burner tube. A fine wire mesh is installed on top of the perforated copper block to prevent flame blow-off during the instability.

The burner tube in both flame configurations is connected to a cylindrical decoupler of diameter $200\ mm$ and height $200\ mm$. The decoupler creates an acoustically open end for the burner tube and arrests the propagation of acoustic oscillations into the fuel and air supply lines. Upstream of the decoupler, LPG and air are mixed in a premixing

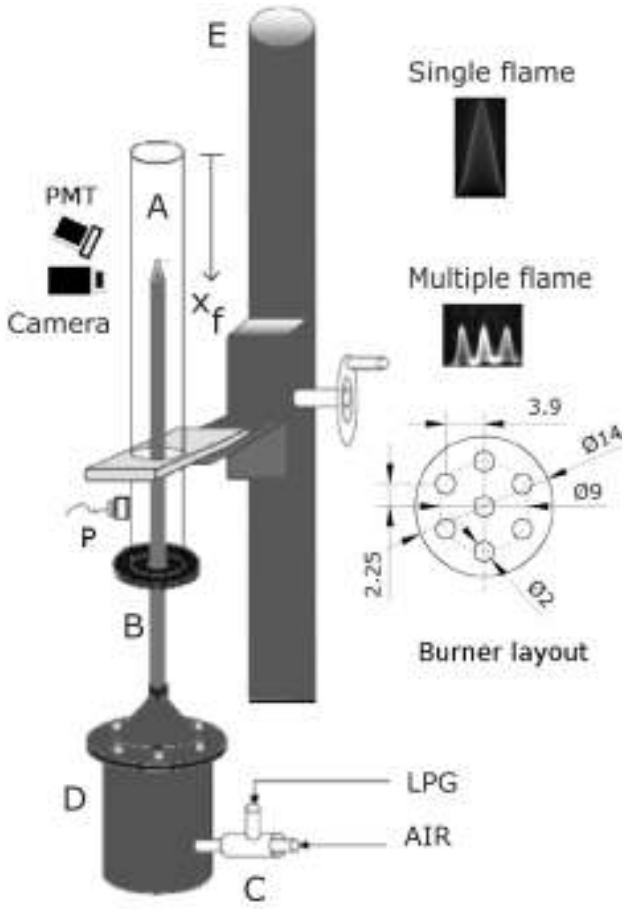

Figure 3.1: Schematic of the thermoacoustic setup. A: open-closed glass duct, B: burner tube, C: LPG-air premixing chamber, D: decoupler, E: traverse, P: pressure sensor, PMT: photomultiplier tube. Two flame configurations were investigated - single and multiple premixed flame. On the top right corner are steady state images (line of sight) of the two configurations. A burner layout for multiple flames is also shown just below the steady flame image of the multiple flame.

chamber of 100 mm in length and 6 mm in diameter. Steel wool is stuffed inside the premixing chamber to ensure proper mixing. In addition to this, the inlet of air and LPG to the chamber is made perpendicular to each other for enhanced mixing.

The dimension of the burner tubes and the equivalence ratio at which experiments were conducted for both flame configurations are summarized in Table 3.1.

In addition to the above stated specifications, the choice of the bifurcation parameter is an essential detail. Net flow rate or the equivalence ratio are obvious choices. However, these are not the most appropriate because firstly, changes in the flow rate and/or equivalence ratio directly cause changes in mean flame characteristics such as

Table 3.1: Burner configuration and operating conditions for results presented in the thesis

Flame types	Burner configuration	ϕ	Volumetric air flow rate (lpm)
Single flame	Tube length= 860 mm Material brass Inner diameter = 10 mm Tube wall thickness = 0.50 mm	0.51$\pm$0.014	7
Multiple flames	Tube length= 800 mm Inner diameter = 14 mm Material mild steel Tube wall thickness = 1.50 mm Individual hole diameter = 2 mm Number of holes = 7	0.48$\pm$0.014	4

the flame height, angle and flame speed. Secondly, the available range for bifurcation analysis with net flow rate/equivalence ratio as the bifurcation parameter is limited. The resulting bifurcation diagram would be coarse with large uncertainties resulting from available measurement equipment. To side step these issues, a suitable bifurcation parameter would be the flame location in the confinement. As results show later, this choice of the bifurcation parameter suits ideally to the objective of this investigation.

Bifurcation analysis forms the basis of the present investigation and the flame location relative to the glass duct confinement is considered as the control parameter for both the setups. In order to facilitate variation in relative flame location (x_f), a traverse mechanism using which the flame location can be mechanically varied in steps of $1\ mm$ has been constructed. Traversing the glass duct was performed smoothly and mechanically (using a rack and pinion mechanism), without the use of electrical motors that create noise and vibration, to ensure that the test setup is not affected by sound and vibration associated with the traverse system. The burner is ignited by bringing the burner exit close to the open end of the enclosing duct. The flame location is then varied slow enough to maintain a quasi-equilibrium state. Measurements were recorded at every $1\ mm$ only after a waiting time of at least $2\ minutes$ to ensure that only

asymptotic dynamics is captured. Following this, data is acquired for a time interval of $30\ seconds$. It is to be noted that the spatial temperature distribution in the glass duct will depend on the speed of traverse motion and whether the flame location is changed from closed towards open end or the opposite. Although, an attempt has been made to avoid these effects by moving the traverse very slowly (traversing speed determined from preliminary investigations involving temperature measurements), reported results could include minor effects of differences in the spatial distribution.

3.2 Measurements and Data Acquisition

For the analysis of self-excited instability, time series data for duct acoustic pressure and *CH** radical emission from the flame were acquired. Pressure sensors (PCB piezotronics, model number 103B02) were mounted at different locations on the glass duct. At locations unaffected by hot combustion products, for example near the closed end, microphones were flush mounted as shown in Fig. 3.1. Pressure fluctuations due to standing waves in the duct have a maximum amplitude near the acoustically rigid end and hence, the signal-to-noise ratio will be higher for pressure signals acquired by microphones mounted near to the closed end of the duct. Microphone P is located at a distance of $50\ mm$ from the bottom of the glass duct. Results are presented for acoustic pressure acquired by the microphone labelled P in the setup (Fig. 3.1). Volumetric fuel and air flow rates were metered using calibrated glass rotameters with an accuracy of 2% of the full-scale reading.

*CH** radical emission (chemiluminescence measurements $I(t)$) is known to be proportional to heat release rate from premixed flames (Langhorne, 1988). Hence, simultaneously with pressure oscillations, time series of *CH** emission has been acquired using a photomultiplier tube (Hamamatsu, H5784) equipped with a narrowband filter (bandwidth $10\ nm$, centered at $431.4\ nm$). A 16-bit analog to digital conversion card (NI-6143), interfaced to the pressure sensor via a signal conditioner, was used to acquire data at a sampling rate of $10\ kHz$ for a duration of $30\ sec$. High speed flame images were acquired using a high speed monochrome digital camera (Phantom V. 12) at $5\ kHz$ and additionally on a video camera (Panasonic) at a framing rate of $25\ Hz$ as

a method for visualization of mean flame shape and position in the analysis of single flame configuration.

In the preliminary experiments, it was found that environmental conditions affected experiments. Hence, it is important to maintain a certain control over the conditions at which measurements are performed. In particular, the system acoustics, a major element of the phenomenon under investigation, is quite sensitive to fluctuations in ambient environment conditions (the conditions of the test facility environment are different for instance, when conditions on a rainy day are compared to those on a sunny day, even when the room is air-conditioned). Prior to every experiment, the exponential decay rate of the acoustic pressure generated in the system in response to an internally introduced acoustic pulse was evaluated (at cold flow conditions) for the characterization of inherent acoustic damping. To ensure a consistency in conditions for different sets of experiments, experiments were performed when the exponent of the measured exponential decay falls within 10% of $16/s$.

The analysis of results presented here is largely based on the implementation of nonlinear time series analysis techniques. The theory behind the techniques and certain details of their implementation are presented in the next chapter.

CHAPTER 4

DYNAMICAL SYSTEMS AND NONLINEAR TIME SERIES ANALYSIS

4.1 Introduction

In this thesis, we have performed a nonlinear analysis of experimentally obtained results on thermoacoustic instability, based on dynamical systems theory. A discussion of the concepts involved and their implementation on the obtained results have been presented in this chapter. Certain specific details regarding the implementation of the techniques described here have also been described along with the obtained results. The discussion of the techniques used for nonlinear analysis requires introduction of terminologies from the dynamical systems theory, which is presented next. Center of our discussion will the evolution of system *trajectories* in the *phase space*. In particular, We will be focusing on the long term, asymptotic dynamics whose phase space representation is termed as an *attractor*. The discussion here is limited to the requirements of the thesis. Readers interested in the topics of dynamical systems and nonlinear time series analysis may refer to specialized texts((Abarbanel *et al.*, 1993; Kantz, 1994; Strogatz, 1994; Hilborn, 2000; Nayfeh and Balachandran, 2004)).

4.2 Dynamical Systems

$$\dot{\mathbf{X}} = \mathbf{\Phi}(\mathbf{X}) \tag{4.1}$$

Equation 4.1 represents the evolution of a general dynamical system, defined by a set of time-varying *state variables,* $\mathbf{X}$. $\dot{\mathbf{X}}$ is the first order time-derivative of the state variables. The evolution follows a well-defined rule contained in $\mathbf{\Phi}$. Given an initial condition that assigns specific values to the state variables at a reference time, the evolution of a *deterministic* dynamical system, represented by Eqn. (4.1) can be used to

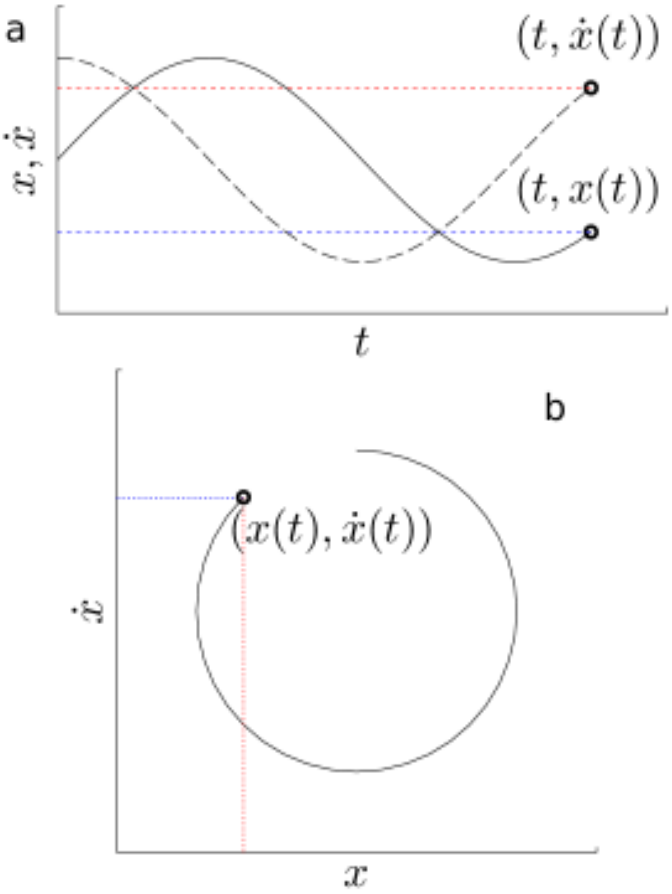

Figure 4.1: Illustration of the phase space trajectory (b) created from sinusoidally varying state variables (a) of a hypothetical dynamical system. Plotting the state variables ($\mathbf{X} = [x, \dot{x}]$) against each other gives the phase space. Accordingly, the values of the state variables at a particular time ($x(t)$, $\dot{x}(t)$) gives the coordinates of a single point in the phase space.

determine a future state. The evolution rule, $\mathbf{\Phi}$ can assume a linear or a nonlinear form. In the paragraphs that follow, a geometric approach the *phase space* analysis, which is particularly effective in the analysis of nonlinear dynamical systems is discussed.

4.2.1 The Phase Space Representation

Going back to the general equation for dynamical systems, Eqn. (4.1), the state vector $\mathbf{X}$ consists of individual state variables that define the considered system.

$$\mathbf{X} \equiv [x_1, x_2, x_3, \ldots, x_n] \tag{4.2}$$

represents a dynamical system which requires n state variables to define its state at any given time. The *phase space* of the system is then an n-dimensional geometrical space where every dimension corresponds to a single variable. Accordingly, values that the state variables assume at a particular time correspond to a single point in the phase space; i.e., at a particular instant of time, t, the system state corresponds to a point $\mathbf{X_t} = (x_{1_t}, x_{2_t}, x_{3_t}, \ldots, x_{n_t})$.

4.2.2 Trajectories in Phase Space

Based on the above discussion, an initial condition at reference time $t = 0$, assigned to the dynamical system, is given by a point in the phase space given by

$$\mathbf{X_0} = (x_{1_0}, x_{2_0}, x_{3_0}, \ldots, x_{n_0}). \tag{4.3}$$

The system then evolves in time according to the governing rule in Eqn. (4.1). In the phase space, this evolution is represented as a line that traverses the n-dimensional space, passing through points as they are being created by the dynamical system. This line is the *trajectory* that represents the system's time evolution graphically.

The concept of a phase space trajectory is illustrated in Fig. 4.1. The sinusoidal time evolution of the state variables x and $\dot{x}$, shown in Fig. 4.1 (a) is represented in a phase space by a trajectory constructed by plotting (x, $\dot{x}$) at different time instants.

4.2.3 Attractors in Phase Space

Different initial conditions assigned to a dynamical system will lead to different trajectories in the phase space, that never intersect each other. In the phase space, there exist regions that attract phase space trajectories (attractors), regions that repel phase space trajectories (repellers) and regions that attract phase space trajectories approaching from certain directions but repels in other directions (saddle). After a certain transient, every phase space trajectories are attracted towards a definite structure in the phase space. This structure is the *attractor* of system dynamics. The attractor defines asymptotic

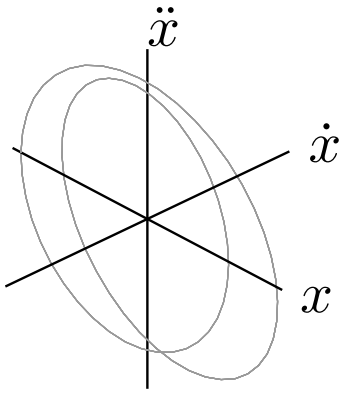

Figure 4.2: A period-2 attractor. $x = asin(2\pi f_1 t) + bsin(2\pi f_2 t);\ f_1/f_2 = 2$. The double-looped closed structure is due to the presence of a subharmonic.

system dynamics and its topological features correspond to a point or a loop or a fractal object in the phase space depending on the dynamical system. For a single parameter set (dependence of a dynamical system on system parameters is discussed in Sec. 4.4), the phase space can contain more than just a single attractor. Each attractor has its region of influence called the *basin of attraction* (Hilborn, 2000).

In the case of multiple attractors, trajectories starting within the basin of attraction of a particular attractor have their fate tied to that specific attractor. This gives rise to an interesting situation, that different initial conditions, could lead to different asymptotic states. The asymptotic dynamics of a dynamical system is related to the topological characteristics of the phase space attractor. Dynamics observed in most physical systems correspond to attractors that can be classified into three types.

4.3 Attractor Classification

4.3.1 Fixed-point

A point is the most fundamental geometrical construction in the phase space. The stable/unstable *fixed-point attractor* is a point in the phase space that attracts/repels trajectories. At a fixed-point attractor, the system dynamics corresponds state variables that do not change in time. In multi-dimensional systems, where dynamics is not constrained to a one-dimensional phase space, more geometrical structures in addition to

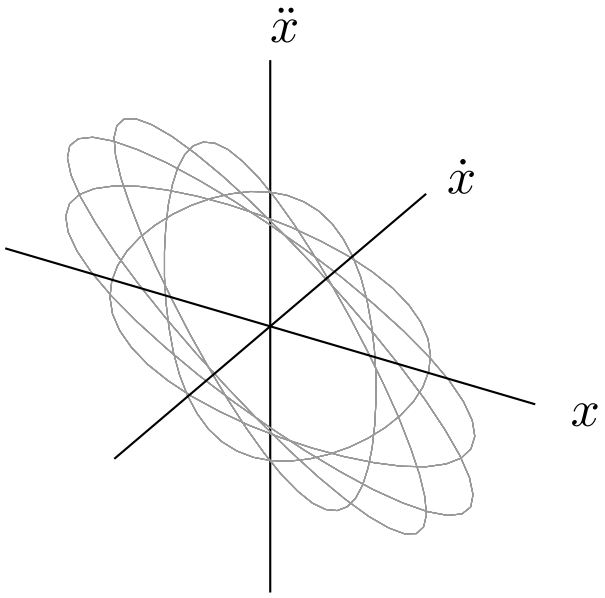

Figure 4.3: Attractor for a frequency-locked state. Such an attractor is formed when system dynamics is a result of two contributing frequency components related rationally to each other $x = asin(2\pi f_1 t) + bsin(2\pi f_2 t)$; for this illustration, the frequency ratio is chosen as $f_1/f_2 = 7/5$.

fixed points for the phase space attractor are possible.

4.3.2 Periodic Attractor

Often in physical systems including thermoacoustic systems, one finds periodic solutions/dynamics where the state variables or an observed physical quantity varies periodically in time. Such system dynamics forms closed loops in the phase space. Depending on the number of rotations made in the phase space before closing on itself, periodic attractors are termed as period-n attractors, where n is $1, 2, 3, \ldots$. The period-1 attractor is more often recognized by the name, *limit cycle*. Figure 4.2 illustrates a period-2 attractor with the distinct double loop structure formed due to the subharmonic. A limit cycle is a single loop, a period-4 has 4 loops and so on. Such period-n attractors are formed due to the presence of subharmonics in a system.

There exists another category of periodic attractors corresponding to the frequency-locked state. For frequency-locking, the system has frequencies which are related by a rational ratio. Such an attractor is shown in Fig. 4.3. In a frequency-locked state, phase space trajectories form form several loops before closing on itself.

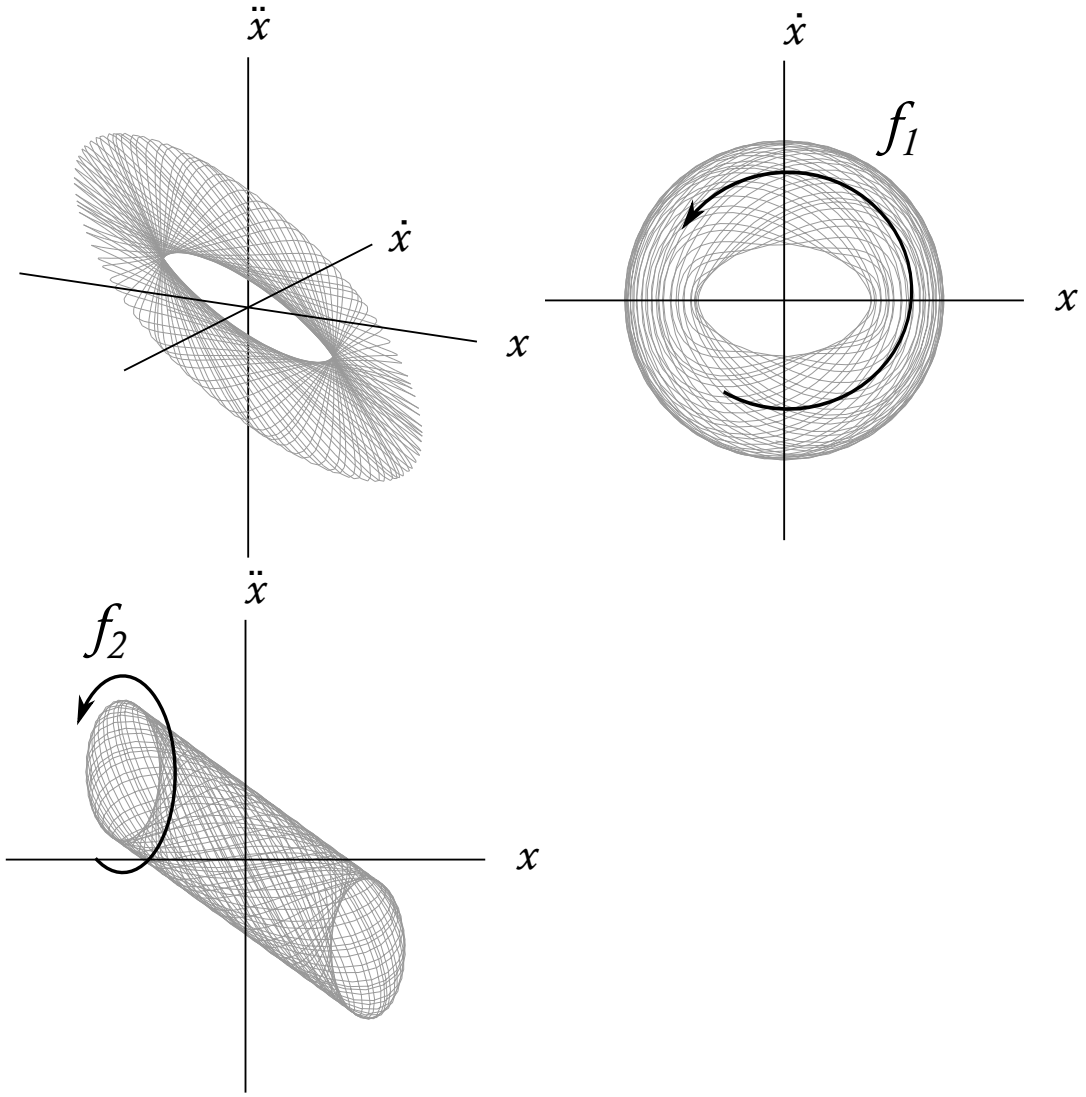

Figure 4.4: Irrationally related frequency components in a dynamical system lead to quasi-periodic motion of the trajectories where they evolve on a torus never closing on itself. $x = asin(2\pi f_1 t) + bsin(2\pi f_2 t)$. For this illustration, the frequency ratio, f_1/f_2 is chosen as the golden ratio, $\frac{1+\sqrt{5}}{2}$.

4.3.3 Quasi-periodic Attractor

Quasi- or almost periodic attractors are formed in systems where two or more than two frequencies that contribute to the dynamics in a system are incommensurate or irrationally related. As a result, the phase space trajectory can never close itself. Presence of quasi-periodic dynamics results in a toroidal structure: a two-torus for two incommensurate frequencies, a three-torus for three and likewise. Quasi-periodicity is also commonly observed in physical systems. An illustration of a quasi-periodic trajectory is presented in Fig. 4.4. Trajectories following a torus can be clearly identified. Only

a finite evolution of the trajectories is plotted resulting an apparently weaved structure of the torus. The trajectories will further evolve and form a dense closed torus, never exactly going back the initial point.

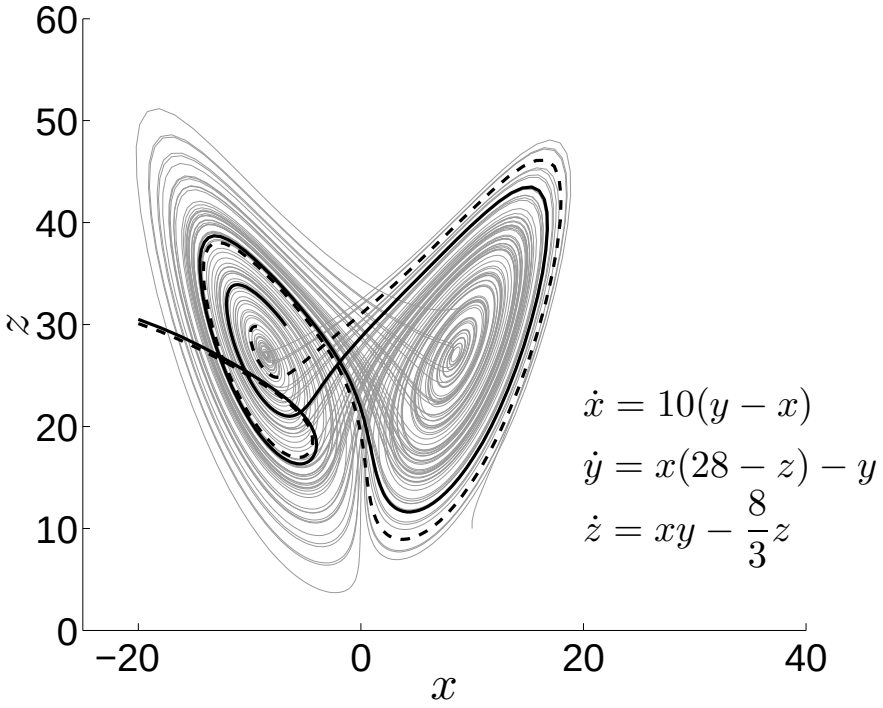

Figure 4.5: The Lorenz attractor (gray) obtained by solving the Lorenz system of equations. The solid black lines and the dashed line are two trajectories starting as neighboring trajectories. Due to the chaotic nature of the Lorenz attractor, the separation between the trajectories increases as it evolves on the attractor.

4.3.4 Aperiodic Attractor

Aperiodic attractors in the phase space are identified by an strange structure and a highly sensitive dependence of trajectories on the initial conditions. In dissipative systems, the irregular structure associated with the chaotic attractor is a fractal, possessing a non-integer inherent dimension. In discussions on transition scenarios to chaos, we will find that chaotic attractors appear as a result of the breakdown of regular periodic/quasi-periodic attractors. The sensitive dependence of trajectories to errors in the initial condition means that two trajectories originating from initial conditions differing by a small measure deviate as they evolve on the chaotic attractor. This implies that a small error in the prediction of the initial condition results in growing prediction errors subsequently.

The well-known 'butterfly effect' is a hypothetical illustration of the sensitivity of a chaotic system to initial conditions. The chaotic Lorenz attractor associated with the inception of the 'butterfly effect' is given in Fig. 4.5. The dark solid line and dashed lines in the phase space Fig. 4.5 illustrate how two neighboring trajectories diverge from each other as it evolves on the phase space.

4.4 Bifurcations

Physical mechanisms and interactions observed in a dynamical system often depend on certain critical parameters of the system. Dependence on system parameters is a feature inseparable from nonlinear dynamical systems. Changing critical parameters would cause changes in the dynamical behavior of the system. Including this parametric dependence in Eqn. (4.1), a more general formulation is obtained as:

$$\dot{\mathbf{X}} = \mathbf{\Phi}(\mathbf{X}, \mu) \tag{4.4}$$

$\dot{\mathbf{X}} = 0$ gives the fixed points of the dynamical system. Variation of system parameter, μ can switch the stability of fixed points. The presence of an unstable fixed point gives rise to the possibility of the several possible attractors that govern the asymptotic system dynamics: limit cycles, quasi-periodic oscillations and even chaotic states. Depending on $\mathbf{\Phi}$, the spectrum of possible equilibrium states for a particular dynamical system is defined. Among these, the asymptotic state that the system will correspond to depends on μ. In addition to changes in the fixed point stability, as a parameter μ is varied, the phase space undergoes transformations. Existing attractors can morph or disappear and new attractors can be be created. Therefore, system dynamics for different system parameters can be drastically different. By changing a system parameter systematically, transitions or *bifurcations* of a nonlinear dynamical system to different nonlinear asymptotic states can be observed. According to the dynamical systems theory, bifurcations have been categorized depending on the equilibrium states participating in the transition. It is well-understood that physical systems follow standard bifurcations such as pitch-fork, transcritical, saddle-node and the Hopf bifurcations (Strogatz, 1994).

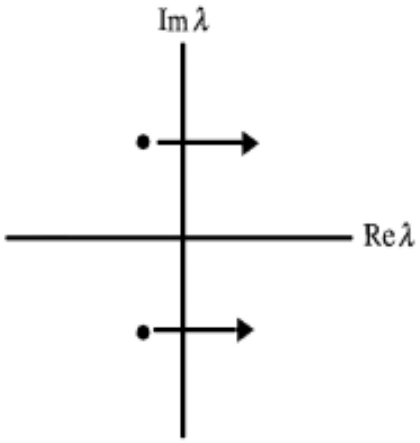

Figure 4.6: Movement of conjugate pair towards the right half plane is an indication for the occurrence of Hopf bifurcation in the system. λ is the eigenvalue.

For the discussion of results in the present investigation the saddle-node, Hopf and the Neimark-Sacker bifurcations are of particular importance. A saddle-node bifurcation, also referred to as the fold bifurcation, is when stable and unstable solutions merge together. The point at which the merging occurs is the fold point. The Hopf bifurcation results in the birth of a limit cycle solution while a Neimark-Sacker bifurcation is the name given to secondary (Hopf) bifurcation of a limit cycle.

While on one hand, such bifurcations lend nonlinear systems their intrinsic complexity, identical bifurcation scenarios in completely unrelated physical systems bring together different systems giving rise to a certain universality.

4.4.1 Hopf Bifurcation, a Case Study

In the context of thermoacoustic instability, the Hopf bifurcation associated with the formation of limit cycles and the subsequent bifurcations are of particular importance. A Hopf bifurcation is characterized by a conjugate pair of eigenvalues of the system crossing the imaginary axis indicating loss of stability of the fixed point. Figure 4.6 shows the crossing of eigenvalues in the imaginary plane, a characteristic feature of Hopf bifurcation. Hopf bifurcation is further classified as subcritical Hopf bifurcation and supercritical Hopf bifurcation. A limit cycle corresponds to periodic oscillations of the state variables appears when the system parameter μ crosses the critical point i.e., the Hopf point. The onset of thermoacoustic oscillations occurs through Hopf bifurca-

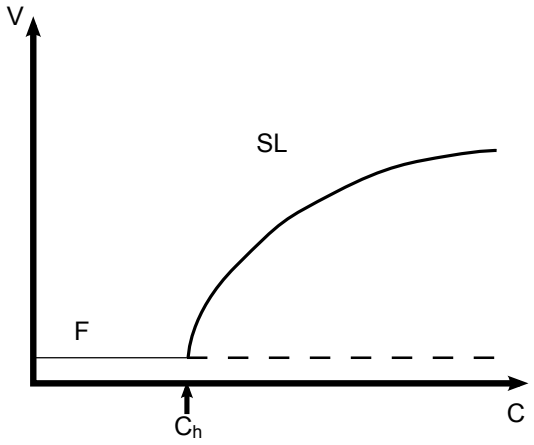

Figure 4.7: An illustration of a supercritical Hopf bifurcation. Solid lines indicate stable states and the dashed line indicates unstable states. The Hopf point is the point (C_h) where transition to a limit cycle state (SL) from fixed point (F) occurs. The fixed point solution (F) loses stability beyond the Hopf point.

tion (Knoop *et al.*, 1997; Zinn and Lieuwen, 2005). In nonlinear systems, two categories of Hopf bifurcations exist, supercritical and subcritical Hopf bifurcation. Both these are schematically explained in Fig. 4.7 & Fig. 4.8 respectively. The horizontal axis is the parameter (C) axis and the vertical axis is the measured amplitude (V) of a state variable from the system (for instance acoustic pressure). The dashed line denotes unstable state. The solid curve in the bifurcation diagrams denote stable state/attractors. In a supercritical bifurcation (Fig. 4.7), a stable limit cycle attractor is created at the Hopf point. Beyond the Hopf point, the fixed point solution is always attracted towards the available stable attractor (SL) and hence, the asymptotic state of the dynamical system is a limit cycle oscillation (SL).

In contrast, in a subcritical bifurcation (Fig. 4.8), the fixed point solution loses stability at the Hopf point (C_h) and simultaneously, an unstable limit cycle solution is created (UL). In addition, the unstable limit cycle oscillation exists before the Hopf point along with the stable fixed point state (F). As a result, theoretically, beyond the Hopf point, any infinitesimal deviation from the fixed point will cause the oscillation to grow infinitely. However, this is not physical and the system is attracted to a distant stable attractor (SL) and eventually settles onto that attractor. It is important to note that it is often reported that the distant attractor is also a limit cycle. This is not a requirement for a subcritical Hopf bifurcation and the distant attractor can be a period-2 or a quasi-periodic or any other variant of stable attractors (Strogatz, 1994; Nayfeh and

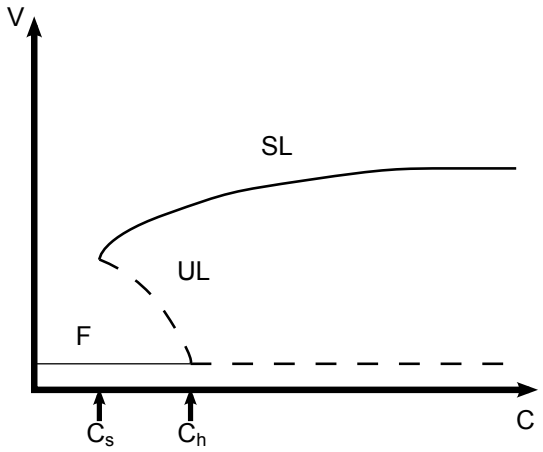

Figure 4.8: A schematic representation of subcritical Hopf bifurcation. The unstable limit cycle (UL) is represented by dashed lines and solid lines represent a stable limit cycle (SL). F denotes the fixed point state. The grey inner region from the basin of attraction for the fixed point and the outer shaded region forms the basin of attraction for SL. UL is a curve on the basin boundary. For a two dimensional system, it is the separatix (Strogatz, 1994).

Balachandran, 2004; Moon, 2004).

The subcritical Hopf bifurcation scenario is explained in Fig. 4.8. A stable fixed point attractor (F) losses its stability and a new branch - an unstable limit cycle (UL) is born at the Hopf point (C_h). Beyond the Hopf point, the only solution is the unstable fixed point and trajectories will be repelled until a distant stable attractor is found (shown as a limit cycle (SL) here for illustration). We see that in the region C_s-C_h is a region of bistability where two stable attractors, F and SL co-exist along with the unstable attractor/repeller UL, which acts as a separator between the *basins of attraction* of the two stable attractors.

The concept of basins of attraction within the bistable region in the case of subcritical bifurcation for a two dimensional system is illustrated in Fig. 4.9. The basin of attraction of an attractor is the set of all the initial conditions in the phase space (Strogatz, 1994) such that the asymptotic state of the system is given by the attractor. The fixed point solution F, unstable limit cycle UL and stable limit cycle SL are graphically represented in the phase space representation as a point, a dashed loop and a solid loop. Any initial condition of the system that lies within the dark shaded regions will spiral away from UL towards F. This set of points denoted by the dark shaded region forms the basin of attraction of F. Initial conditions outside the UL loop will spiral away to-

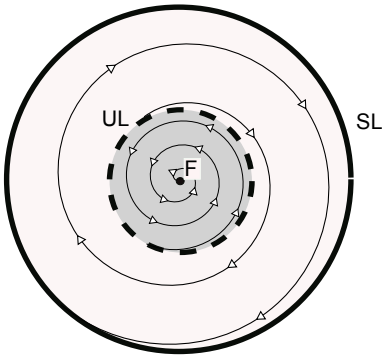

Figure 4.9: Phase space illustration of the subcritical zone for a two dimensional system that exhibits subcritical Hopf bifurcation. The unstable limit cycle (UL) is represented by dashed lines and solid lines represent a stable limit cycle (SL). F denotes the fixed point state. The grey inner region forms the basin of attraction for the fixed point and the outer shaded region forms the basin of attraction for SL. UL then acts as a basin boundary shared by F and SL.

wards SL. Such points in the phase space form the basin of attraction of SL. As such, UL forms the basin boundary between the two attractors. Any initial condition on the basin boundary continues to stay on the boundary. This, however, is an ideal situation and as soon as perturbations or noise is present in the system, the system will always posses either of the two stable states asymptotically. In general, the basin boundary is a multi-dimensional hyper-surface with a complicated shape. The attributes of the basin boundary govern transient system dynamics of thermoacoustic systems as we have observed in experiments (See Appendix A for more discussions on the dynamics involved in bistable region of a thermoacoustic system).

It can be seen that in the bistable region, if the dynamical system is forced away from the stable fixed point towards the stable limit cycle through some mechanism, it is possible to trigger a transition. According to the diagram, one would have to introduce a finite perturbation such that the initial condition falls in the basin of attraction of the stable limit cycle. The explosions and pulses that were introduced in liquid and solid propellant rocket motors mentioned in Chapter 2, provided a mechanism for the mentioned transition and pulse-triggered instability or triggering was observed. Additionally to triggering, a system undergoing a subcritical bifurcation would also display hysteresis behavior. With reference to Fig. 4.8, without externally introduced perturbations, transition to limit cycle oscillations will occur at C_h. However, variation of

the system parameter backwards will cause transition from limit cycle oscillations to a steady state at C_s instead of C_h. Therefore, the entire bistable region or the subcritical zone is also a region of hysteresis. Both triggering instability and hysteresis were subjects of early investigations on thermoacoustic systems and continue to be so due to the lack of a complete understanding of the phenomenon.

4.5 Transition to Chaos

The transition from regular behavior to chaotic states in the variety of nonlinear physical systems occurs via a small number of well-defined bifurcation scenarios. As a result, these few classes of transition scenarios are often referred to by the dramatic term '*routes to chaos*'. The most commonly observed routes to chaos in nonlinear systems, which are of importance also to this investigation are discussed next.

4.5.1 Period-doubling Route to Chaos

The period-doubling scenario consists of a cascade of period-doubling bifurcations. A period-1 attractor undergoes transition to a period-2 which undergoes bifurcation to a period-4 attractor and so on, until chaos. Between different systems that undergo period-doubling bifurcations to chaos, the similarity is not only in the scenario but also in the parameter values at which individual bifurcations take place. It was pointed out by Feigenbaum analytically (Feigenbaum, 1978) and has also been found in experiments (Libchaber *et al.*, 1982) that a constant governs the parameter spacings at which successive period-doubling bifurcations occur. If C_n, C_{n+1} and C_{n+2} are the parameters at which the n^{th}, $(n+1)^{th}$, $(n+2)^{th}$ period-doubling bifurcations respectively, then

$$\lim_{n\to\infty} \frac{C_n - C_{n+1}}{C_{n+1} - C_{n+2}} = 4.669\ldots \tag{4.5}$$

The number $4.669\ldots$ is a constant (also called the Feigenbaum number) regardless of the system undergoing period-doubling bifurcations to chaos.

4.5.2 Quasi-periodic Route to Chaos

In the quasi-periodic scenario, a limit cycle is first generated via a Hopf bifurcation. With the introduction of a second frequency, incommensurate to the oscillation frequency corresponding to the limit cycle, quasi-periodicity appears in the system. This causes phase space trajectories to evolve on a quasi-periodic torus. The quasi-periodic torus exists for a certain range of parameter values and then eventually ruptures leading to chaos. Unlike the period-doubling route, the quasi-periodic route to chaos involves incommensurate frequencies. This route was identified by Ruelle and Takens (1971) in hydrodynamics systems and hence is also referred to as the Ruelle-Takens scenario.

It is important in the context of results presented in this thesis, to mention about the phenomenon of *frequency-locking*. The bifurcation parameter is often associated with the natural frequencies of the system. Changing the bifurcation parameter might lead to a change in the frequency excited in the system. If one of the frequencies leading to quasi-periodicity varies, the ratio between the two frequency might at some parameters become rationally related. Strong interaction between the two rationally related frequencies could resist further changes in system dynamics in response to variations in the bifurcation parameter. This would lead to frequency-locking in the system which exists for a range of parameters before switching to quasi-periodicity or chaos.

4.5.3 Intermittency Route to Chaos

This third route is associated with an apparently irregular switching of a system between chaotic and regular behavior. This phenomenon is known as *intermittency*. The intermittency route to chaos was described by Pomeau and Manneville (1980). On the basis of theoretical analysis, they categorized intermittency into three types: type-I, type-II and type-III. Each type is associated with a particular bifurcation prior to the intermittent state. Type-I intermittency is associated with a saddle-node bifurcation. Type-II occurs due to a Hopf bifurcation and is associated with the appearance of a quasi-periodic state. Finally, type-III intermittency is associated with a reverse-period doubling bifurcation (Okamoto *et al.*, 1998). Intermittency was first studied in the Rayleigh-Bénard convection experiments and has been identified as a route to turbulence in hydrody-

namic flows (Gollub and Benson, 1980; Swinney, 1983; Bérge *et al.*, 1980). In most observations of intermittency, the intermittent state is followed by a chaotic regime. The evolution of the intermittent state with changes in the bifurcation parameter corresponds to statistical features specific to the type of intermittency present (Pomeau *et al.*, 1981; Pomeau and Manneville, 1980).

All the above stated routes to chaos have been predicted in theoretical models and subsequently observed in experiments. The chaotic state is a dynamical behavior of the system and not an irregularity due to errors and noise. Based on the theory of chaotic dynamics, it is possible to quantitatively analyze the characteristics of the chaotic attractor. The divergence between neighboring trajectories due to chaos, associated with the loss of determinism and predictability and the dimension occupied by the fractal structure of the chaotic attractor in dissipative systems can be used to quantify chaotic behavior and have been discussed next.

4.6 Measures of a Chaotic Attractor

The fundamental feature of the trajectories of a chaotic attractor is that neighboring trajectories diverge in time as they evolve. The attractor and its trajectories are always bounded. Hence, due to the divergence, after a certain time interval two trajectories starting from nearby points might lie in different parts of the attractor. To quantify these diverging trajectories in an attractor, the concept of Lyapunov exponent was established. A second feature of chaos in dissipative systems is that the phase space attractor is a fractal object occupying a non-integer dimension in the phase space. The correlation dimension is the most commonly employed technique to calculate the dimension of the phase space attractor formed by a chaotic oscillations. Complexity of chaotic attractors also lies in the fractal nature of the phase space attractors.

4.6.1 Lyapunov Exponent

Figure 4.10 illustrates the concept of diverging trajectories of a chaotic attractor within a bounded region in a two dimensional phase space. Due to system dynamics, it is seen

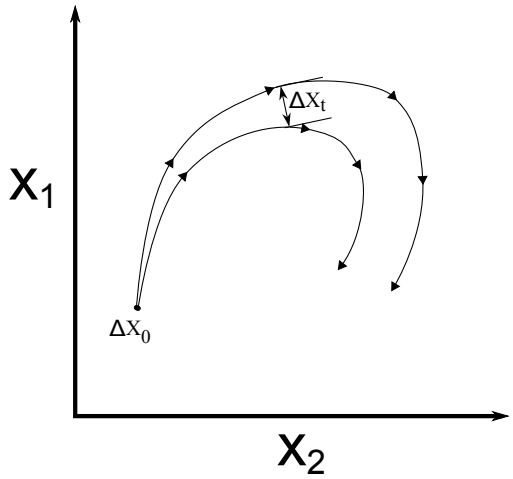

Figure 4.10: Divergence of neighboring trajectories of a chaotic system. The initial separation between the trajectories, $\Delta\ \mathbf{X}_0$, increases as the trajectories evolve. The Lyapunov exponent characterizing the chaotic system is based on this divergence (further discussion presented in text).

that the initial distance between closely spaced trajectories grows with time. Considering an exponential divergence of trajectories, the local Lyapunov exponent is the rate of exponential divergence of the trajectories. An attractor will have a *spectrum* of Lyapunov exponents, each corresponding to a single phase space coordinate. An average of the local Lyapunov exponents over the trajectory represents the divergence characteristics of the attractor. A positive average Lyapunov exponent confirms the presence of chaotic dynamics. Accordingly, for the identification of chaos in a system, it is sufficient to calculate the average maximal Lyapunov exponent which is defined as (Kantz, 1994),

$$\lambda_m = \lim_{t\to\infty}\lim_{d\to 0}\frac{1}{t}ln\left(\frac{|\Delta\mathbf{X}_t|}{d}\right) \tag{4.6}$$

where $d = |\Delta\mathbf{X}_0|$, the initial distance between the neighboring trajectories.

A positive maximal Lyapunov exponent indicates that on an average, there is divergence between neighboring in the phase space attractor and therefore, the system is chaotic.

4.6.2 Correlation Dimension

In the discussion on chaotic attractors, the interesting property of the attractor being a fractal was mentioned. To establish the inherent dimension of a phase space attractor,

the organization of phase space trajectories making up the attractor needs to be quantified by an appropriate measure. The correlation dimension is one such measure. Taking the analogy of a time-varying function, where correlation indicates how the dependence between values of the function occurring with a time difference varies with the time difference, correlation for points on the phase space attractor can be defined. In the phase space, correlation between two points varies with the spatial separation between them. In strange attractors (fractal attractors associated with chaos), this correlation decays with separation. The magnitude of decay is related to the inherent fractal dimension.

To calculate the correlation dimension, the correlation sum C(r), given by Eqn. (4.7), is calculated for the attractor.

$$\mathrm{C(r)} = \lim_{\mathrm{r}\to 0} \frac{1}{N^2} \Bigg(\text{number of pairs of points with } Euc.dist. < \mathrm{r} \Bigg), \tag{4.7}$$

where, N is the number of points in the phase space and $Euc.dist.$ is the Euclidean distance between two points on the attractor. The correlation sum has a power law dependence on r as $\mathrm{r} \to 0$ and the power on r gives the correlation dimension of the attractor (Moon, 2004). A non-integer correlation dimension is a direct indication that the attractor is a fractal.

4.7 Nonlinear Time Series Analysis

It is clear from the introduction chapter of the thesis that thermoacoustic instability is a phenomenon appears in the thermoacoustic system in the form of high amplitude pressure oscillation. The limit cycle nature and the chaotic nature of the system is also well known. Therefore, it is clear that like other physical system in nature, thermoacoustic system should also follow a definite path towards aperiodic or periodic behavior. This can be obtained even by solving the governing equations of the system. The presence of limitation in modeling and measurements in experiments makes difficult to explain the natural phenomena. In reality it is possible only to measure a few system state variables such as pressure, temperature, velocity. However, the hostile nature of the thermoacoustic system makes it even difficult for measuring these variables. The embedding

theory given by Takens (1981) becomes very useful for such complicated systems, as from measurements of a single quantity it is possible to extract the information about the system dynamics without any ambiguity.

As linear stability theory can only give the decay, growth in oscillations and the corresponding frequency, in order to understand dynamical behavior of a system from system variables, nonlinear time series analysis is essential. Explaining the dynamical nature of self-excited thermoacoustic oscillations through experimentally acquired data is the basis of the thesis.

The most important step in the time series analysis techniques used here is the representation of the asymptotic state of nonlinear oscillations in an appropriate phase space and investigation of the structure of the resulting attractor of system dynamics. This attractor is a mapping of the actual process in a finite dimensional space created from scalar observations. Topological measures of the so formed attractor, such as the correlation dimension and the Lyapunov exponents of the attractor can then be calculated. These quantities are direct measures of the complexity in the system. Several nonlinear systems have been successfully investigated in the light of these techniques and from this study, it can be seen that the nonlinear nature of thermoacoustic oscillations can also be studied through the application of these methods. The fundamental idea behind the time series analysis techniques employed in this work is given below.

4.7.1 Reconstructed Phase Space

The asymptotic dynamics of any physical system as discussed can be viewed in terms of its evolution in a space formed by a set of independent variables that unambiguously define the system. The phase space attractor so formed is an invariant, which means that the asymptotic state of the system always corresponds to the particular attractor. Additionally, once the system reaches the attractor, it continues to evolve on the attractor. This would mean that identifying the topology of the phase space attractor is identifying the system dynamics. Scalar measurements of the system obtained in an experiment can be viewed at best as a mapping from the system state variables.

Clearly, the aim is to obtain system dynamics from the available scalar measure-

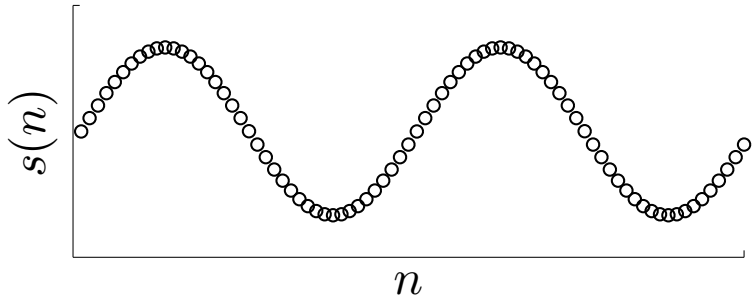

Figure 4.11: A Sinusoidal time series generated in order to show the significance of optimum time delay; the significance is shown in Figs. 4.12.

ments. The embedding theorem was first proposed by Takens (1981) for *reconstruction* of a phase space from scalar measurements within which a representative attractor of system dynamics can be obtained. He proved that it is possible to reconstruct phase space information from time series of a single measurement using time-delayed vectors. The resulting phase space attractor would preserve topological information that quantifies system dynamics and system complexity. The 'method of delays' is the most practical and widely applied method of reconstructing the attractor of system dynamics from experimental measurements as opposed to other techniques such as the method of obtaining derivatives from time series data suggested by Packard *et al.* (1980).

4.7.2 Optimum Time Delay

Time delay embedding involves obtaining n time-delayed vectors (with a time-delay between vectors corresponding to τ) from a single time series data. For a proper reconstruction, one is left with the task of obtaining an optimum time-delay τ and an optimum embedding dimension. Several methods exist for obtaining optimum values for each of the quantities. The general prescription for an optimum time-delay comes from the fact that the vectors representing the system dynamics should be independent. Subsequently, the optimum embedding dimension is the lowest dimension at which trajectory crossings occur due to the system dynamics and not due to their projection onto a lower than required dimension. This is of course to ensure that while evaluating the reconstructed phase space structure, the topological characteristics obtained should be due to system dynamics and not because the dimension chosen for reconstruction is too small to unambiguously represent the phase space structure. A detailed discussion on

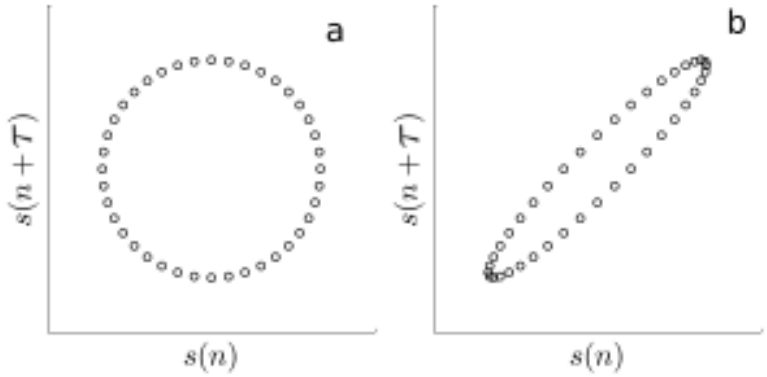

Figure 4.12: Importance of choosing an optimum time delay for reconstruction. In this figure, a sinusoidal time series is used for reconstruction. The correct phase space trajectory is a circle which can be seen as in the reconstructed phase space (a). The time delay chosen corresponds to one-fourth of the time period. When a non-optimal time delay is chosen, the phase space trajectories are distorted (b). As a result, the geometrical characteristics of the phase space trajectories does not represent dynamics of the system correctly.

the various algorithms for choosing the optimum time delay and embedding dimension can be found in Kantz and Schreiber (2003) and Abarbanel (1996).

Accordingly, the time-delayed coordinates from a time series data (Abarbanel *et al.*, 1993), $s(n) = s(t_0 + n\tau_s)$, where τ_s is the sampling time interval would be

$$y(n) = [s(n), s(n+\tau), s(n+2\tau), s(n+3\tau), \ldots]$$

Consider a sinusoidal signal as shown in Fig. 4.11. For a pure sine wave, at a time-lag corresponding to $1/4th$ of the time period i.e. a phase shift of $\pi/2$, correlation goes to 0 (a cosine, which is equivalent to a sine being shifted by a phase of $\pi/2$, and a sine are an orthogonal pair of functions). By choosing a time delay τ for reconstruction of the phase space equal to a quarter of the signal time period, we get the familiar limit cycle loop in Fig. 4.12 a. However, choosing a time delay differently leads to a distorted limit cycle as seen in Fig. 4.12 b. By choosing vectors for phase space reconstruction which are by some measure (here correlation), the least correlated, the optimum phase space representation is reconstructed. The concept of signal correlation works in the case of a single frequency limit cycle, but being essentially a linear approach, it is not effective for more complex oscillations such as quasi-periodic and chaotic oscillations.

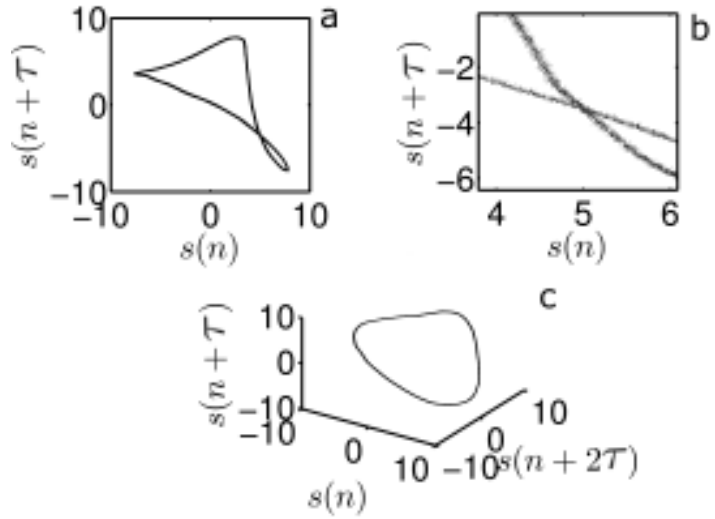

Figure 4.13: This figure shows a closed orbit in reconstructed phase spaces of different dimensions. In the two dimensional reconstruction (a), trajectories appear to intersect each other. All the points at this intersection would be falsely considered neighbors in the phase space (as seen in the zoomed-in view, b). This false intersection is resolved in a three dimensional reconstruction (c) where a distinct limit cycle loop is observed. It is important not to choose a lower than optimal embedding dimension for reconstruction.

4.7.3 Optimum Embedding Dimension

Once the delayed vectors are obtained, it is essential to calculate the embedding dimension that produces a proper reconstruction. Phase space reconstruction is essentially a mapping of the original multivariate phase space, of dimensionality d_A to a subspace created from the time-delayed vector obtained from experiments, in a manner such that the invariants of the system remain constant. The dimension of the subspace, referred to as the embedding dimension, d_E, is one of the two important entities to be derived for a proper mapping or embedding. A dimension equal to or larger than the embedding dimension can be used for phase space reconstruction but choosing a dimension lower than the embedding dimension will lead to false embedding. Appropriate embedding dimension can be calculated from the measured times series using one of the several techniques available. A review of commonly used techniques such as singular-value decomposition of the sample covariance matrix, saturation with dimension of some system invariant, the method of false nearest neighbors and the method of true vector fields is given by Abarbanel *et al.* (1993).

In Fig. 4.13, the situation of a false embedding caused due to lower than optimum

embedding dimension is shown. The phase space trajectory when seen on a two dimensional space (Fig. 4.13 a) contains false crossings (Fig. 4.13 b, zoomed view). Only by choosing a higher dimension (Fig.4.13 c), this false embedding is remedied. As will be seen later, the false nearest neighbor algorithm is based on detecting the percentage of false crossings for an embedding dimension. Unless this percentage goes to zero, the dimension is not appropriate for reconstruction and a higher dimension will be required.

Once the phase space trajectories are reconstructed in an appropriate phase space, quantitative information about the phase space attractors, namely the maximal Lyapunov exponent and the correlation dimension can be obtained. Also, other phase space analysis techniques such as recurrence plots that have been implemented in the analysis here require a correct phase space reconstruction. The implementation of algorithms for the calculation of the Lyapunov exponent and correlation dimension as well as other techniques have been discussed together with results in subsequent chapters.

CHAPTER 5

FLAME ACOUSTIC INTERACTION LEADING TO INTERMITTENCY AND LEAN FLAME BLOWOUT

5.1 Introduction

In the present study, we investigate the bifurcation behavior of a confined, burner stabilized, single conical premixed flame system. Such a configuration is the most basic combustion-driven thermoacoustic system. In this simple configuration, we will attempt to study the fundamental dynamics associated with thermoacoustic instability. As we will see later in the results of the bifurcation analysis, a transition occurs from steady to oscillatory dynamics through a Hopf bifurcation. This bifurcation is then followed by further bifurcations resulting in complex dynamical states. Eventually, thermoacoustic oscillations lead to flame blowout. The oscillation dynamics prior to flame blowout resemble the phenomenon of intermittency which we will discuss in detail in the following section. The present study provides a more detailed investigation of the occurrence of intermittency in thermoacoustic oscillations.

5.2 Bifurcation Analysis

The experimental bifurcation analysis of the system under study suggests that the nonlinear interaction between the laminar conical flame and the acoustic field of the duct results in different oscillation states. As seen in the bifurcation plot in Fig. 5.1, a clear transition exists between oscillations with different characteristics. This bifurcation plot, has been obtained using flame location as the control parameter, maintaining a constant equivalence ratio ($\phi = 0.51$). Starting with a steady state (absence of oscillations), the flame location was gradually varied in steps of $5\ mm$ and the acoustic pressure data

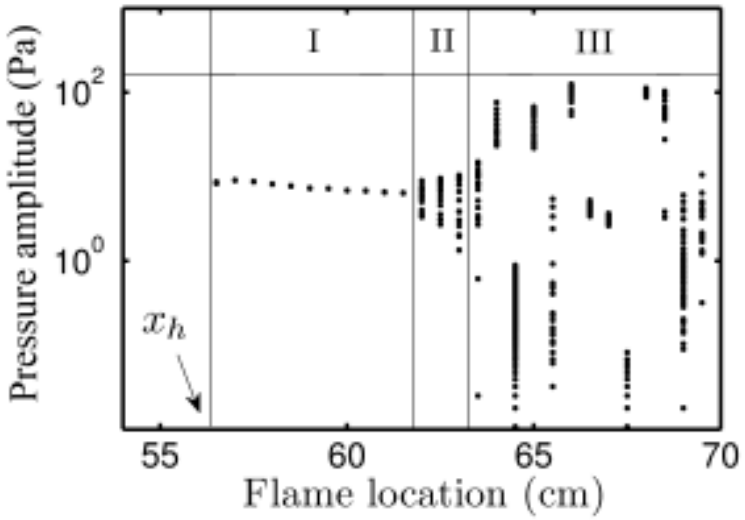

Figure 5.1: Experimental bifurcation plot for equivalence ratio, $\phi = 0.51$. The plot is divided into regions according to the nonlinear characteristics of the self-excited oscillations. Transition to instability occurs via a subcritical Hopf bifurcation at the flame location, $x_f = 56.5\ cm$, marked as x_h. Region I, II and III correspond to limit cycle oscillations, quasi-periodic oscillations and intermittent behavior respectively.

was acquired corresponding to each location. The oscillation state for each flame location is then represented by plotting the amplitude of all the local maxima in the pressure time series present in a time interval of $0.5\ s$. In the plot, the ordinate corresponds to the values of the amplitude of local maxima in the acquired acoustic pressure time series, corresponding to each flame location that was investigated, given by the abscissa. It is clear that all the local maxima amplitudes in limit cycle oscillations, characterized by periodic oscillations of a single dominant frequency, will coincide, resulting in a single point on the bifurcation plot. Oscillations characteristically different from limit cycle oscillation will result in a set of points (corresponding to the flame location at which the oscillations occur) whose distribution will depend on the variations in the local maxima amplitude values. In the light of this discussion, it is observed from the bifurcation plot, Fig. 5.1, that at $x_f = x_h$, a bifurcation occurs in the system and results in the occurrence of thermoacoustic instability in the form of limit cycle oscillation. This bifurcation is a subcritical Hopf bifurcation whose subcritical nature is evident from the sudden jump ($x_f = 56.5\ cm$) in the pressure amplitude, clearly seen in the bifurcation plot. Interestingly, at $x_f = 62\ cm$, a second bifurcation is observed to occur which is clearly indicated by the appearance of a spread in the amplitudes of the local maxima.

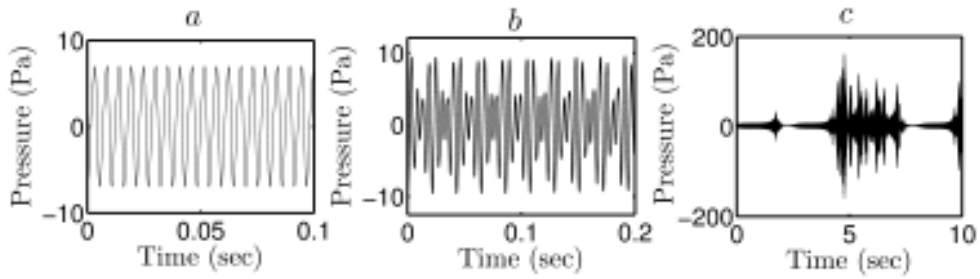

Figure 5.2: Time series data of pressure fluctuations for limit cycle oscillation (*a*) at $x_f = 56.5\ cm$, quasi-periodic at $x_f = 62\ cm$ (*b*) and intermittent oscillations (*c*) at $x_f = 63.5\ cm$. In the case of intermittent oscillation, the pressure time series is shown for $10\ sec$ to show the two types of burst and the fixed point in between.

This spread increases gradually as the flame location is varied further and is followed by a sudden change at $x_f = 63.5\ cm$, indicating the presence of another bifurcation of the system. The points on the bifurcation plot after this bifurcation are highly irregular. No further bifurcation is observed to appear in the system and eventually at $x_f = 69.5\ cm$, flame blowout occurs due to violent oscillations in acoustic pressure as well as the flame, as we shall see later. From the observed behavior, the entire bifurcation plot can be divided into three parts, marked as region I, II and III in Fig. 5.1.

The acquired pressure time series at $x_f = 56.5\ cm$ (region I), $62\ cm$ (region II) and $63.5\ cm$ (region III) are shown in Fig. 5.2. Limit cycle oscillation (with noticeable effects of the presence of superharmonics) in region I are seen in Fig. 5.2 a. Oscillations in Fig. 5.2 b & c posses dynamics that are quite different and need further treatment. These oscillations are a direct consequence of the respective bifurcations and identification of the characteristics of the oscillations will directly indicate the nature of the bifurcations. Towards this purpose, we will utilize the techniques for reconstruction of the system dynamics in the phase space (representative attractor of system dynamics) from the time series data of the pressure fluctuations.

5.2.1 Implementation of Nonlinear Time Series Analysis

For the investigations presented here, we have obtained optimum time-delays for phase space reconstruction based on the calculation of average mutual information (Fraser

and Swinney, 1986). The average mutual information between the original vector and a time-delayed vector indicates the extent of information, I, shared between the two. Clearly, for reconstruction, the optimum time-delay will correspond to a small value of the corresponding average mutual information. As pointed out by Fraser and Swinney (1986), the time-delay at which the average mutual information attains its first local minima will result in a good reconstruction.

Considering a scalar time series data acquired at a sampling time interval τ_s, $p(n) = p(t_0 + n\tau_s)$, the average mutual information at a time-delay τ is given as

$$AMI(\tau) = \sum_{i,j} P(p_i(n), p_j(n+\tau)) \log_2 \frac{P(p_i(n), p_j(n+\tau))}{P(p_i(n))\ P(p_j(n+\tau))} .$$

The probability that the time series, $p(n)$, assumes a value $p_i(n)$ is given by $P(p_i(n))$. The joint probability of the event that the original time series, $p(n)$, and the delayed time series, $p(n+\tau)$, simultaneously assume a value $p_i(n)$ and $p_j(n+\tau))$ respectively, is denoted by $P(p_i(n), p_j(n+\tau))$.

The reconstruction matrix constructed using the optimum time-delay, τ can be represented as

$$\mathbf{y} \ = \ [p(n), p(n+\tau), p(n+2\tau), p(n+3\tau), \dots] .$$

Average mutual information calculated for pressure oscillations during thermoacoustic instability acquired in our experiments is plotted in Fig. 5.3 a, corresponding to the three cases given in Fig. 5.2. The first minima of the plot of average mutual information is the time delay recommended for phase space reconstruction. We have reconstructed a three-dimensional projection (Fig. 5.4 a to c) of the actual multi-dimensional attractor that governs the system dynamics during the occurrence of instability.

5.2.2 Reconstructed Phase Space

After obtaining the delayed vectors, we can represent system dynamics in a reconstructed phase space with an appropriate dimension. In order to avoid false crossings of the trajectories in the phase space due to a lower than required reconstruction dimen-

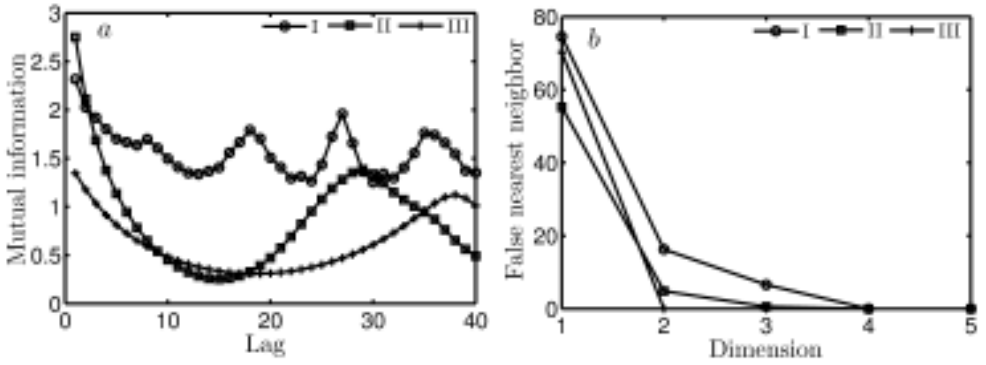

Figure 5.3: Average mutual information (a) and percentage of false nearest neighbor (b) calculations for the determination of optimum time delay and embedding dimension respectively. The first minimum in the plot of average mutual information gives the time-lag to be used for optimum time delay. At an optimum embedding dimension, the percentage of false nearest neighbors vanishes. Curves have been plotted corresponding to the time series data presented in Fig. 5.2.

sion, it is important to calculate the optimum embedding dimension. For the analysis presented here, we have used the false nearest neighbor method proposed by Kennel *et al.* (1992). According to the false nearest neighbor algorithm, for every dimension, the false crossings of the reconstructed trajectories is calculated in terms of the percentage of points that falsely appear in the vicinity of other points. Percentage of false neighbors is calculated for increasing the reconstruction dimension and the dimension for which this percentage goes very close to zero is an optimum embedding dimension. Figure 5.3 b presents the plot between the percentage of false neighbors as a function of the dimension for pressure time series acquired in our investigation. This plot shows that the dynamics of oscillations in all the three regions is restricted to a four dimensional phase space. The dominant features of the attractor can also be visualized in a three dimensional projection with minimum loss of information about the system dynamics. For recurrence analysis, we have used a four dimensional phase space.

The frequency spectrum of each of the three oscillation states are shown in Fig. 5.4 ($d-f$). Figure 5.4 a is the reconstructed phase portrait for limit cycle oscillations. Limit cycle oscillations exists for flame locations ranging from $56.5\ cm$ to $61.5\ cm$ (Fig. 5.1). The single closed loop and the presence of a single dominating frequency with its higher harmonics confirms periodic behavior. The limit cycle oscillations undergo a bifurcation leading to oscillations whose phase space attractor resembles a torus. Such

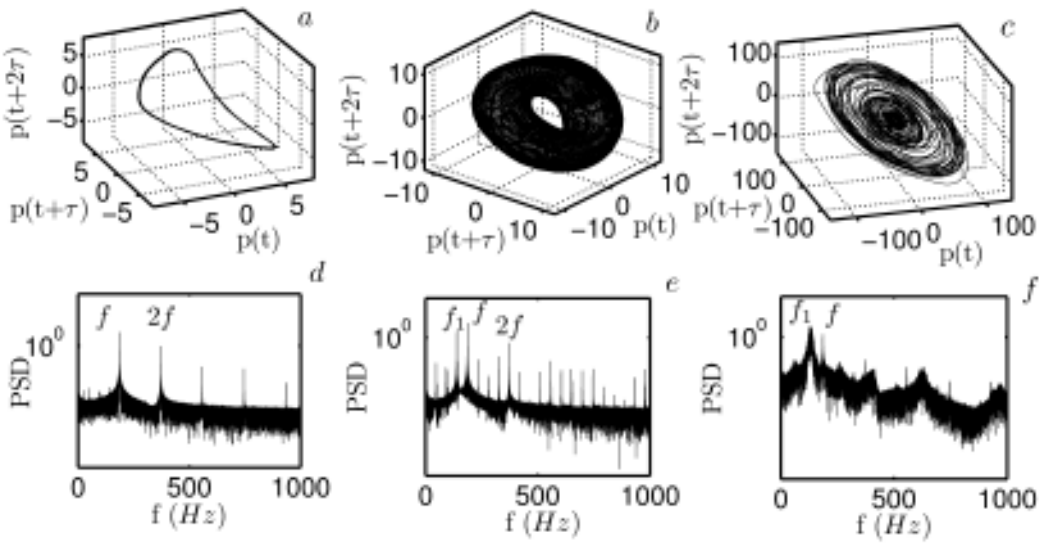

Figure 5.4: Reconstructed phase space attractors (a, b, c) from time series data of pressure fluctuations (see Fig. 5.1) and corresponding frequency spectrum (d, e, f) for limit cycle, quasi-periodic and intermittent oscillations observed in the system in region I, II and III respectively. The frequencies are $f = 186\ Hz$, f_1=139 Hz.

a structure indicates the presence of quasi-periodic behavior, where unlike limit cycle oscillation, the trajectory forming the phase space attractor does not come back to the same point after every oscillation. The trajectory evolves on a toroidal structure instead, never coming back to the initial point. This is also reflected in the frequency spectrum which shows the presence of *incommensurate* frequency components ($f = 186\ Hz$ and $f_1 = 139\ Hz$). Essentially due to the presence of incommensurate frequencies ($f - f_1 = 47\ Hz$, $2f_1 - f = 92\ Hz$), the oscillations are technically aperiodic. The unique feature of quasi-periodic oscillation is the presence of linear combination of dominating frequency (f_1) in the system which helps to form the dense toroidal structure in the phase space. Emergence of a quasi-periodic state from limit cycle oscillations is a result of a secondary Hopf bifurcation, also referred to as the Neimark-Sacker bifurcation (Nayfeh and Balachandran, 2004). This particular bifurcation is quite common in nonlinear systems (Nayfeh and Balachandran, 2004).

The next interesting behavior appears in the system as it crosses x_f = 61.5 cm. In the time series plot, Fig. 5.2, we find that the oscillation is characterized by sudden, irregular and *intermittent* bursts. In the frequency spectrum, Fig. 5.4 f, we see a broadband frequency content as opposed to clear dominant peaks. The reconstructed phase space,

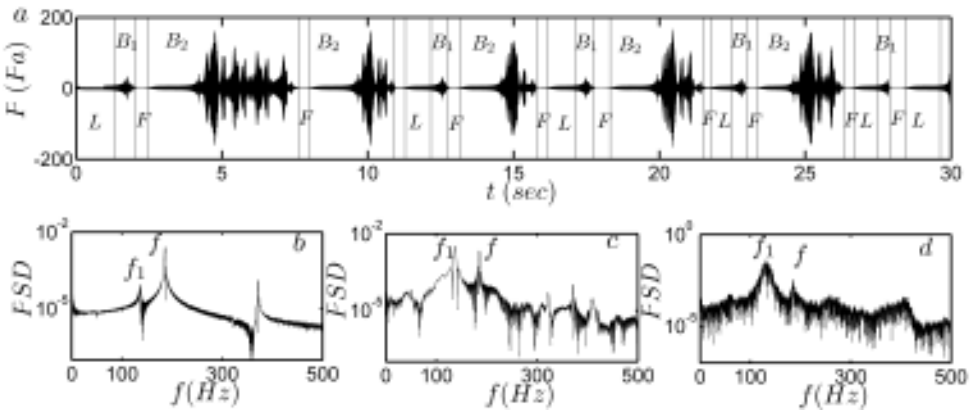

Figure 5.5: (a) Pressure time trace acquired at flame location $x_f = 63.5\ cm$ (Fig. 5.1, region IV). Two types of bursts are present, B_1 and B_2. b, c and d - Frequency spectrum of the laminar state L, B_1 and B_2 respectively.

Fig. 5.4 c, has two dense, concentric disks - an outer and an inner disk. Most of the dynamics occurs in these two disks. During the bursts, the trajectories are pushed to the outer disk and then are re-injected back to the inner region. This oscillation is similar to the intermittent oscillations observed in many other nonlinear systems as a result of the phenomenon referred to as *intermittency*. This particular dynamics occurs as a result of the breakdown of the quasi-periodic attractor, suggesting that the intermittency observed in our system is a type-II intermittency.

Bifurcation of quasi-periodic oscillations leads to burst oscillations in region IV of the bifurcation plot. In the pressure time series, irregular bursts are observed where the amplitude attains about 10 times the amplitude observed in limit cycle and quasi-periodic states. Pressure time trace, frequency spectrum and phase space representation for this state are shown in Fig. 5.2 and Fig. 5.1 respectively. Pressure time series corresponding to $30\ s$ of burst oscillations is given in Fig. 5.5 a.

Intermittency in dynamical systems is the repeated transition between quiescent or regular and burst or irregular states of the system. Such phenomenon has been captured in a number of experiments on fluid systems (Bérge *et al.*, 1980), solar activity (Platt *et al.*, 1993) and chemical kinetics (Pomeau *et al.*, 1981). Several models explaining intermittency have also been constructed. However, the occurrence of intermittency in different systems are characteristically different. Hence, categories of intermittency (Type I, II and III, crisis-induced and on-off intermittency being the major categories) have been proposed by theoreticians, primarily based on statistical characteristics of

the apparently random transitions and associated bifurcations. Intermittency also is one of the routes from periodic to chaotic oscillations. In the following, we discuss the dynamics of thermoacoustic oscillations observed in the system under investigation, with emphasis on comparison with intermittency.

As marked in Fig. 5.5 a, two types of bursts were observed - B_1 & B_2, along with sections of laminar (L) state. Laminar state refers to regular periodic sections in between burst oscillations. Power spectrum corresponding to the three states are given in Figs. 5.5 b, c & d. Frequency spectra for the smaller burst B_1 (Fig. 5.5 c) and the laminar state (Fig. 5.5 b) consist of dominant peaks at identical frequencies. However, in the frequency spectrum for B_1, we find additional peaks due to its deviation from the laminar state. During the smaller burst, B_1, the system attempts to escape the laminar state but is unable to escape and the burst eventually ends with a steady state. For B_2, the power spectrum shows a broadband frequency centered at f_1. In this state, the system leaves the laminar state (periodic orbit) and temporarily settles to another non-periodic (B_1 & B_2) dynamical state. After spending some time in the non-periodic state, oscillations decay to a steady state. A sudden decay in oscillations marks the end of a burst. A laminar state follows where there is a growth of oscillations of a single dominant frequency. Beyond a certain oscillation amplitude, the system leaves the laminar state leading to either B_1 or B_2 (Fig. 5.5 a).

5.3 Characterization of Intermittent Oscillations

5.3.1 Return Map

We use a mapping technique for dynamical systems, the *return map* (Nayfeh and Balachandran, 2004; Strogatz, 1994) to further analyze the different dynamical states observed in the thermoacoustic system under investigation. This technique can be used to investigate the evolution of extreme events such as local maxima and minima or evolution of the periodicity, drift with time and so on. For instance, in the first return map, all the maxima, p_n are collected and each maxima is plotted against the next maxima that occurs and a two-dimensional plot, p_n vs. p_{n+1} is obtained. This would be equiv-

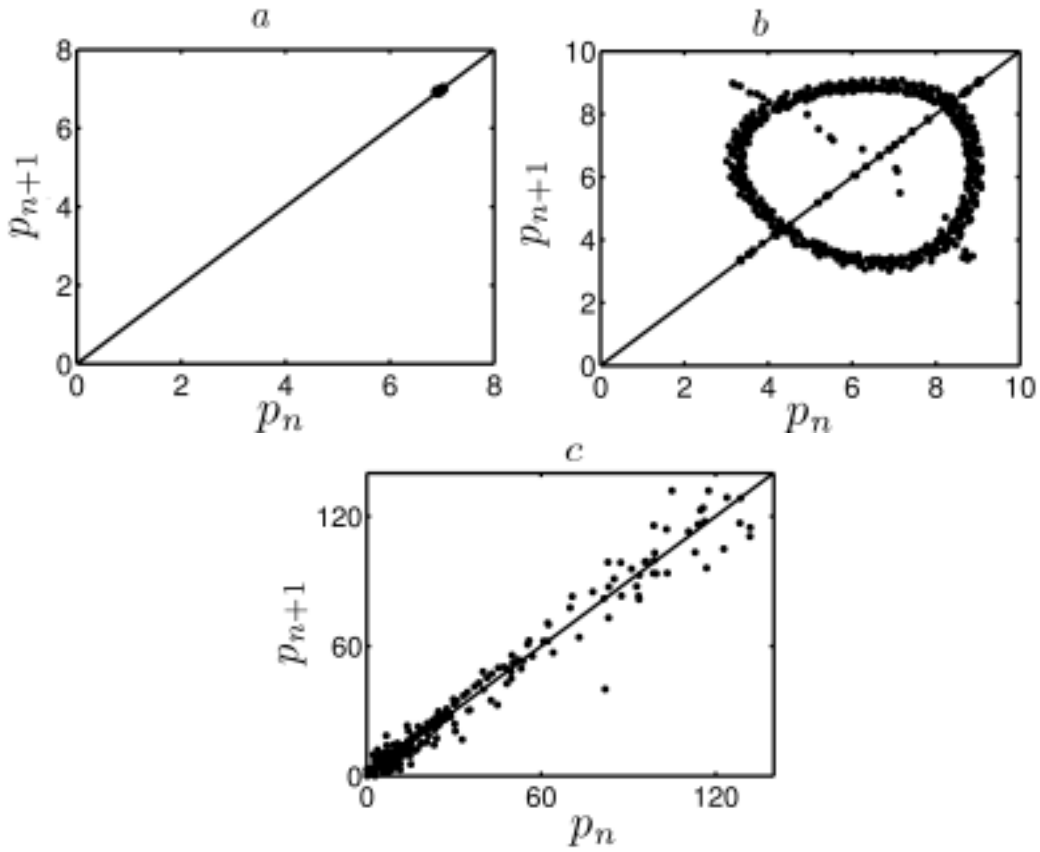

Figure 5.6: Comparison of first return map for (a) limit cycle oscillation ($x_f = 56.5\ cm$), (b) Quasi-periodic oscillation ($x_f = 62\ cm$) and (c) intermittent burst oscillation ($x_f = 63.5\ cm$).

alent to simply plotting successive values of a system variable, at points where the first derivative goes to zero, against each other. If successive maxima/minima are equal, mapping lies on the $x = y$ main diagonal; else it moves away from the main diagonal. Hence, through this approach, significant information about a dynamical system can be obtained even in two dimensions. It is an important technique that can be utilized to study the underlying dynamics of the system. Return maps also makes it possible to directly compare continuous systems with standard discrete maps such as the logistic map, circle map and tent map for instance.

In Fig. 5.6, we have plotted the first return map for limit cycle (a), quasi-periodic (b) and intermittent (c) oscillations. We used values of local maxima extracted from the acoustic pressure time series for creating the plots. For limit cycle oscillations, the return map is a single point on the main diagonal. This is because as discussed for the bifurcation plot, all the local maxima are of the same amplitude. For quasi-periodic

oscillations, the return map gives a circular loop around the main diagonal. Bifurcation of the quasi-periodic state results in breaking down of the quasi-periodic return map pattern. The burst oscillations that emerge, when projected on a first return map gives scattered points. On careful inspection, we find that along the $x = y$ diagonal, the points follow a trend of gradually drifting away from it. This resembles the return map of the simple logistic map which displays similar distribution of points on the return map during its intermittent state. Several other systems such as intermittent states in hydrodynamic systems (Batiste *et al.*, 2001) where one finds turbulent bursts distributed among laminar states also show such resemblance. Looking at this resemblance, we can say that the nonlinear phenomenon of intermittency and the burst oscillations observed in our system may be related. If so, intermittency (Pomeau and Manneville, 1980), which has been investigated in rigorous detail by specialists in the field of nonlinear dynamics, could to certain extent describe features of thermoacoustic instability and its behavior just before flame blowout phenomena. Additionally, the fact that a subcritical Hopf bifurcation gives rise to oscillations indicates that the type of intermittency involved with burst oscillations could be type-II intermittency.

We analyse the dynamics of the observed thermoacoustic oscillations in a reconstructed phase space derived from the time series measurements of acoustic pressure. In particular, we investigate the intermittent behavior occurring prior to flame blowout as a result of nonlinear bifurcations in the system by studying the recurrence behavior of the system dynamics (Klimaszewska and Zebrowski, 2009). A more elaborate discussion is presented below.

5.3.2 Recurrence Plots

Recurrence plots (RPs) were introduced by Eckmann *et al.* (1987) as a tool for studying the recurrences of phase space trajectories. An RP is created from a recurrence matrix which contains information about whether or not pairs of points in the phase space occur close to each other (indicating the recurrence of phase space trajectories). Starting from the phase space attractor (the reconstructed attractor using time-delay embedding for experimentally acquired data), every region in the phase space occupied by the phase

space attractor is checked for recurrences by the phase space trajectory. The binary recurrence matrix $\mathbf{R}_{ij}|_{N\times N}$ is then defined for a phase space attractor with N points as:

$$\mathbf{R}_{ij} = \Theta(\epsilon - ||\vec{x}_i - \vec{x}_j||), \quad i, j = 1, \ldots, N$$

where Θ is the Heaviside function, ϵ is a predefined threshold, $||.||$ is the norm between two points that is evaluated for recurrence, $\vec{x}_i$ is a point on the attractor in the phase space. The threshold for recurrence, ϵ determines the upper limit of the separation between pairs of points in the phase space that can qualify as a recurrence pair. It is important to choose a suitable ϵ for the recurrence plots. If the threshold is high, too many recurrence pairs in the recurrence plot will mask the fine features of the recurrence plot. If chosen too low, recurrences due to system dynamics will be underestimated. There are several approaches to choosing an optimum threshold (see Marwan *et al.*, 2007). One method for choosing ϵ is to fix the recurrence density such that for each point considered, the number of points qualifying recurrence is fixed (Marwan, 2003). This method however is computationally more expensive than using a fixed the recurrence threshold. Our implementation uses a fixed ϵ for all points, with a value equal to 10% of the attractor diameter (Marwan, 2003). For evaluating recurrence, commonly the L_2 norm is used. However, the L_1 and L_∞ norm can also be used (a more detailed discussion is presented in Marwan, 2003). For results presented here, the L_2 norm was applied for recurrence analysis.

The recurrence plot then consists of black and white points, black denoting that two points are sufficiently close-by in the phase space indicating a recurrence of the phase space trajectory. Points on the main diagonal are always black (due to the trivial fact that every point is definitely close to itself). Several salient features of the dynamical system can be studied on a recurrence plot. For periodic oscillation such as limit cycle, the 45° lines parallel to the main diagonal line are always equally spaced, indicating the single time period with which the system is oscillating. The recurrence plot of a periodic signal is dominated by long dark lines parallel to the main diagonal. Random uncorrelated noise will result in a uniform but random distribution of black and white points. The salient features of RP has been discussed very clearly by Marwan (2003) for periodic, aperiodic and noisy system. The features of an RP can be changed depend-

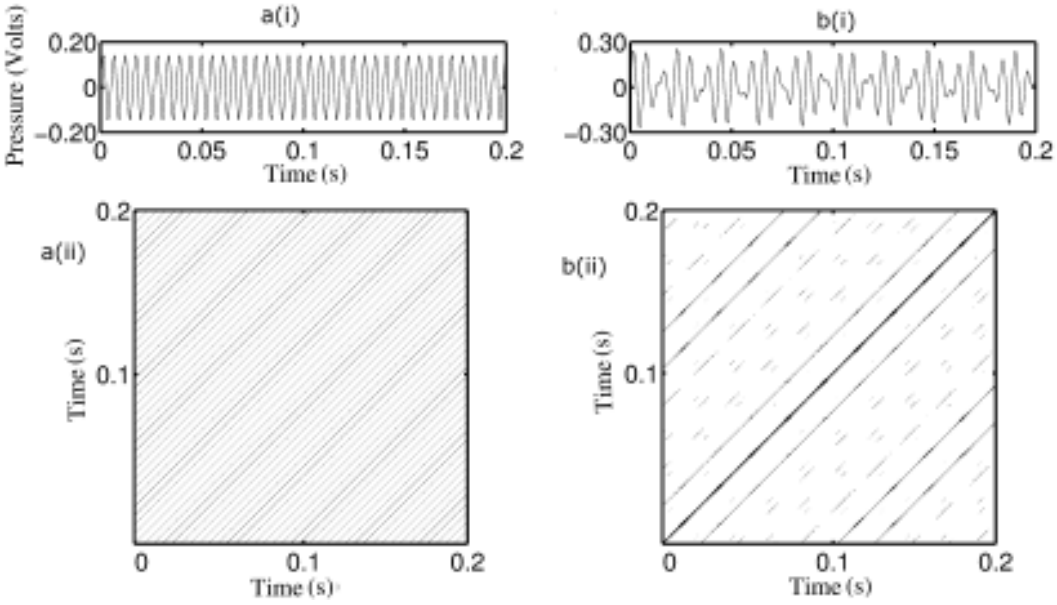

Figure 5.7: Recurrence plots for limit cycle oscillations (a(ii)) and quasi-periodic oscillations (b(ii)). Equally spaced diagonal lines indicate the presence of a single dominant frequency in the limit cycle oscillations. For quasi-periodic oscillations it is seen that diagonal line segments are separated by unequal vertical spacings; a manifestation of irrationally related frequencies comprising the quasi-periodic state. A four dimensional space was used to construct the recurrence plot, with a specified recurrence threshold (ϵ) of $0.03V$ and $0.07V$ for limit cycle and quasi-periodic oscillations respectively.

ing on the system dynamics. To quantify the dynamical behavior further, treatment of the RP is needed depending on the amount of quantitative information ones is seeking about the system dynamics. A significant advantage is the ability to infer critical information about the dynamical system even from short time series data. As mentioned by Eckmann *et al.* (1987), an RP is essentially a time plot and through the RP it is possible to identify dynamics on large and small time scales simultaneously. Owing to its potential, the method of recurrence plots has been applied to physical and physiological data in several investigations, more recently by Marwan (2003). In the presence of intermittency, the structure of diagonal segments in an RP is modified depending on the type of intermittency present (Klimaszewska and Zebrowski, 2009).

The recurrence plots for the pressure time series for $x_f = 56.5\ cm$ and $x_f = 63\ cm$, are shown in Fig. 5.7. From our previous discussion, we know that at $x_f = 56.5\ cm$ the pressure oscillations exhibits limit cycle behavior whereas for $x_f = 63\ cm$ the oscillations are quasi-periodic in nature. The dynamics is clearly represented in the RPs.

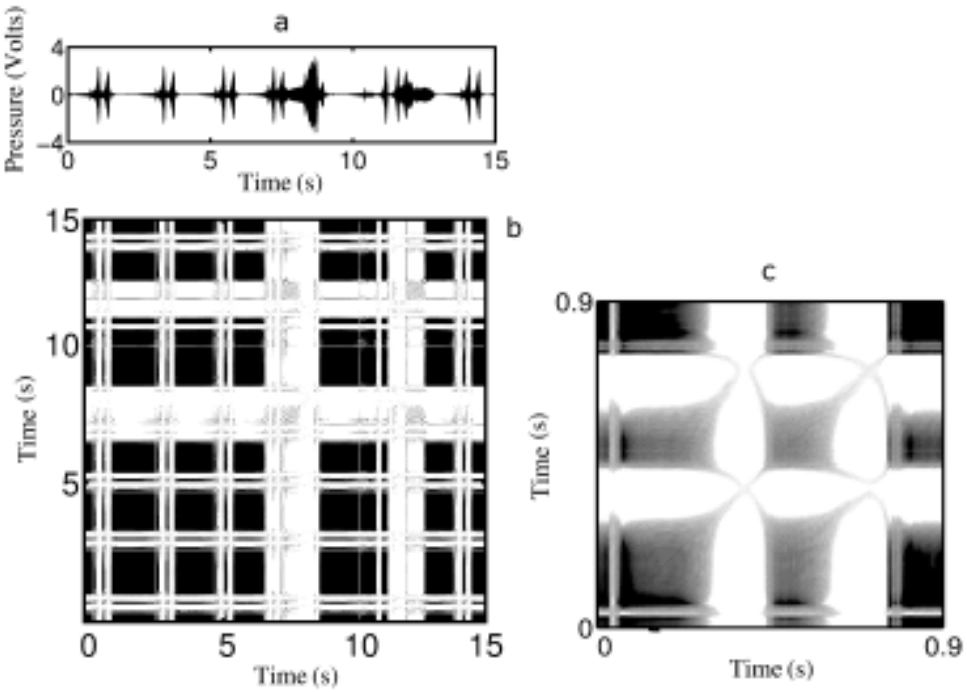

Figure 5.8: Intermittent oscillation for flame location $x_f = 63.5\ cm$ is shown in plot a and recurrence plot corresponding to intermittent oscillations (a) is shown in (b). Embedding dimension = 4, ϵ = $0.4V$. In c, a closer look into the patterns comprising the recurrence plot is presented. The end of laminar phases correspond to elongated structures, whose kite-like appearance indicates type-II intermittency. Acoustic pressure amplitude in the time series corresponding to recurrence plots is in Volts.

Equally spaced diagonal lines parallel to the main diagonal denote periodic behavior as is seen in Fig. 5.7 a(ii) which corresponds to limit cycle oscillation. As already discussed, a RP is essentially a time plot and hence temporal features such as the time period (vertical spacing between diagonal lines) can be directly obtained. Presence of a second incommensurate frequency in quasi-periodic oscillations translates to diagonal lines parallel to the main diagonal but separated by unequal vertical spacings (Zou, 2007). This is also what is observed in the RP corresponding to quasi-periodic oscillation, as seen in Fig. 5.7 b(ii).

The obtained RP from the time series data of acoustic pressure corresponding to intermittent oscillations is showed in Fig. 5.8 b. The dense black patches on the RP plot correspond to laminar states (dynamics prior to bursts) in the system. The laminar states are interrupted by bursts, which are still oscillatory in nature, as seen in the time series. During these bursts, the system dynamics is such that the recurrence of phase

space trajectories is significantly reduced. In effect, the density of the black region is thinned by white regions. This can be seen clearly by comparing the pressure oscillation time series, Fig. 5.8 a with the corresponding RP shown in Fig. 5.8 b. Bursts are associated with the absence of recurrence in the RP. A zoomed-in view of the RP is given in Fig. 5.8 c. The kite like elongation (Fig. 5.8 c) seen on the top right is a characteristic of type-II intermittency (Klimaszewska and Zebrowski, 2009). Klimaszewska and Zebrowski (2009) presented an analysis to identify the intermittency types based on the recurrence plot analysis. Type-II and type-III were found to have similar large scale patterns, black squares. However, a closer look indicated that the kite-like structure differentiates type-II from type-III. Accordingly, the recurrence plot obtained for the intermittent oscillations in our system indicates type-II intermittency.

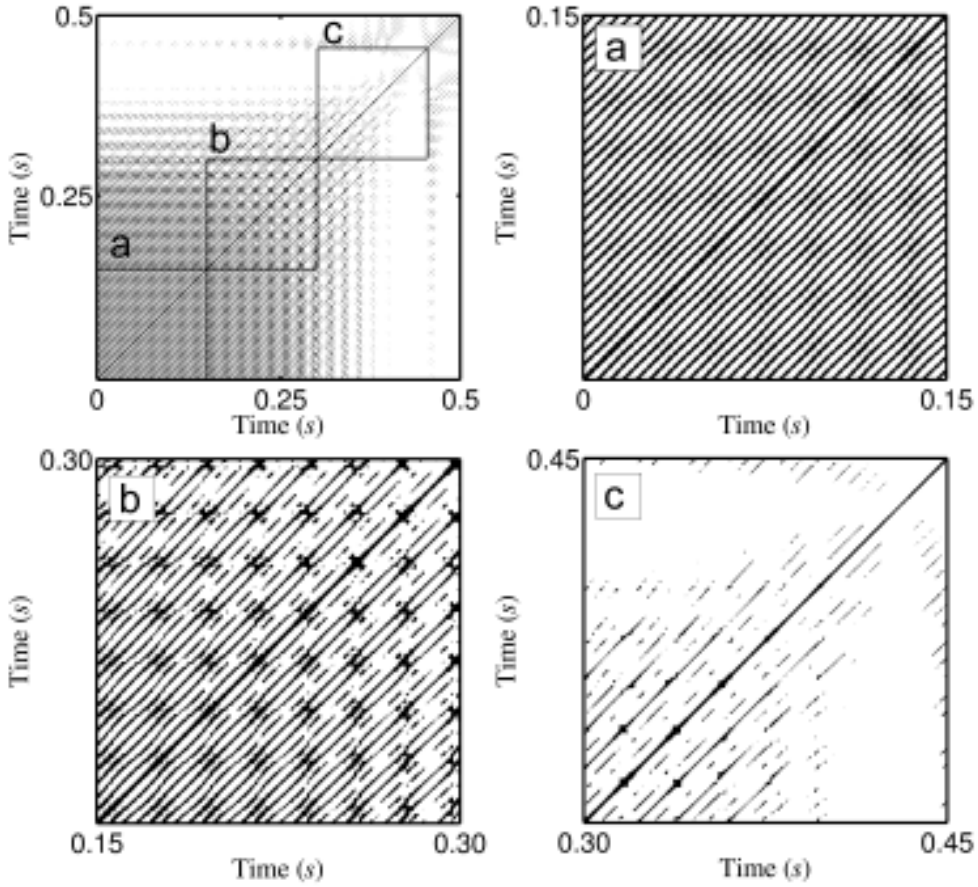

Figure 5.9: Recurrence behavior of the system prior to a burst (top-left frame). The evolution of the system entering a burst state is analyzed by following the main diagonal. Windows a-c as marked indicate the transition of the system from limit cycle to quasi-periodic oscillations before the occurrence of a burst.

Further magnification of the recurrence plot reveals that within the kite-like structure, more detail about the system transition to bursts is embedded. An RP indicating system dynamics prior to entering the burst phase is given in Fig. 5.9. Figures marked a, b and c are windows taken from the RP on the top left. Following the main diagonal in RPs is essentially following the temporal evolution of the system. Before entering a burst, the system dynamics is characterized by limit cycle oscillations (window a). Gradually, the limit cycle undergoes transformation towards quasi-periodic behavior (window b). Just before a burst, the RP is strongly indicative of quasi-periodic dynamics.

An additional feature associated with intermittency is the change in the intermittent behavior itself as the control parameter is changed. Pomeau and Manneville (1980) reported that for intermittent oscillations, the average length of laminar phases decreases as the control parameter is gradually varied. A similar trend is seen in the present case for the flame locations x_f between $63.5\ cm$ and $69.5\ cm$ (see Fig. 5.1), region IV. Initially, just after the transition from quasi-periodic state to intermittent state, bursts are temporally spaced quite distant from each other. As the flame location is varied, the occurrence of bursts become more frequent. At a flame location of $69.5\ cm$, the flame is unable to form a stable attachment point to the burner rim and therefore oscillates violently while in a lifted position and then blows off. Any further change in flame location leads to flame blowout.

Figure 5.11 shows the evolution of bursts as the flame location is varied further from the bifurcation point. As the flame location is gradually varied, a higher number of bursts are seen for the total data acquisition time. This is in agreement with the trends reported in the literature on intermittency. Prior to flame blowout, in Fig. 5.10 l, the intermittent bursts occur quite frequently. Comparing the recurrence plots for oscillations states at a flame location close to bifurcation, Fig. 5.8 and at a flame location close to lean blowout, Fig. 5.11 b, shows that close to lean blowout, laminar states states become smaller and bursts occur more frequently (Fig. 5.11 a). This is seen as smaller but a considerably greater number of closely spaced dark patches in the recurrence plot, Fig. 5.8. A magnified view of the recurrence plot is presented in Fig. 5.11 d. The high amplitude pressure oscillations occurring rapidly during the intermittent state disturbs the flame

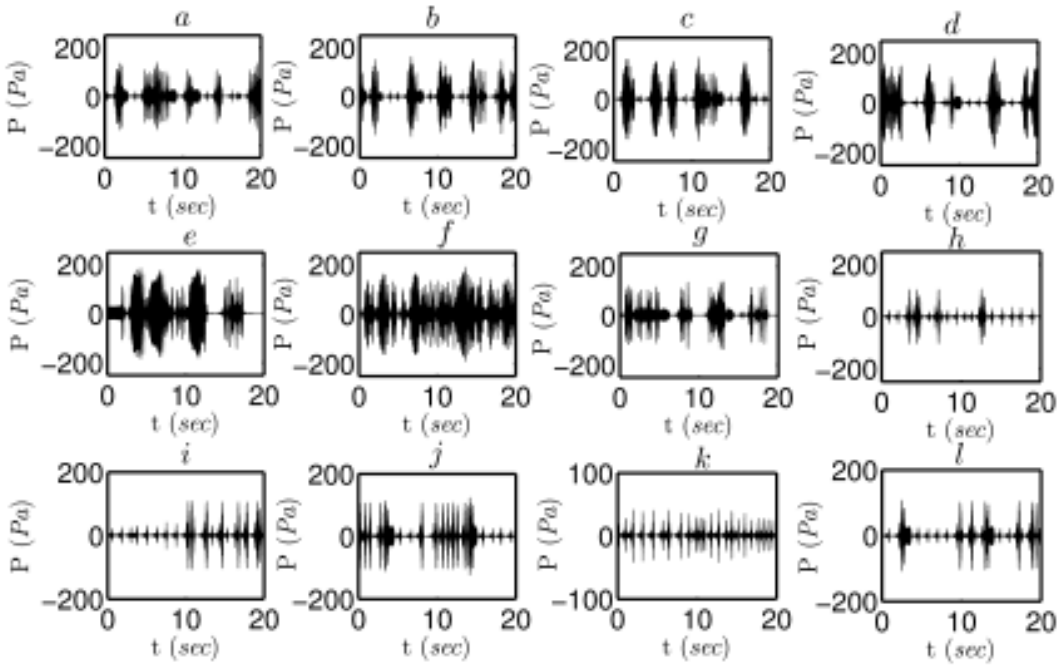

Figure 5.10: Pressure time series, $p\ (t)$ for flame locations, $x_f = 64.5\ cm$ till $x_f = 69.5\ cm$, arranged (a to l) in the increasing order of flame locations. Flame blowout limit for the system at the given operating conditions occurs after $x_f = 69.5\ cm$ (i.e., after l).

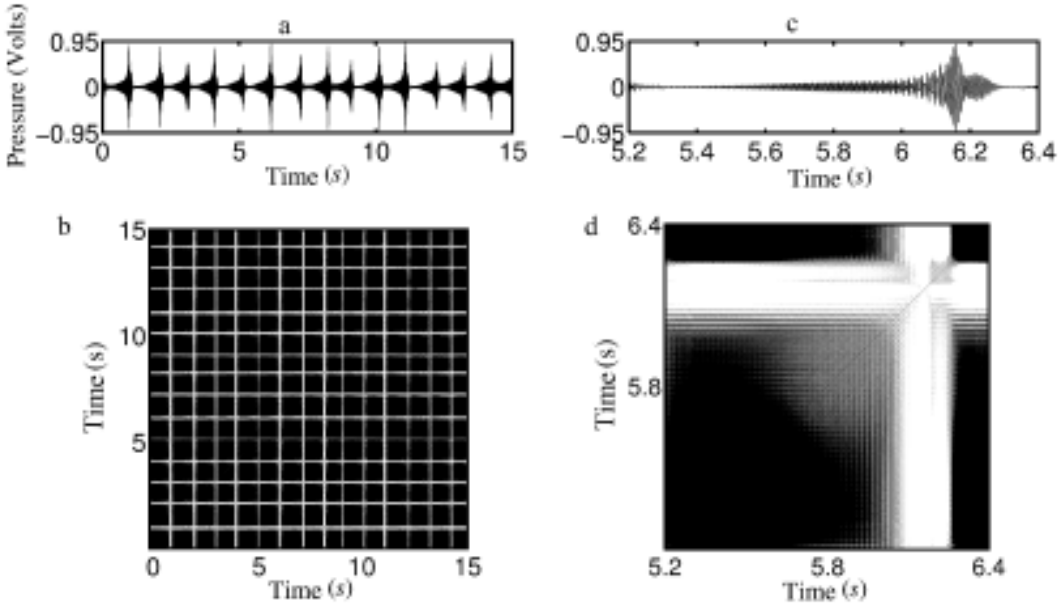

Figure 5.11: System dynamics analyzed through a recurrence plot at a flame location ($x_f = 69\ cm$) close to blowout. Embedding dimension = 4 and ϵ = 0.4V. Near flame blowout, bursts occur more rapidly (a). Acoustic pressure amplitude in a and c are represented in volts.

stabilization point as we will discuss through flame imaging later and eventually leads to flame blowout.

The large scale patterns and the finer textures formed in the recurrence plot are associated directly with the topological characteristics of the phase space attractor. As such, a quantitative study of the recurrence plot will provide information about the system dynamics. Recurrence quantification techniques were suggested by Eckmann *et al.* (1987), who mentions about the patterns and textures of the recurrence plot in her investigation. A detailed study on recurrence quantification analysis has been put forth by Zbilut and Webber (1992) and Marwan (2003). According to these reports, one can obtain the degree of determinism involved with a dynamical system by examining the ratio of points contributing to linear structures and individual points distributed in the recurrence plot.

As an illustration, by definition, positive Lyapunov exponents in system dynamics indicate divergence between nearby trajectories. Divergence between two trajectories would lead to an end of recurrence between the trajectories after a certain time which is determined by the magnitude of divergence between them. Hence the Lyapunov exponent is then related to the longest linear structures in the recurrence plot. Accordingly, the degree of determinism of a system goes down as linear structures become shorter and less pronounced in the recurrence plot. Here, we examine the recurrence plot for the intermittent states graphically. From the kite-like structure present in the recurrence plot, we arrive at the inference that the system has a type-II intermittency as pointed out by Klimaszewska and Zebrowski (2009). However, further investigation of intermittency in thermoacoustic systems with the help of recurrence analysis techniques should provide more details on the phenomenon.

5.4 Flame Dynamics

A qualitative analysis of flame oscillations at the observed nonlinear states gives further insight into the process. By analysing high speed flame images, it was found that nonlinear dynamics of thermoacoustic oscillations identified through nonlinear time series

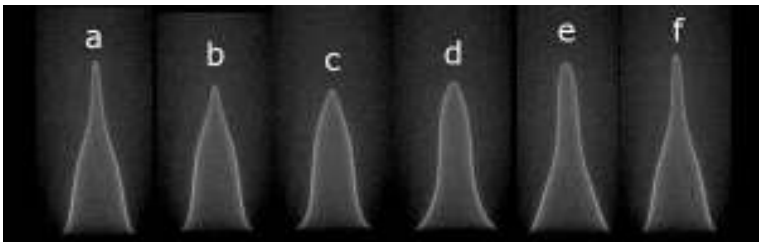

Figure 5.12: Sequence of instantaneous flame images (framing rate, $5\ kHz$) for limit cycle oscillation, a = $0\ ms$, b = $0.8\ ms$, c = $1.4\ ms$, d = $2.8\ ms$, e = $4.2\ ms$ and f = $5.4\ ms$. A uniform periodic flame wrinkling about the mean flame shape is observed during limit cycle oscillations

analysis of pressure oscillations is reflected in the flame dynamics. Results show that uniform flame surface modulation (Fig. 5.12) is restricted only for periodic limit cycle oscillations. Figure 5.12 a to f are the instantaneous flame images corresponding to one time period of oscillation ($5.4\ ms$). During a single time period, wrinkles appear to originate at the base of the flame and propagate downstream along the flame surface. The flame surface area modulations occur about the mean flame shape.

Flame oscillations corresponding to quasi-periodic oscillations feature flame elongation, neck-formation, pinch-off and cusping, in addition to fluctuations about the mean flame shape. The various events associated with a quasi-periodic flame oscillation behavior are highlighted in Fig. 5.13. The arrows indicate flame surface elongation and the circles mark neck-formation, pinch-off and cusping of the flame that follows elongation. Flames images presented are not equally spaced in time but have been chosen to illustrate the differences with flame oscillations observed during limit cycle oscillations. The dynamics are largely influenced by the oscillations in the acoustic variables around the burner exit. The amplitude of acoustic pressure oscillations for limit cycle and quasi-periodic oscillations at a given duct location are comparable (refer to Fig. 5.2). The flame and the burner exit however experience different acoustic fields for the two oscillation states in terms of pressure amplitude, which is the reason for differences in the flame-acoustic interaction.

Nonlinear features in flame dynamics such as pinch-off have been reported previously in experiments based on forcing of unconfined flames (cf Bondar, 2007). The introduction of acoustic forcing results in the creation of disturbances at the flame base. These disturbances travel along the flame surface convectively and lead to a global flame

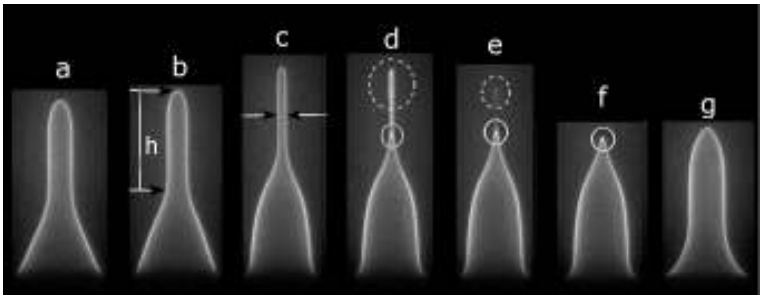

Figure 5.13: Sequence of instantaneous flame images (framing rate, $5\ kHz$) at quasi-periodic oscillations. a = $0\ ms$, b = $2.6\ ms$, c = $4\ ms$, d = $4.2\ ms$, e = $4.4\ ms$, f = $4.6\ ms$ and g = $8\ ms$. Characteristic flame surface area modulations during quasi-periodic oscillations involve flame elongation (b), neck-formation (c), pinch-off (d, e) and subsequent cusp formation (f). The arrows and circles mark the evolution of flame elongation and subsequent pinch-off during the quasi-periodic state. The height of the flame tip is marked with the alphabet h to show that the flame tip gets elongated as it moves towards cusping.

response. As the amplitude of acoustic forcing introduced on the flame is increased, the strength of disturbances generated at the flame base increases and eventually flame response characteristics such as pinch-off appear. In the context of this discussion and the observation of complex nonlinear self-excited state in our experiments, the experimental investigation presented by Bourehla and Baillot (1998) is of particular relevance. Through an exhaustive analysis they reported that the flame response can be quite varied, ranging from uniform wrinkling to subharmonic and chaotic response, depending on the amplitudes and the frequency of acoustic forcing. The mechanism of flame surface area fluctuations in our experiments is also similar to forcing experiments, as observed from the flame images. Variation in the flame location changes the characteristics of acoustic field affecting the flame and correspondingly the flame response. However, unlike forced flame behavior, in a self-excited case, the interaction between flame and acoustics is a feedback interaction. This means that changes in flame response to changing acoustic field interacts with the system acoustics. This interactions in turn governs the asymptotic system dynamics; bifurcation of a limit cycle state to quasi-periodic oscillations and subsequent bifurcations are identified in this present study. Bifurcation of the quasi-periodic state leads to intermittency and the characteristic flame dynamics during intermittency are discussed next.

A sequence of flame images acquired during intermittency by a video camera and

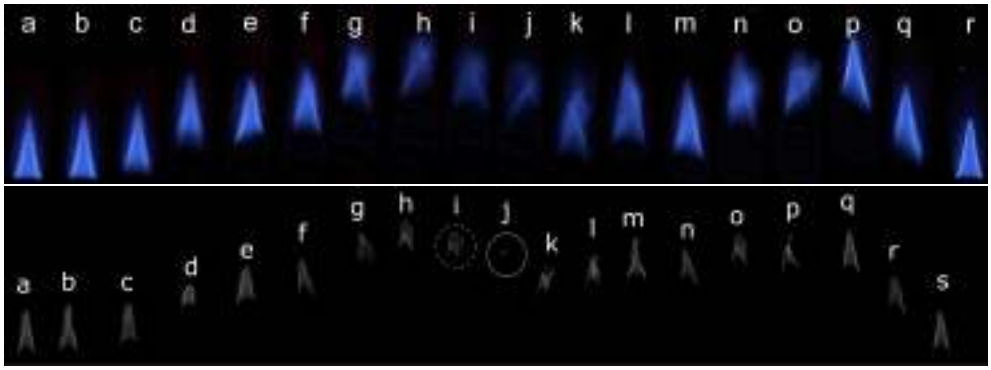

Figure 5.14: Flame dynamics during intermittent oscillations - long exposure images acquired at 25 Hz (top row) indicate the variation in mean flame shape and location during intermittent oscillations. Images are arranged in the order of their occurrence (left to right). Frames acquired at: a = 0 s, b = 0.76 s, c = 1.36 s, d = 1.4 s, e = 1.44 s, f = 1.52 s, g = 1.56 s, h = 1.6 s, i = 1.68 s, j = 1.84 s, k = 1.88 s, l = 1.92 s, m = 2.0 s, n = 2.12 s, o = 2.16 s, p = 2.32 s, q = 2.52 s, r = 2.6 s. Exposure time corresponds to approximately 5 cycles of the oscillation. Instantaneous images (bottom row) marked with circles highlight the characteristic stretching, folding (i) and local extinction (j) in the flame. The lifted flame oscillates in the jet transition region, at about 5 burner tube diameters from the burner exit plane indicating a non-trivial impact of jet flow dynamics. The chaotic flame oscillations during the lifted state is clearly discernible.

instantaneous high speed images acquired by a high speed camera are presented in Fig. 5.14. Sudden bursts in acoustic oscillations (Fig. 5.10) are accompanied by repeated flame lift-off and reattachment behavior. Lifting-off of the flame occurs due to the inability of the flame to sustain a stable attachment with the burner during high amplitude oscillations. The images correspond to flame oscillations prior to lift-off, during lift-off and during reattachment. The low sampling rate video images give an idea of the amplitude of flame oscillations and the mean flame shape during the different stages of the flame during intermittency and the instantaneous images illustrate the stretching and folding undergone by the flame. Oscillations in the flame surface prior to the burst phase, while it is still attached to the burner rim (image frame a, b in Fig. 5.14) are similar to the flame surface area modulation as seen in limit cycle oscillations (Fig. 5.7). Even following the detachment of the flame from the burner rim (beginning of the burst phase), flame oscillations continue to exist (image frame d-o) as in the acoustic pressure (see Fig. 5.2). It is seen that during this phase, flame oscillations are composed of high frequency oscillations (seen as blurred flame images in the top row of Fig. 5.14) superimposed over a slower trend of changing flame position and mean shape.

The intermittent state is characterized by a chaotic flame dynamics marked by highly irregular oscillations in the lifted flame. Prior to flame lift-off, changes in system dynamics were discussed earlier in terms of the acoustic pressure fluctuation (see Fig. 5.9). The lifting up of the flame marks the beginning of a burst state and occurs simultaneously with the transition of the system dynamics from limit cycle to quasi-periodic. During the lifted state, the flame is not stabilized on the burner rim and hence, flame dynamics is not only affected by acoustics but significant flame oscillatory behavior is governed by the hydrodynamics associated with the circular jet emanating from the burner tube and entering the glass duct confinement. Hydrodynamics associated with a circular jet flow at Reynolds numbers has been extensively studied before (Becker and Massaro, 1968; Liepmann and Gharib, 1992). At Reynolds number $\sim (10^3)$ (Reynolds number associated with the circular jet for the configuration we have studied here), the exit flow from the burner tube forms a shear layer resulting in the development of Kelvin-Helmholtz instability in the flow upstream of the lifted flame. The lifted flame oscillates at about 5 burner diameters downstream of the burner exit plane (see Fig. 5.15). This location corresponds to the transitional region of the circular jet where instabilities originating in the shear flow develop into coherent structures (Paschereit *et al.*, 1992). Hence, during intermittency, it is suspected that coherent flow structures affect dynamics of the flame which is lifted during the occurrence of bursts. The inter-

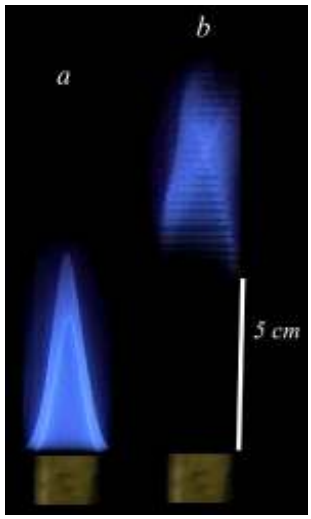

Figure 5.15: Comparison of attached flame to the burner rim (a) and lifted oscillating flame (b) during an intermittent burst oscillation, the white thick line indicate the lifted distance ($5\ cm$). Flame images were acquired using a video camera (Panasonic, AGDVC62) with framing rate of $25\ Hz$

mittent state, as explained with the bifurcation plot (region III in Fig. 5.1) eventually leads to flame blowout.

5.5 Discussions

The appearance of thermoacoustic instability in combustion systems due to interaction between the acoustic field and the combustion processes is an issue of significant concern. Recent experiments have shown that the nonlinear nature of this interaction is reflected in the complex dynamics of the self-excited oscillations.

In this investigation, we reported results of an experimental bifurcation analysis of a ducted conical premixed flame, with flame location as the control parameter. At the onset of instability, the interaction between the heat release rate oscillations due to flame surface fluctuations and acoustic oscillations leads to limit cycle oscillations via a subcritical Hopf bifurcation. The subcritical nature is clearly seen in the bifurcation plot. On changing the flame location further a secondary Hopf bifurcation was observed leading to quasi-periodic oscillations. The quasi-periodic oscillations undergo further transition to an intermittent state which in accordance with the bifurcation scenario is a type-II intermittency. The different oscillatory states were analyzed through phase space reconstruction using nonlinear time series analysis. Flame dynamics associated with limit cycle oscillations was characterized by uniform, periodic flame wrinkling behavior. Whereas, for quasi-periodic oscillations, nonlinear features such as flame pinch-off were observed in addition to flame surface wrinkling.

The intermittent state was characterized and discussed in detail through the application of phase space based nonlinear time series analysis techniques. Features of type-II intermittency were also observed in further analysis of the intermittent state via recurrence plots. Simultaneously during intermittency, interesting flame dynamics were observed as seen in high speed flame images. Bursts in acoustic oscillations were observed to occur simultaneously with flame lift-off. Through recurrence plots, the repeated flame lift-off behavior was found to be associated with the temporal transition of the system to quasi-periodic dynamics. Extreme stretching, folding and local extinction

that characterize flame dynamics during intermittency suggests complex dynamics governing the flame behavior during the intermittent state. These intermittent oscillations eventually lead to flame blowout indicating that the dynamical state of intermittency is a precursor to flame blowout induced by thermoacoustic oscillations.

The high speed flame images provide some evidence that the observed dynamics of the system in this bifurcation analysis is a result of variations in flame dynamics in response to changes in the acoustic field affecting the flame, which occurs as the flame location is varied. This hypothesis is supported by flame response studies (Bourehla and Baillot, 1998; Bondar, 2007; Candel, 2002). However, as flame dynamics is significantly affected also by hydrodynamics, the cause of complex nonlinear behavior could be the effect of acoustic perturbations on a confined jet flow, particularly during intermittency when the flame is detached from the burner. Further investigations on combustion systems conducted from the point of view of dynamical systems theory are necessary to extend the results presented here to industrial applications.

5.6 Interim Conclusions

The results reported here demonstrate that thermoacoustic interaction possesses rich nonlinear behavior. Analysis of results from the point of view of dynamical systems theory sheds new light into the nonlinear aspects of thermoacoustic instability. The observation of intermittency indicates firstly that the nonlinear process of thermoacoustic instability can posses quite complex dynamics, similar in several attributes to nonlinear interactions in other physical systems. A second issue associated with lean combustion is the problem of lean flame blowout (Shanbhogue *et al.*, 2009). Although a vast amount of literature is available on lean flame blowout, the problem is still far from solved. Studies on lean flame blowout involve developing techniques for blowout detection (Nair and Lieuwen, 2005) and efforts to suppress the appearance of blowout (Shashvat, 2007). Overcoming problems associated with flame blowout in practical systems primarily involve strategies that increase the safe operating range. For instance, in gas turbine combustors, a swirl stabilized flame configuration is commonly used, where in the wake of recirculation zone mixing of the reactants takes place. Due

to vortex breakdown, a region of reverse flow exists which stabilizes the flame. However, swirl flames too are prone to flame blowout. Chemiluminescence imaging and laser scattering results on swirl dump combustor shown by Murganandam and Seitzman (Tuscon, Arizon, 10-13 July, 2005) shows that the presence of cold reactants in the inner core of the recirculation zone is the sole reason for flame extinction. Stöhr *et al.* (2011) investigated lean blowout using chemiluminescence imaging, stereo-PIV (Particle Image Velocimetry) and PLIF (Planar Laser Induced Fluorescence) to demonstrate mechanisms involved with flame stabilization close to blowout. This is a step towards a complete understanding, prediction and control of thermoacoustic instability and thermoacoustically induced flame blowout.

CHAPTER 6

ROUTES TO CHAOS IN THERMOACOUSTIC OSCILLATIONS

In the previous chapter we saw that even in the most simple thermoacoustic configuration, complex oscillations in acoustic pressure and flame intensity were observed. Furthermore, through the analysis, it was found that nonlinear aspects of thermoacoustic instability are related to the process of lean flame blowout. However, due to lean flame blowout, a comprehensive bifurcation scenario leading to chaos could not be covered. Towards this objective, a second configuration is adapted - a confined multiple premixed flame system. The configuration has the advantage that the properties of combustion instability can be studied without significant interference from hydrodynamic instability. In addition, the dynamics of laminar flames exposed to acoustic perturbations has been extensively studied through experiments (Candel, 2002) and numerical investigations (Noiray *et al.*, 2008). This makes the configuration ideal for fundamental studies on self-excited combustion instability.

6.1 Transition to Chaos via the Ruelle-Takens Scenario

Similar to the single flame, an experimental bifurcation analysis of the system was performed. Interestingly, the main features of the earlier bifurcations, namely subcritical Hopf bifurcation leading to limit cycle oscillations and a secondary bifurcation to quasi-periodic oscillations was observed in this configuration as well. The application of nonlinear time series analysis, particularly, techniques based on phase space reconstruction from acquired pressure data, reveals rich dynamical behavior and the existence of several complex states. Route to chaos for thermoacoustic instability is established experimentally for the first time. We show that, as the flame location gradually varied, self-excited periodic thermoacoustic oscillations undergo transition to chaos.

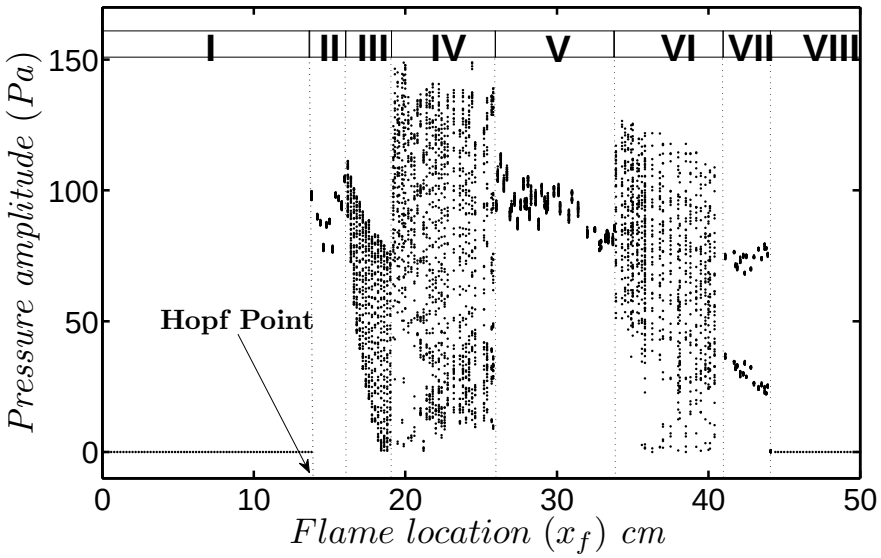

Figure 6.1: Bifurcation plot summarizing the experiment performed for equivalence ratio ϕ = 0.48: Hopf point at $x_f = 13.8\ cm$. The Roman numerals (I-VIII) are used to indicate different regions in the bifurcation plot. Region I-steady state and region VIII-steady state.

6.2 Bifurcation Analysis

As we gradually change the flame location, the system goes from a steady state to a self-excited oscillatory state. From the point of the onset of thermoacoustic instability, if the flame location is varied further, properties of the self-excited state change dramatically. In order to track the changes in oscillations with respect to the flame location, we plot bifurcation diagram (Fig. 6.1). Corresponding to every flame location (x_f), we plot the amplitudes of the local maxima (Strogatz, 1994) in the acquired pressure time series for that particular x_f. The number of local maxima, at a given parameter, gives the period of oscillations: a single local maxima indicates a limit cycle oscillation, two local maxima values suggest period two oscillations and so on. The Roman numerals (I-VIII) are used to indicate different regions in the bifurcation plot. Time series and frequency spectra for oscillations in these regions are presented in Fig. 6.2. A longer time window is used for more complicated oscillations so that the essential features of the oscillations are clearly depicted.

The onset of instability occurs at $x_f = 13.8\ cm$, one-eighth of the total duct length from the open end. At this point, there is a qualitative change in the system from steady state to finite amplitude oscillations. This is an indication of a subcritical Hopf bifur-

cation (Strogatz, 1994). It is quite common to encounter subcritical Hopf bifurcation in practical combustion-driven thermoacoustic systems such as gas-turbine combustors and rocket combustors (Zinn and Lieuwen, 2005). The point at which the bifurcation occurs is referred to as the Hopf point. The bifurcation results in a single frequency, 'limit cycle' oscillation with a frequency $f \sim 570\ Hz$. This is close to the second harmonic of the duct acoustic mode. The time series and frequency spectrum of this state are shown in Fig. 6.2 IIa & IIb respectively.

The limit cycle oscillation state persists for a small range of x_f values beyond which it is followed by a bifurcation of the limit cycle to another type of oscillation with more than one dominating frequency ($f_1 \sim 570\ Hz, f_2 \sim 364.1\ Hz$), as shown in Fig. 6.2 IIIa. As we change the flame location, the frequencies compete with each other and eventually towards the end of this state, the time series (Fig. 6.2 IIIa) and the frequency spectrum (Fig. 6.2 IIIb) changes to the one depicted in Fig. 6.2 IIIc & IIId respectively. The dominant frequency also changes from f_1 to f_2, which is close to the first harmonic duct acoustic mode.

The next bifurcation occurs at $x_f = 19.2\ cm$, the amplitude of local maxima increases to about 1.5 times (150 *Pa*). The irregularity in the oscillations can be clearly seen in Fig. 6.2 IVa. The corresponding frequency spectrum, Fig. 6.2 IVb shows the presence of a broad band of frequencies (along with the appearance of a new independent frequency, $f_3 \sim 524\ Hz$) suggesting the presence of low dimensional chaos. On changing the flame location, we observe that the signature of the time series has changes at $x_f = 21\ cm$, within region IV. We observe regularity in the time series and distinct peaks in the frequency spectrum plots (Figs. 6.2 IVc & IVd). The frequencies in the spectrum are rationally related as opposed to the broadband frequencies. Following this state, the oscillations become regular again in region V .

Figure 6.2 Va & Vb gives the time series and frequency spectrum plots of a representative state in region V (Fig. 6.1). The peaks in the frequency spectrum correspond to f_2, $f_2/2$ and $f_2/4$. This is an indication of the oscillations being period four in nature, but since the contribution from the sub-harmonics is very less compared to the dominant frequency, it is not clearly visible in the time series or in the bifurcation plot (Fig. 6.1). The system exists in this state for a large range of x_f values ($x_f = 25.8\ cm$

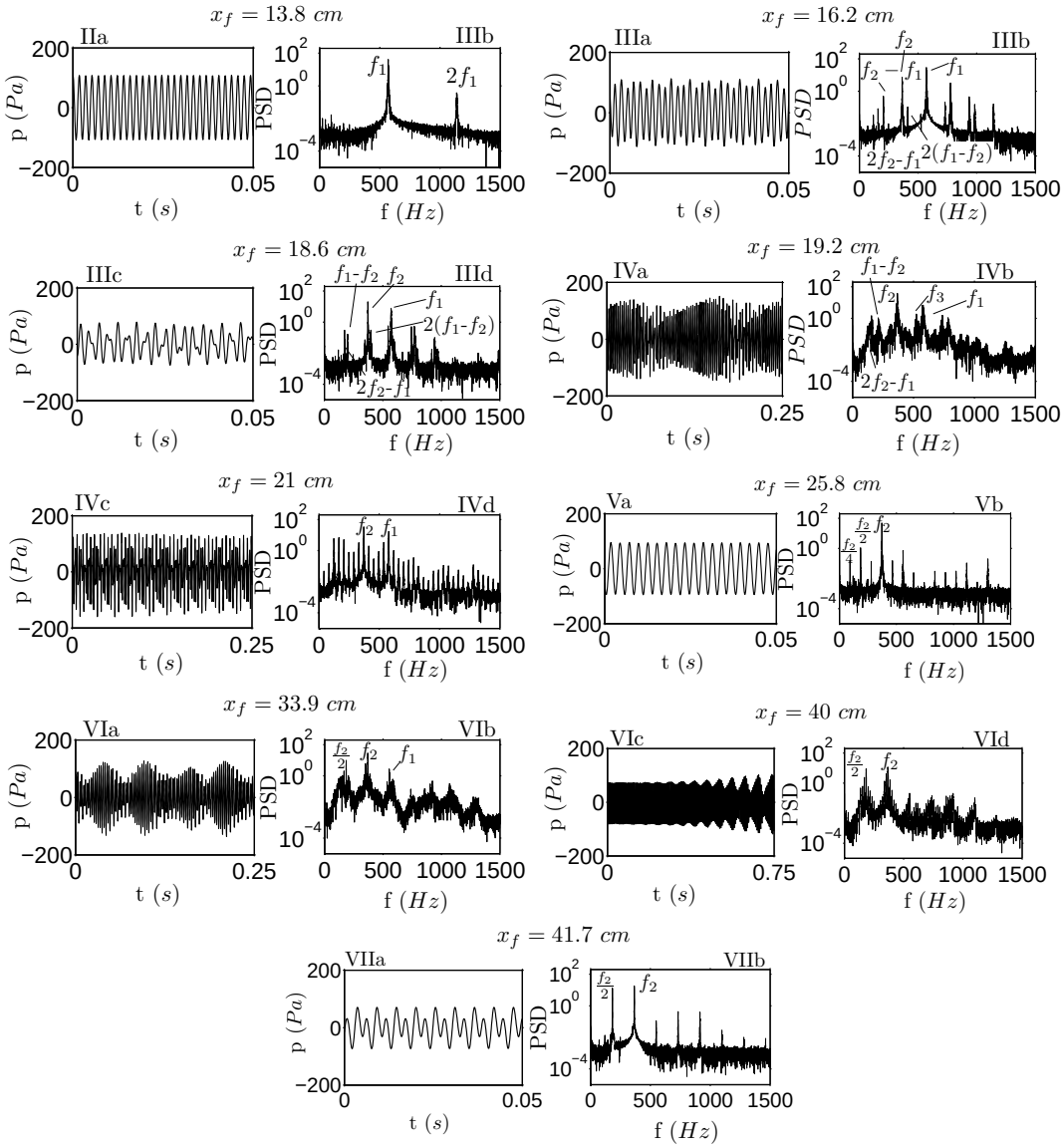

Figure 6.2: Time series and power spectrum for various oscillating states observed in the system, labeled according to the bifurcation plot, Fig. 6.1. The flame location corresponding to each dynamical state is marked above the time series and power spectrum density. The dominating frequency first appeared in the system along with higher harmonics is $f \sim 570\ Hz$. This is close to the second harmonic of the duct acoustic mode. $f_2 \sim 364.1\ Hz$ seen for flame location $x_f = 19.2\ cm$. The third frequency which appears in the system and causes the bifurcation of torus is $f_3 \sim 524\ Hz$ suggesting the presence of low dimensional chaos. To confirm on the torus and presence of low dimensional chaos nonlinear time series analysis is implemented systematically on the time series presents above.

to $x_f = 33.9\ cm$) and is followed by another state similar to the state corresponding to Fig. 6.2 IVa, as depicted in Fig. 6.2 VIa & b. The frequency spectrum shows three broadband regions centered around $553\ Hz$, $370.2\ Hz$ and $185.1\ Hz$, where $185.1\ Hz$

is the sub-harmonic of $370.2\ Hz$. We increase the flame location further and this state changes to a period two oscillation in region VII (Fig. 6.1) via an intermittent state. The time series and frequency spectrum of the intermittent and the period two oscillatory state are given in Figs. 6.2 VIc & d and VIIa & b respectively. The intermittent state has intervals of period two and the irregular state coexisting together. A transition from period two to irregular oscillations can be observed in Fig. 6.2 VIc. Beyond this region, changing the flame location brings the system back to a steady state at $x_f = 43.9\ cm$, which is close to half the duct length.

6.3 Nonlinear Time Series Analysis

For further analysis, techniques that specifically deal with nonlinear systems are called for. It is crucial to implement nonlinear time series analysis techniques for understanding the dynamics of the thermoacoustic system. Nonlinear time series analysis techniques provide tools for systematic analysis and identification of characteristics and structures in time series data generated by nonlinear processes with emphasis on the determination of properties of a special class of nonlinear oscillations, the chaotic oscillations. Chaotic oscillations are quite commonly observed in nonlinear systems and in the absence of appropriate analysis, the broadband frequency spectrum resulting from chaotic dynamics could be misinterpreted to be a result of noise. Therefore, implementation of phase-space based nonlinear time series analysis techniques is essential to extract detailed information about the complex nonlinear processes.

6.3.1 Average Mutual Information

The variation of $AMI(\tau)$ with time delay for all the time series discussed above is shown in Fig. 6.3. The top three curves in Fig. 6.3 are for periodic oscillations with rationally related frequencies, regions II, V and VII (Fig. 6.1). The other curves belong to oscillations with either irrationally related frequencies or broadband frequencies, regions III, IV and VI (Fig. 6.1). The optimal time delay for phase space reconstruction varies from $0.4 - 0.9\ ms$, in the various regions, as seen in Fig. 6.3.

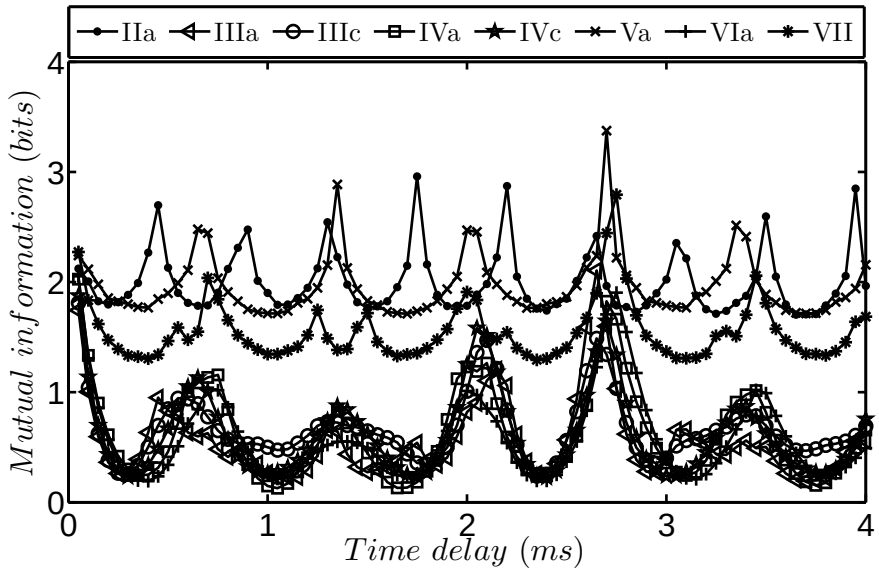

Figure 6.3: Results for the calculation of optimum time-delay for phase space reconstruction using the average mutual information between time-delayed vectors from acquired time series. The Roman numerals marked with markers are in accordance to the different regions in the bifurcation plot (Fig. 6.1).

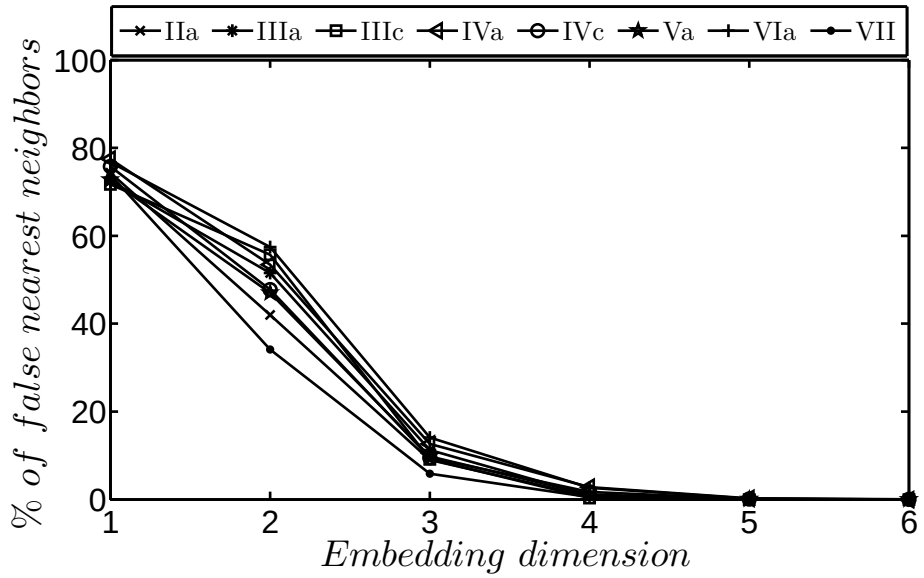

Figure 6.4: The plot presents calculated false nearest neighbor percentage for different embedding dimensions. The dimension at which the percentage goes to zero is taken as the optimum embedding dimension. The Roman numerals marked with markers are in accordance to the different regions in the bifurcation plot (Fig. 6.1).

6.3.2 False Nearest Neighbors

A typical plot obtained for each of the cases discussed in the thesis has been reported in Fig. 6.4. The trend of the variation of the percentage of false nearest neighbor estimates for different oscillations with respect to the embedding dimension, d_E, suggests $d_E = 5$ as an optimum embedding dimension since the percentage of false nearest neighbors for all the states vanishes at $d_E = 5$. Henceforth, quantitative information from phase space reconstruction of strange attractors has been derived using $d_E = 5$.

6.3.3 Reconstructed Phase Portraits

The three-dimensional phase portrait representations of the various states obtained in our system are arranged in the order of their occurrence in the bifurcation plot (Fig. 6.1) in Fig. 6.5, starting with the limit cycle. We find that the characteristics of simultaneously measured flame intensity time series data are similar to the pressure time series data in Sec. 6.6. Phase space structures seen in the reconstructed phase portraits from chemiluminescence time series (Fig. 6.6) are observed to be similar to those obtained from the pressure time series (Fig. 6.5).

Limit cycle (Fig. 6.5 IIa), as expected, is represented by a single loop in the phase space. But, the introduction of new frequencies due to the next bifurcation results in aperiodic oscillations and the loop turns into a dense toroidal structure, as can be seen in pressure oscillations (Figs. 6.5 IIIa & IIIb). A toroidal structure in the phase space, is an indication of quasi-periodic oscillations. Quasi-periodicity is also reflected in the power spectrum (Figs. 6.2 IIIb & IIId) in the form of incommensurate frequency components (365.3 & 571.3 Hz). Due to the presence of incommensurate frequencies, the phase space trajectory evolves on the surface of a torus, never closing on itself. As we change the control parameter, flame position within the quasi-periodic region (region III) in Fig. 6.1, there is a competition between the two major frequencies eventually leading to the introduction of a third incommensurate frequency (f_3 in Fig. 6.2 IVb) causes the toroidal structure to become unstable and break down resulting in a strange attractor as seen in Fig. 6.5 IVa. This structure corresponds to the time series and the frequency spectrum that shows the presence of broadband frequency con-

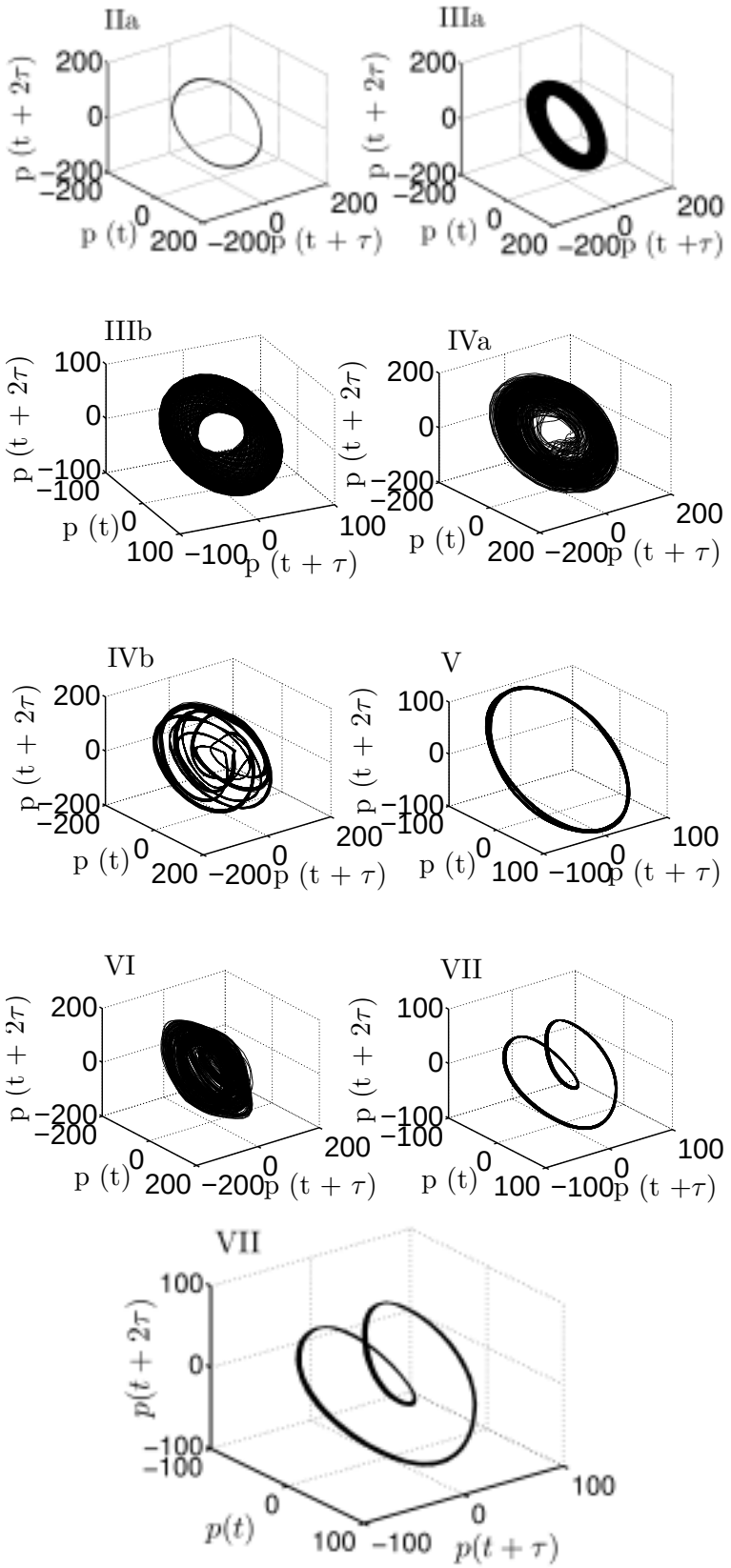

Figure 6.5: Reconstructed phase portraits from measured pressure time series for different oscillation states, sequentially arranged in the order of their occurrence in the bifurcation diagram, Fig. 6.1. The labels are in accordance with the bifurcation plot.

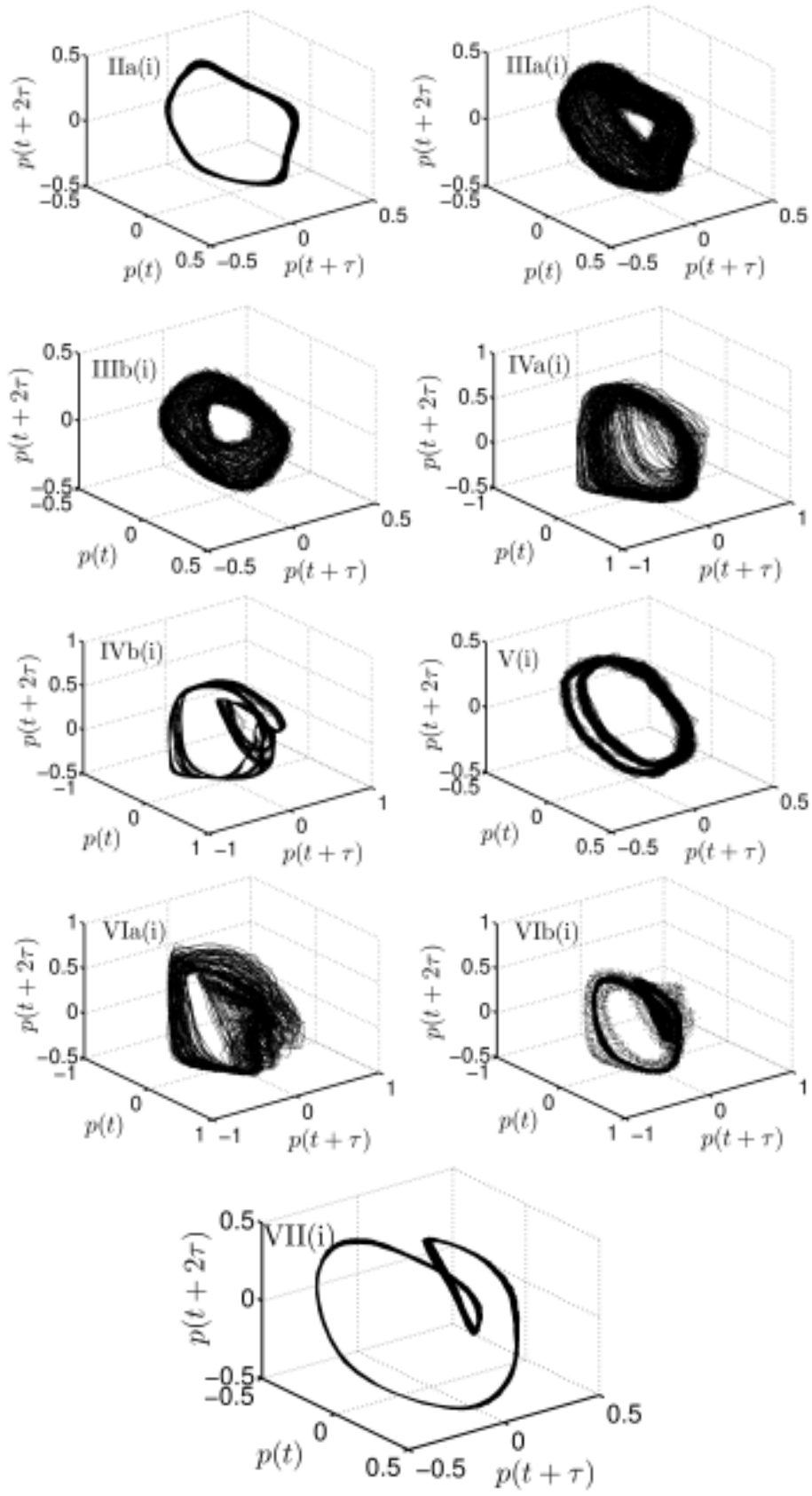

Figure 6.6: Reconstructed phase portraits from measured intensity (*CH**) time series for different oscillation states, sequentially arranged in the order of their occurrence in the bifurcation diagram, Fig. 6.1. The labels are in accordance with the bifurcation plot.

tent in Fig. 6.2 IVb. Broadband frequency content and strange attractor hints towards the presence of chaotic oscillations.

The similar sequence of phase evolution of the system is observed for the system through intensity time series. The reconstructed phase space for limit cycle, quasi-periodic oscillations, two period oscillations, period four oscillation and chaotic oscillation in order of appearance of the oscillations in the system is arranged in Fig. 6.6.

6.4 Strange Attractors

To identify whether the obtained attractor (Fig. 6.5 IVa) is a strange attractor (possesses an inherent dimension which is not an integer but rather a fraction), we evaluate the correlation dimension of the attractor using the Grassberger and Procaccia (1983) algorithm. Subsequently, to find out if the oscillations are chaotic in nature, we calculate the maximal Lyapunov exponent using the algorithm suggested by Kantz (1994). These are discussed in the following paragraphs (see appendix B for algorithm).

6.4.1 Correlation Dimension and Maximal Lyapunov Exponent

According to the Grassberger-Procaccia algorithm, the correlation dimension is obtained from the calculation of the correlation sum of all the points in the phase space. This correlation sum is given by

$$\mathrm{C(r)} = \lim_{N\to\infty} \frac{1}{N^2} \begin{pmatrix} \text{number of pairs of points} \\ \mathbf{x_i}, \mathbf{x_j} \text{ with distances } \mathbf{Euc.dist.} < \mathbf{r} \end{pmatrix}, \tag{6.1}$$

where N is the total number of points, Euc.dist is the Euclidean distance in the phase space, between points $\mathbf{x_i}$ and $\mathbf{x_j}$). As r $\to 0$, this function is found to have a power law dependence,

$$\lim_{\mathrm{r}\to 0} \mathrm{C(r)} \propto \mathrm{r}^{d_c}, \tag{6.2}$$

where d_c is an estimate of the correlation dimension of the attractor. In Figs. 6.7 and 6.9 the plot for C(r) vs. r for the attractors, corresponding to region IV and VI is given. It is seen that a scaling region where the power law dependence can be seen is found for r in the range $\sim 20 - 100$. Corresponding to these plots, the value of local slope with respect to r, for dimensions 6, 8, 10 and 12 have been given in Figs. 6.8 and 6.10. In the scaling region, the value of slopes gives an estimate of the correlation dimension of the particular attractor. For region IV, the value of slope in the scaling region fluctuates significantly. However, at high dimensions, it seems to have saturated. For region VI, slopes in the scaling region, calculated for different dimensions follow a more robust trend. For the two attractors in region IV and region VI, the correlation dimension, calculated from the curve at dimension 12 is found to be 5.5 ± 0.4 and 4.6 ± 0.3 respectively.

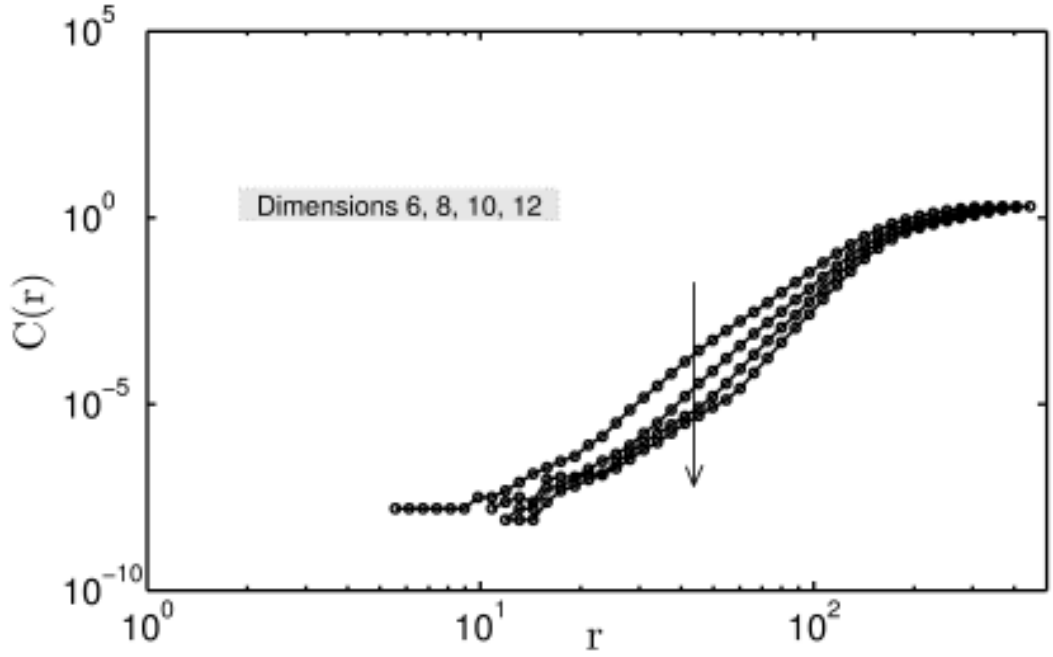

Figure 6.7: Variation of correlation sum as a function of r for the attractor in region IV, Fig. 6.5 IVa. The variation with respect to r is plotted for dimensions 6, 8, 10 and 12. Arrow points towards increasing embedding dimension. A data set with 16000 points was considered for obtaining the plot.

Chaotic dynamics in a dynamical system is indicated by the presence of positive Lyapunov exponents. Lyapunov exponents, by definition are a measure of the exponential divergence in time, of two neighboring phase space trajectories. A positive exponent implies that any uncertainty in estimation of the dynamical state of the system

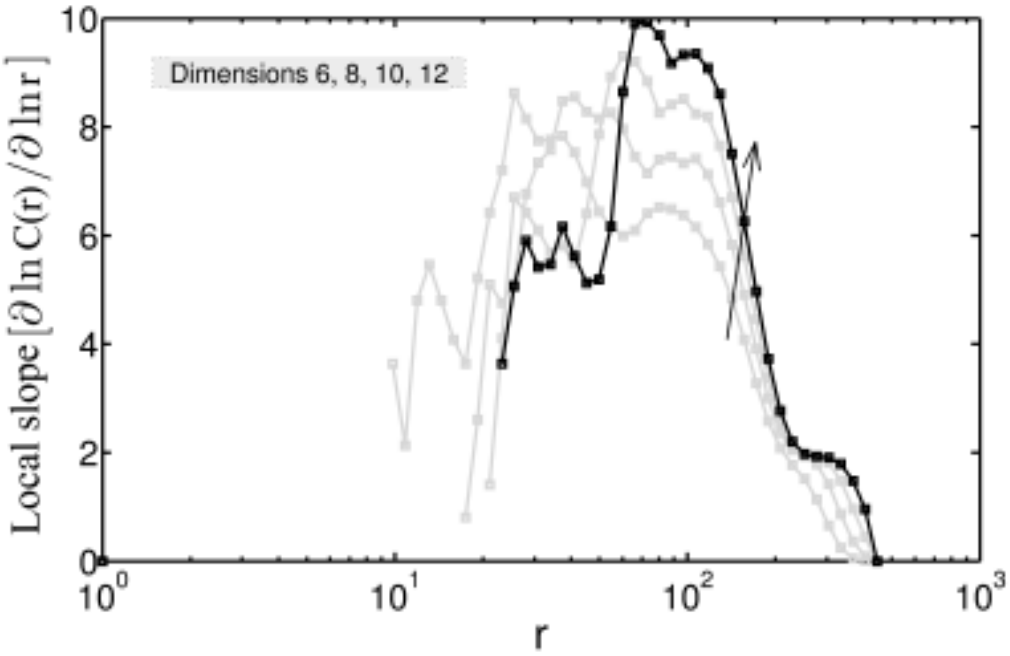

Figure 6.8: Slopes of the correlation sum in Fig. 6.7 as a function of r. The correlation dimension is evaluated from the curve corresponding to a dimension 12 (in black). Arrow points towards increasing embedding dimension. The correlation dimension is obtained from the scaling region where a constant slope exists for a range of correlation radius, r.

will grow exponentially in time. To identify the presence of chaotic dynamics in our system, we calculate the maximal Lyapunov exponent using the method given by Kantz (1994). According to the algorithm, one finds the average separation between neighboring trajectories in the reconstructed phase space as time evolves and the evolution in the average separation is searched for an exponential trend. More specifically, the average separation $S(\Delta n)$ is calculated as a function of temporal separation Δn:

$$S(\Delta n) = \frac{1}{T}\sum_{t=1}^{T} \ln\left(\frac{1}{|\mathcal{U}_t|}\sum_{i\in\mathcal{U}_t} dist\left(\mathbf{x_t}, \mathbf{x_i}; \mathbf{\Delta n}\right)\right), \tag{6.3}$$

where $\mathcal{U}_t$ is the neighborhood of any point $\underset{\sim}{x}_t$ in the phase space and $dist(\mathbf{x_t}, \mathbf{x_i}; \mathbf{\Delta n})$ is defined as

$$dist(\mathbf{x_t}, \mathbf{x_i}; \mathbf{\Delta n}) = |\mathbf{x_{t+\Delta n}} - \mathbf{x_{i+\Delta n}}| \ . \tag{6.4}$$

The quantity $S(\Delta n)$ scales linearly with Δn in an intermediate range with a slope cor-

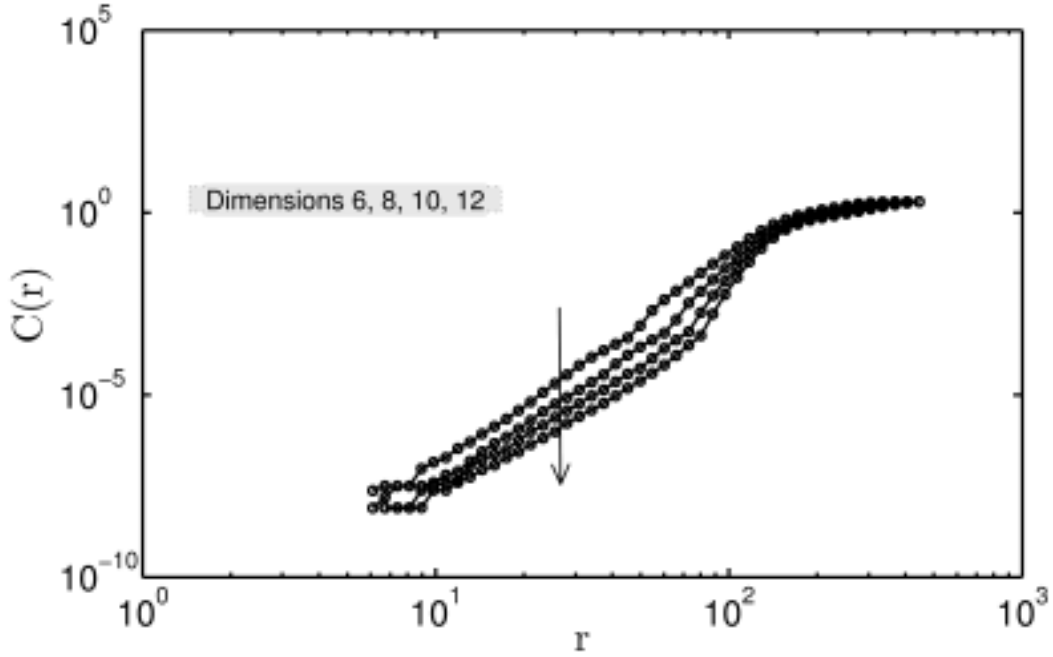

Figure 6.9: Plot for the correlation sum for the attractor in region IV, Fig. 6.5 VIa. The variation with respect to r is plotted for dimensions 6, 8, 10 and 12. Arrow points towards increasing embedding dimension. A data set with 16000 points was considered for obtaining the plot.

responding to the maximal Lyapunov exponent. Further details about the algorithm and its implementation on experimentally acquired time series data can be found in Kantz (1994), Kantz and Schreiber Kantz and Schreiber (2003).

According to the bifurcation analysis of our system, regions IV and VI in the bifurcation plot are the possible chaotic states. In accordance with the Kantz algorithm, variation in $S(\Delta n)$ with Δn with an embedding dimension of 4, 6, 8, 10 and 12 for region IV and VI is given in Fig. 6.11 and Fig. 6.12 respectively. The slope of a linear fit to the curves for embedding dimension 12, shown by the dashed line gives values 0.00041 and 0.00051 per time step. As data has been acquired with a sampling rate of $10kHz$, the maximal Lyapunov exponent corresponding to these slopes, comes out to be 4.1 $\pm$ 1.4 and 5.1 $\pm$ 0.6 for region IV and region VI respectively. The range of Δn to be searched for, to obtain the scaling region is quite large in both cases owing to the high sampling rate. In both cases, exponential divergence between neighboring trajectories occurs amidst a highly cyclic trend of the time series (number of cycles corresponding to a Δn of 1000 $\sim O(10)$). The maximal Lyapunov exponent for both the regions is a

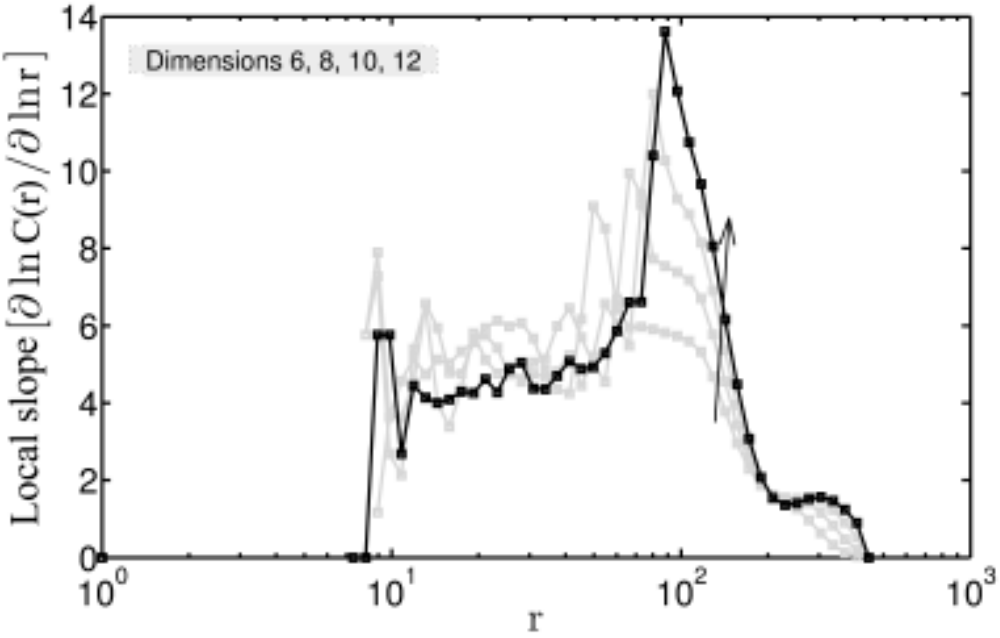

Figure 6.10: Local slopes of the correlation sum in Fig. 6.9. The correlation dimension is evaluated from the curve corresponding to a dimension 12 (in black). Arrow points towards increasing embedding dimension.

positive value, indicating the chaotic nature of the system. Now that all the states have been characterized individually, we will discuss the entire bifurcation scenario.

In our experiments, the quasi-periodic state is followed by chaotic oscillations. The system follows a torus breaking route to chaos starting from a limit cycle evolving into a two-frequency quasi-periodic state and eventually the two torus structure of the quasi-periodic attractor breaks down as a result of a third incommensurate frequency, thus leading to the emergence of a chaotic state. This torus breaking route to chaos is also called the Ruelle-Takens scenario (Ruelle and Takens, 1971). The strange attractor is then followed by periodic mode-locked oscillations featuring several rationally related frequencies (Fig. 6.2 IVd). The phase space representation is given by Fig. 6.5 IVb. The structure is a closed loop which indicates a periodic nature of the oscillation, while following several turns before closing on itself which is because of the presence of a number of frequencies.

Following this state, the system once again enters a state with periodic oscillations given in Fig. 6.2 Va. The frequency spectrum (Fig. 6.2 Vb) contains frequencies f_2 $f_2/2$, $f_2/4$ indicating this could be a period-4 state. The contribution from $f_2/2$ and

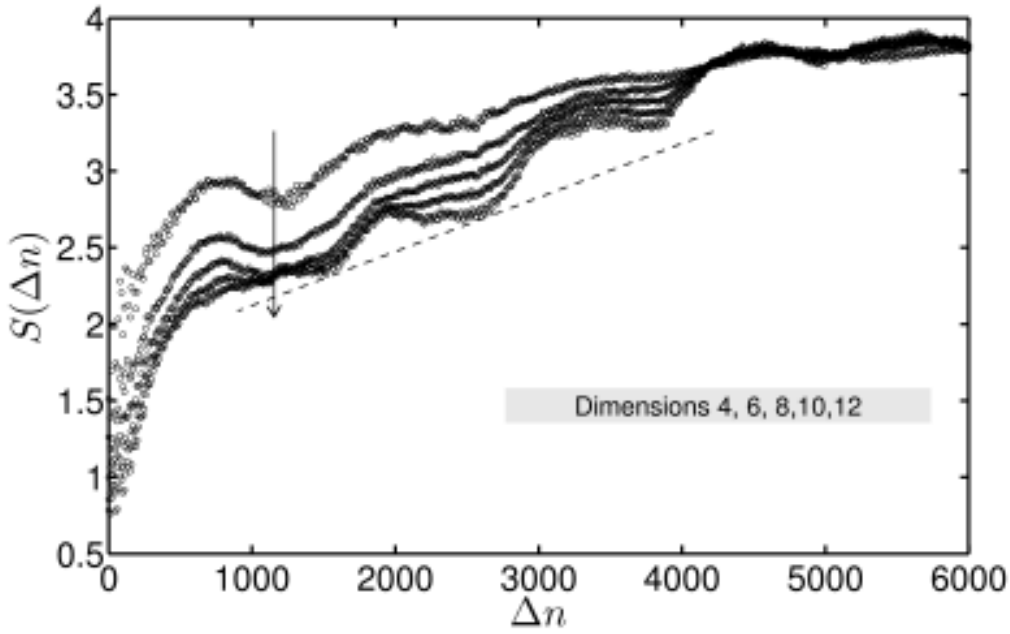

Figure 6.11: Estimation of the maximal Lyapunov exponent (4.1 ± 1.4) (region IV) for dimensions 4, 6, 8, 10 and 12. A data set of 16000 points was considered for calculations. Arrow points towards increasing embedding dimension. The dashed line indicates a linear fit the arrow points towards increasing embedding dimension

$f_2/4$ being of very low order when compared to f_2 result in an attractor which consists of two very closely spaced loops in Fig. 6.5 Vb. This periodic state exists for a long range of control parameter before the next bifurcation which results in another aperiodic state.

Region (VI) exhibits chaotic oscillations resulting from a bifurcation of the periodic state. From the frequency spectrum, Fig. 6.2 VIb and the reconstructed attractor, Fig. 6.5 VIa, it is observed that this could be another strange chaotic attractor. Figure 6.5 VIa is a strange attractor, corresponding to the time series data obtained for $x_f = 33.9\ cm$, and clearly shows the characteristics of the chaotic behavior observed in region (VI). The correlation dimension for this strange attractor is calculated to be 4.6 and the positive maximal Lyapunov exponent is 5.1 ± 0.6. As discussed earlier, this state goes through an intermittent transition to period-2 oscillations.

In the reconstructed phase space for pressure (Fig. 6.5 VIb), we have shown phase space representation of the intermittent oscillations that alternate between period-two and a two-period quasi-periodic attractor. The dark loop is the period-two attractor

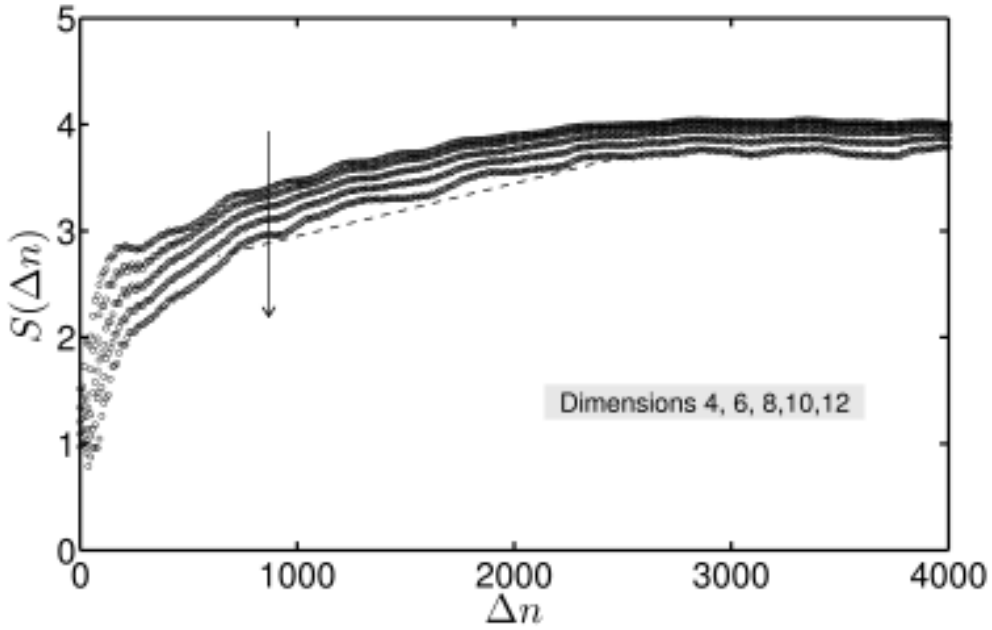

Figure 6.12: Estimation of the maximal Lyapunov exponent (5.1 ± 0.6) (region VI) for dimensions 4, 6, 8 , 10 and 12. Arrow points towards increasing embedding dimension. A data set of 16000 points was considered for calculations. The dashed line indicates a linear fit.

which is embedded within a quasi-periodic attractor represented using light dotted markers in the reconstructed phase portrait. Once the flame location is changed, the system evolves to a period-two attractor via a very narrow window of stable quasi-periodic attractor. The window of this stable quasi-periodic oscillation is too insignificant to be labeled separately as another region. The phase space representation of the period-2 oscillations for region VII (Fig. 6.1) is shown in Fig. 6.5 VII. The system seems to follow a reverse quasi-periodic transition from chaotic to periodic oscillations. Region VIII (Fig. 6.1) is again the steady state (fixed point) to which the system eventually returns.

6.5 Discussions

We have presented an experimental bifurcation analysis conducted on a prototypical combustion driven thermoacoustic system. Changing the position of the combustion zone with respect to the duct causes the appearance of oscillations in the flames and in the acoustic pressure. This first bifurcation in the system is a subcritical Hopf bi-

furcation leading to limit cycle oscillations. However, the dynamics of thermoacoustic oscillations in combustion systems is not limited to limit cycle oscillations and although the system we study is a highly simplified version of a practical combustion system, variation of the flame location induces additional bifurcations. Bifurcation of limit cycle oscillations gives rise to quasi-periodic oscillations and changing the flame location further gives rise to chaotic oscillations. The sequence of bifurcations we observed in our experiments is summarized below:

$$\text{Steady} \xrightarrow{\text{Subcritical Hopf bifurcation}} \text{Periodic} \xrightarrow{\text{Neimark-Sacker Bifurcation}} \text{Quasi-periodic}$$

$$\xrightarrow{\text{Ruelle-Takens Scenario}} \text{Chaotic} \rightarrow \text{Mode-locked} \rightarrow \text{Period-4} \rightarrow \text{Chaotic} \rightarrow$$

$$\text{Two-period quasi-periodic} \rightarrow \text{Period-2} \rightarrow \text{Steady}$$

The sequence of bifurcations to chaotic oscillations, exhibited by the system is similar to the route to chaos in other physical systems, such as the Rayleigh-Bénard convection, popularly known as the quasi-periodic route to chaos or the Ruelle-Takens scenario. Transitions to complex oscillation states and the specific route to chaos observed in the present investigation arise from complex interactions between several processes; flame dynamics, acoustics, hydrodynamics and heat transfer being the most significant processes. A strong coupling between these processes exists during the occurrence of combustion instability. However, it is still possible to shed light on the most likely cause of the presence of interesting system dynamics seen here, based on previous investigations that hint towards the importance of flame-acoustic interaction in combustion driven thermoacoustic systems.

The presence of combustion in an acoustic field, in particular the flame response to acoustic fluctuations, is known to be responsible for nonlinear aspects of thermoacoustic instability. A simplified analytical treatment of combustion instability (for instance, refer to the analysis by Dowling (1999)) indicates that a nonlinear response of the flame to the incident acoustic fluctuations can explain nonlinear features such as the presence of limit cycles, subcritical bifurcation and triggering. This is further supported by the more recent describing function analysis (Noiray *et al.*, 2008) of combustion instability, for a combustor similar to the present investigation. Complex nonlinear states

in addition to limit cycle oscillations have also been reported, for instance by Jahnke and Culick (1994), where quasi-periodic thermoacoustic oscillations were obtained in a dynamical system analysis using numerical continuation approach of thermoacoustic instability and by Sterling (1993) in a numerical bifurcation analysis where a period doubling scenario was observed. Incorporation of nonlinear flame-acoustic interaction to explain the observed results in the analytical/numerical/experimental treatment of thermoacoustic instability is the common feature of the above mentioned studies.

Based on the results summarized above and other previous investigations, we can surmise that a nonlinear flame response largely governs the behavior of thermoacoustic oscillations, including the bifurcations leading to chaos that have been observed in this report. Specifically in our experiments, changes in the flame location directly change the location of the combustion zone with respect to the acoustic field of the duct (standing wave). This in turn leads to changes in flame response and hence the overall dynamics of the self-excited heat release and pressure oscillations.

Flame surface area oscillation is the dominant mechanism generating unsteady heat release rate (cf. Schuller *et al.*, 2003) in our experiments. The unsteady heat release rate gets coupled to pressure fluctuations during combustion instability. Changes in this flame-acoustic interaction at different oscillation states is reflected in pressure oscillations as well as in flame surface oscillations, as can be seen in high speed flame images in Sec. 6.6.

In addition, it should also be noted that along with flame-acoustic interactions, other important processes, also contribute to the dynamics of oscillations. In practical combustion systems, complex fluid flow interactions (Schadow and Gutmark, 1992) in the periphery of the confined combustion zone play a non-trivial role in determining the resulting thermoacoustic oscillations. Also important is the role of oscillatory heat transfer at the burner (Merk, 1956). These processes are significant and need to be considered in detailed modeling approaches. However, concerning our experiments, these processes might not undergo changes at different flame locations and therefore, do not participate in the bifurcation behavior. Hence, we speculate that, nonlinear flame-acoustic response turns out to be the most plausible mechanism responsible for the observed dynamics.

6.6 Frequency Locking Route to Chaos

A qualitative change in the behavior exhibited by any dynamical system on varying a control parameter is termed as bifurcation. Bifurcation plot for the system under investigation is given in Fig. 6.14. The bifurcation plot (Fig. 6.14) has been shown till flame location $x_f = 50\ cm$ as the system remains stable (fixed point) beyond this point. The vertical axis is the pressure amplitude in *Pascals* obtained from pressure microphone P (Fig. 3.1). For each flame location, local maxima from the corresponding pressure time series, about 100 cycles long, have been plotted. For a limit cycle oscillation, this will be a single point, corresponding to the peak amplitude of the oscillation. Figure 6.14 (a) represents the bifurcation diagram for increasing flame location and Fig. 6.14 (b) for decreasing flame location. While increasing the flame location, the system jumps from a stable to an unstable state at $x_f = 13.5\ cm$ (x_{f_1}). The set of ordinates corresponding to this particular x_f i.e., the amplitudes of all the local maxima in the pressure time series are of the same magnitude and hence, the oscillations present at the particular location are limit cycle oscillations. As we go beyond this point, limit cycle oscillations exist till $x_f = 14\ cm$. At this point, there is sudden change in the behavior of oscillations - a second bifurcation occurs. The local maxima in the oscillations no longer have the constant amplitude, which as we will see later, is also reflected in the Fourier spectrum in the form of the emergence of additional frequencies. Further changing the flame location leads to a series of bifurcations in the system. The system returns to its steady state at the flame location $x_f = 48.5\ cm$. In the reverse direction, we find that the system exhibits hysteresis for each region as shown in Fig. 6.14 (b). This hysteresis in system behavior is evident from the fact that there is a jump from the limit cycle oscillation back to the steady state, at $x_{f_2} = 10\ cm$, instead of x_{f_1} (Fig. 6.14). The hysteresis behavior suggests that the bifurcation at the onset of instability is a subcritical Hopf bifurcation. The region of hysteresis, $x_{f_1} - x_{f_2}$, is formally known as the subcritical zone or the bistable region.

From Fig. 6.14, it is seen that the oscillations observed in the system assume several characteristically different periodic and aperiodic states. In the following sections, the oscillating behavior obtained for each flame location (x_f) is characterized from the time series data of pressure and intensity oscillations, with the application of concepts

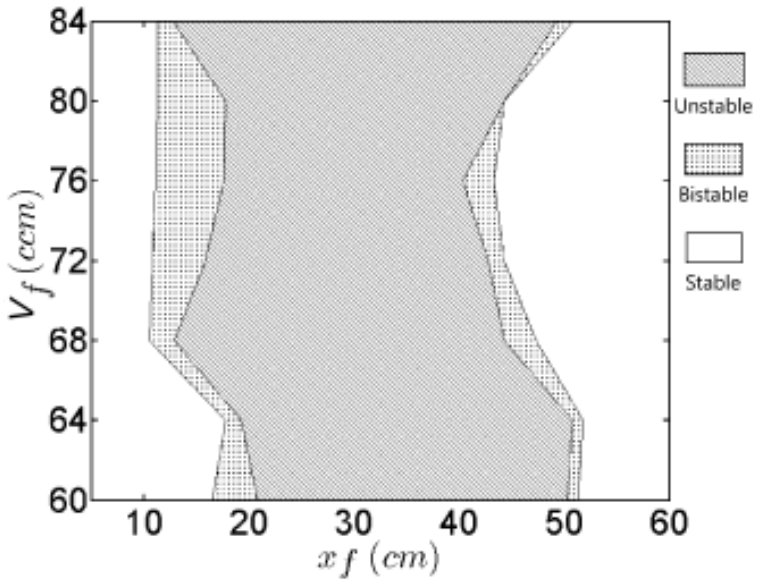

Figure 6.13: Stability map of the system indicating the stability regimes of the system for a air flow rate ($4000\ ccm$). Results have presented here for $\phi = 0.50$

from dynamical systems theory - phase space representation of the system and Poincaré sections. These concepts are briefly discussed below.

We will now continue with the results obtained by nonlinear time series analysis of data acquired for the thermoacoustic system under study. For the results presented here, the maximum embedding dimension was found to be four. A three dimensional space was found adequate to represent the phase portrait and to identify qualitative differences between various classes of oscillations obtained. The phase space representation will be in a three dimensional space constructed from time-delayed vectors ($p(t),\ p(t+\tau),\ p(t+2\tau)$) and ($I(t),\ I(t+\tau),\ I(t+2\tau)$) obtained from pressure time series and intensity time series respectively with time delay calculated for each case. We will discuss these different regimes with reference to Fig. 6.14a.

A Poincaré section depicts the intersection of an orbit in the phase space with a plane called the Poincaré plane. Unlike the phase plots discussed above where we continuously follow the evolution of a system, in a Poincaré section we look at the state of the system only at discrete time intervals. Hence, we get a set of points in the phase plane. Each classification of periodic and aperiodic motion has its own signature in the Poincaré section. To illustrate with examples, the Poincaré section of a simple limit cycle orbit will be a single point in a usual Poincaré section wherein the Poincaré

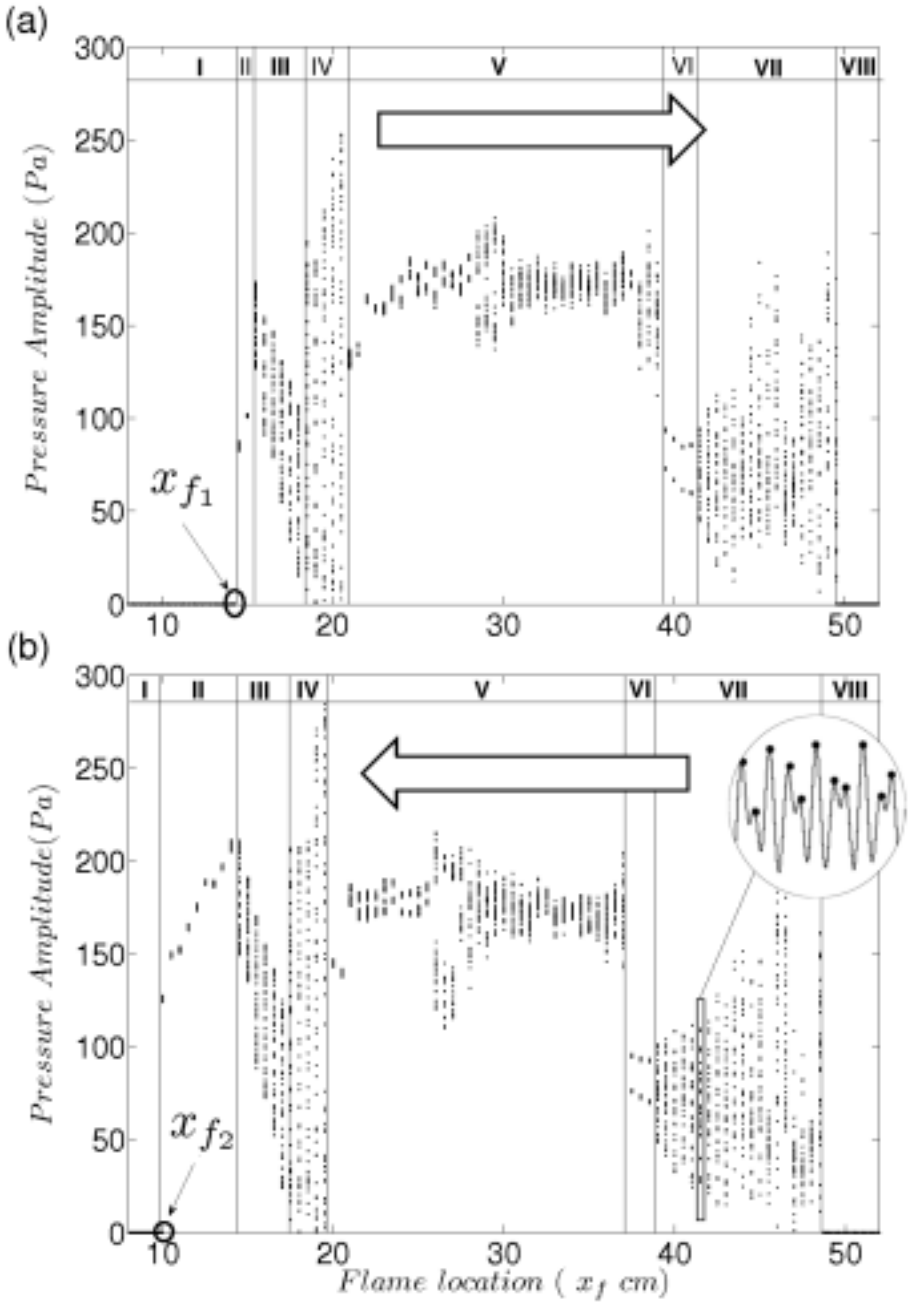

Figure 6.14: Bifurcation diagram with respect to flame location (V_a at $4000\ ccm$, V_f at $68\ ccm$). The block arrows indicate the direction of change in the flame location. (a) Increasing flame location and (b) Decreasing flame location. Local maxima in the pressure time series have been plotted for each flame location. Inset shows a few cycles of a sample time series with local maxima marked with black dots.

plane is a semi-infinite plane, i.e., it extends only in one direction and two points in case of a two-sided Poincaré sections with an infinite plane. For periodic solutions with the presence of a $1/n$ subharmonic in the signal along with the dominant frequency

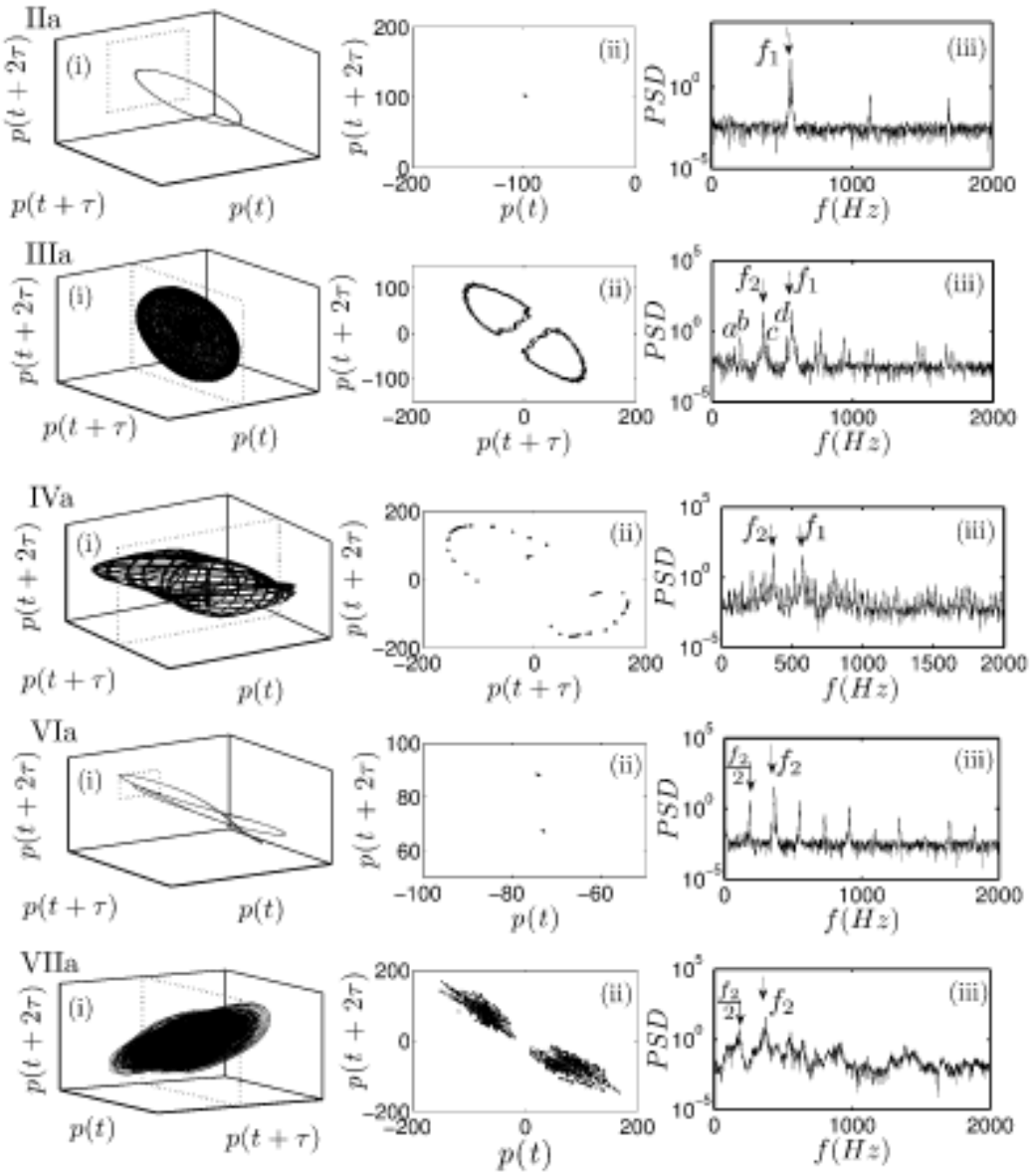

Figure 6.15: Phase portraits (i), Poincaré sections (ii) and frequency spectra (iii) for pressure time series, for different types of oscillations, sequentially arranged in the order of their occurrence in the bifurcation diagram, Fig. 6.14a. $f_1 = 570.2\ Hz$, $f_2 = 366.3\ Hz$. In Fig. iia(iii) and Fig. iib(iii), markers *a*, *b*, *c* and *d* point to frequencies $163.6\ Hz$, $202.7\ Hz$, $406.6\ Hz$ and $529.9\ Hz$ respectively. Properties of acquired data in region V are similar to the attractor in region III and hence, have not been shown here.

(formally called a period n limit cycle), the two sided section will have $2\,n$ points. For quasi-periodic solutions, the two sided Poincaré section consists of bunch of points which fill up two closed curves. In contrast, for chaotic solutions, the points on the Poincaré section fill up regions in the phase space which are more than a curve and these

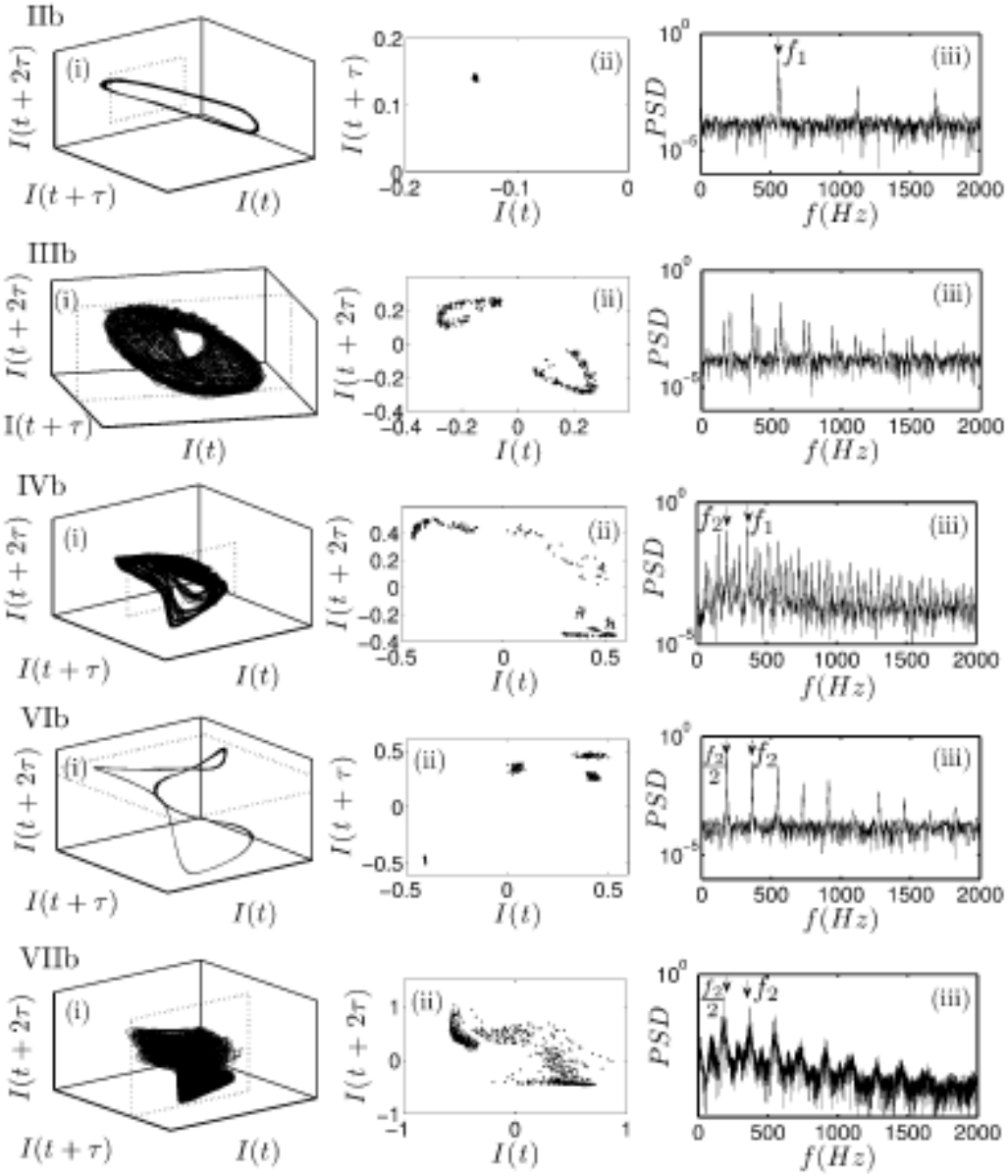

Figure 6.16: Phase portraits (i), Poincaré sections (ii) and frequency spectra (iii) for intensity time series, for different types of oscillations, sequentially arranged in the order of their occurrence in the bifurcation diagram, Fig. 6.14a. $f_1 = 570.2\ Hz$, $f_2 = 366.3\ Hz$. In Fig. iia(iii) and Fig. iib(iii), markers *a*, *b*, *c* and *d* point to frequencies $163.6\ Hz$, $202.7\ Hz$, $406.6\ Hz$ and $529.9\ Hz$ respectively. Properties of acquired data in region V are similar to the attractor in region III and hence, have not been shown here.

regions also form a fractal structure. Poincaré sections obtained from the reconstructed phase portraits using pressure and heat release time series from the experiments will be presented in the following sections.

6.6.1 Limit Cycle Oscillations: Region II

The appearance of periodic oscillations from a steady state is first observed in the system at $x_f = 13.5\ cm$ (see Fig. 6.14 a). The self-excited state is a limit cycle oscillation, resulting from a Hopf bifurcation. Owing to the subcritical nature of the bifurcation, the change in the system dynamics is marked by an abrupt jump in the oscillation amplitude. The characteristics of the resulting oscillations are given in Figs. 6.15-II a & -IIb for the pressure time series and the intensity time series respectively. The frequency spectra (Figs. 6.15-II a(iii) & -II b(iii)) shows the presence of a single frequency f_1 along with the super-harmonics. Correspondingly, the structure representative of the system dynamics (referred to as the attractor henceforth) is a distinct single loop (Figs. 6.16-IIa(i) & -II b(i)). To investigate the structure of the attractor, we use Poincaré sections. A Poincaré section (Nayfeh and Balachandran, 2004) is a surface (a Poincaré plane here) in the phase space, intersecting the trajectories of the phase space attractor. In the case of a limit cycle, the intersection will give a single point, as observed in the Figs. 6.16-IIa(ii) & II b(ii). The Poincaré plane for different cases represented here was chosen differently for different cases for easier visualisation of the dynamics. The Poincaré plane used for the phase portraits for limit cycle and other subsequent cases is given in the phase space diagram as a dotted rectangle.

Simultaneously acquired instantaneous flame images have been presented as images $a - h$ in Fig. 6.17. During the limit cycle oscillations, flames undergo sinusoidal modulations as seen in the flame images. The first six frames $a - f$ represent flame shape during different phases of oscillation, arranged in a sequence. Frames g and h are given to illustrate that for the case of limit cycle oscillations, the flame shapes occurring after time intervals of integral multiples of the oscillation time period are identical - as seen in image pairs e & g and d & h. This regular behavior is as expected since, the time traces also show regular behavior. As the flame location is varied further, we observe interesting changes in the dynamics of the self-excited oscillations.

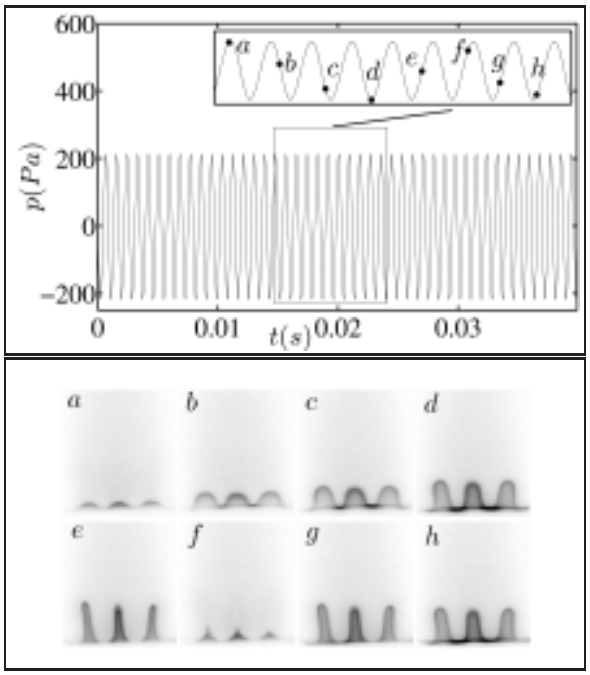

Figure 6.17: Instantaneous flame images for limit cycle oscillations. The tagged dots in the pressure time series have corresponding flame images marked by the same lowercase alphabets as used for the tags.

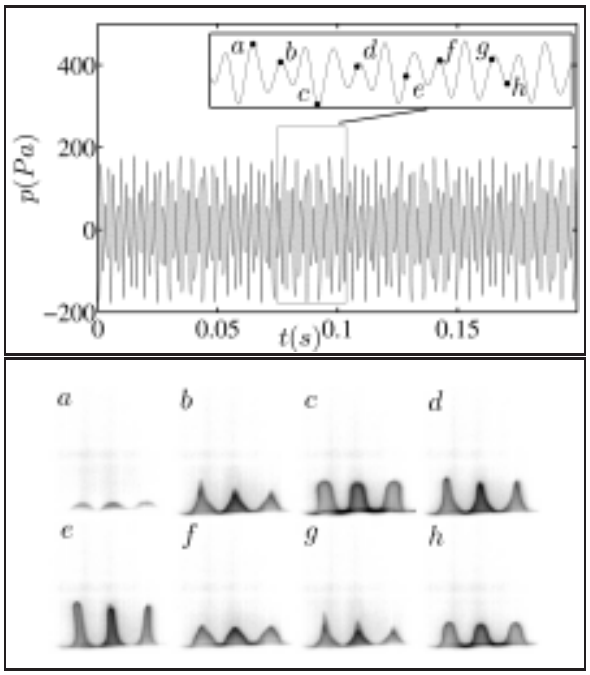

Figure 6.18: Instantaneous flame images for quasi-periodic oscillations. The tagged dots in the pressure time series have corresponding flame images marked by the same lowercase alphabets as used for the tags.

6.6.2 Quasi-periodic Oscillations: Region III

In region-III, oscillations qualitatively different from limit cycle oscillations are observed as a result of subsequent bifurcation of limit cycle oscillations. A second periodicity ensues in the system, which is revealed in the power spectrum (Figs. 6.15-IIIa(iii) & -IIIb(iii)) as a second frequency f_2 along with other frequencies with smaller contributions. When at least two frequencies of an oscillation are irrationally related, the oscillation will be aperiodic and the trajectories cannot form a closed loop, but instead, they evolve on the surface of a torus - a 2-torus if two such frequencies are present and covers the torus densely as it evolves. This is seen in the phase portrait in Figs. 6.15-III a(i) & -III b(i). Such oscillations are referred to as quasi-periodic oscillations. The Poincaré section (Figs. 6.15-III a(ii) & -III b(ii)), further illustrates the inner structure of the quasi-periodic attractor that we have obtained in our case. The intensity time series and the pressure time series both exhibit similar behavior in the phase space and in the power spectra. This secondary bifurcation of a limit cycle leading to the emergence of a second frequency is known formally in the theory of nonlinear dynamics as Hopf-Hopf or a Neimark-Sacker bifurcation (Nayfeh and Balachandran, 2004).

Since, reporting a large number of flame images will not be possible, we have limited the number of image frames to eight. The differences between the trends in flame oscillation have been reported instead. The periodicity, which was present in the case of limit cycle oscillations, is absent in this case. The loss of periodicity can also be seen in the flame shape modulations (Fig. 6.18). Here, although images a, b, d, f and g correspond to local maxima in the pressure time series, each of them is significantly different from the other. Images c and h are observed for two local pressure minima. The image e, showing an elongated flame shape, is acquired while pressure around the flame location is building up towards a local maxima.

6.6.3 Frequency-locked Oscillations: Region IV

As the trajectories are moving on the surface of the torus, the frequencies become rationally related and lead to frequency-locked oscillations. In the power spectrum of the pressure and intensity time series (Figs. 6.15-IV a(iii) & -IV b(iii)), we see frequencies

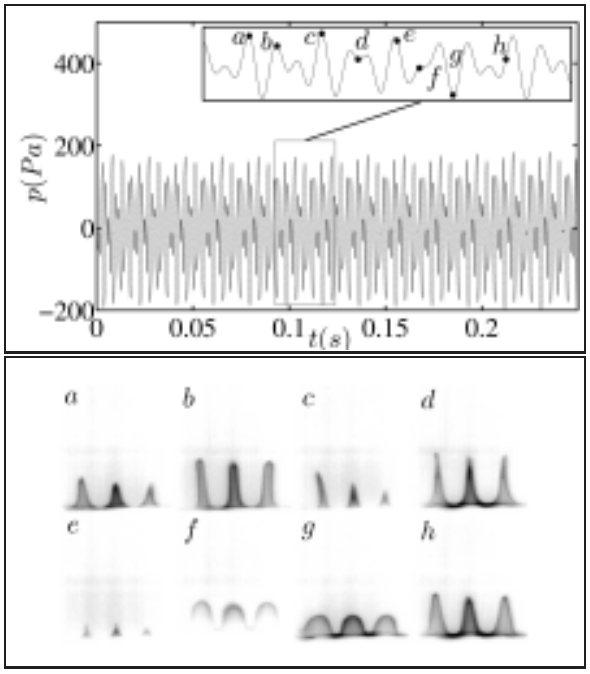

Figure 6.19: Instantaneous flame images for frequency-locked oscillations. The tagged dots in the pressure time series have corresponding flame images marked by the same lowercase alphabets as used for the tags.

that are rationally related to f_1, leading to a frequency-locked behavior (Hilborn, 2000). In the phase portrait (Figs. 6.15-IV a(i) & -IV b(i)), we find the trajectory no longer wanders on a torus, but instead, closes onto itself and hence, a periodic loop is formed. The time period is very long so we see many loops in the phase portrait. This is further seen in the Poincaré section (Figs. 6.15-IV a(ii) & -IV b(ii)) which has distinct points where the loop intersects the dotted Poincaré plane. The time taken by the system to complete one full cycle, seen in the time series, is equivalent to the time duration between point a and the local maxima adjacent to, and following point h (Fig. 6.19). Images $a - h$ correspond to different phases of the signal within this time duration.

Although oscillations are periodic in nature, since the total time period (time required for phase space trajectories to come back to the initial point) is much longer than a limit cycle, it is difficult to come to the same conclusion by looking at the instantaneous flame images. The flame oscillations are stronger when compared to limit cycle and quasi-periodic oscillations although the pressure amplitude from the time traces is the same. In image f, for example, the flame leaves the tip of the burner whereas in image e, it is on the verge of extinction. Images a, b, c and e are all at local maxima in the pressure time series, but each one has a completely different shape. The most

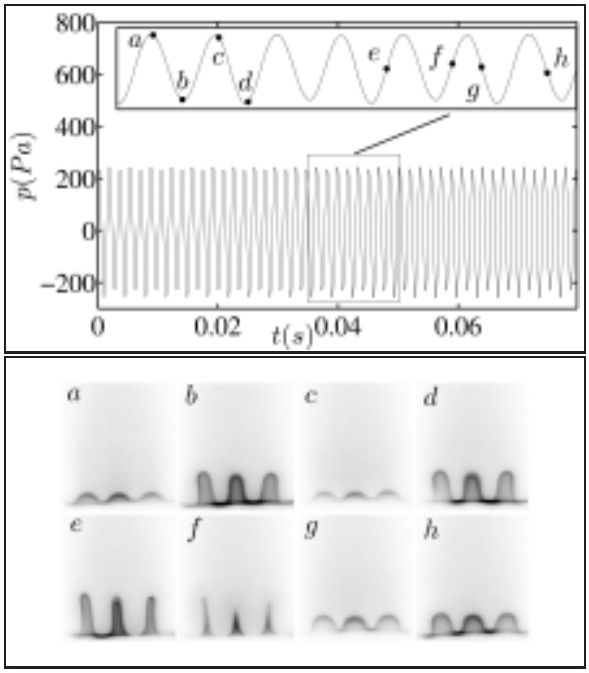

Figure 6.20: Instantaneous flame images for period-2 oscillations. The tagged dots in the pressure time series have corresponding flame images marked by the same lowercase alphabets as used for the tags.

interesting of the images shown is image c, where different flames in the multiple injection burner assume different lengths. As the flame location is varied, the flame location with respect to acoustic modes of the duct gets changed. The effect can be seen in flame images and also in the pressure and intensity time traces since the interaction is coupled.

6.6.4 Quasi-periodic Oscillations with Subharmonic Frequency Content: Region V

Following this state, the next bifurcation at $x_f = 25.5\ cm$, results in a quasi-periodic state where the strength of the frequency f_1 decreases and f_2 emerges as the dominating frequency along with a frequency $\frac{f_2}{2}$. This is region V in Fig. 6.14. The attractor for this case is similar to the one discussed for the quasi-periodic oscillations in region III, the difference being in the presence of a subharmonic. The dynamics is dominated mostly by quasi-periodicity, except for a small region (the bulge within region V, Fig. 6.14a), where the subharmonic content grows but subsides before the system eventually goes to a period-2 oscillation.

6.6.5 Period-2 Oscillations: Region VI

The quasi-periodic region with f_2 and its subharmonic now changes to a periodic oscillation, with frequency components f_2 and $\frac{f_2}{2}$ (Figs. 6.15-VI a(iii) & -VI b(iii)). The presence of a sub-harmonic leads to double-looped attractor in the phase space (Figs. 6.15-VI a(i) & -VI b(i)); i.e. the trajectories need to loop twice before coming back to the initial point. Since the orbit is periodic, we get two distinct dots in the single-sided Poincaré section for the pressure time series (Figs. 6.15-VI a(ii)) and set of four dots (scattered due to the noise in signal) in the double-sided Poincaré section (Figs. 6.15-VI b(ii)), in the case of flame intensity time series measurement.

In the flame shape modulations (Fig. 6.20), it can be seen that because of the period-2 nature, image frames separated by the time period corresponding to $2f_2$ are different. The pairs of images, *a* & *c*, *b* & *d*, *e* & *f* and *g* & *h* are each acquired almost at the same phase, separated by a time interval $\frac{1}{2f_2}$ and are different in their intensities due to the period-2 nature of oscillations. One period of the oscillations corresponds $\frac{1}{f_2}$.

As we vary the flame location gradually, the system moves from period-2 oscillation to a chaotic state via quasi-periodic states. The quasi-periodic route to chaotic oscillations has been observed in several nonlinear systems such as Taylor-Couette flow (Brandstäter *et al.*, 1983) and Rayleigh-Bénard convection (Gollub and Benson, 1980).

6.6.6 Chaotic Oscillations: Region VII

At the onset of region VII, a strange attractor (Nayfeh and Balachandran, 2004; Strogatz, 1994) emerges in the system. An attractor is termed as strange when its calculated dimension is not an integer i.e. when the structure is a fractal. There are several measures to estimate the dimension of a set of points (Moon, 2004; Grassberger and Procaccia, 1983). The correlation dimension is one such measure.

The correlation dimension calculated for the attractor shown in Fig. 6.15-VII a(i) observed in region (VII) is 2.63 - an indication that it is a strange attractor. To check if the oscillations are chaotic, we need to calculate the maximal Lyapunov exponent.

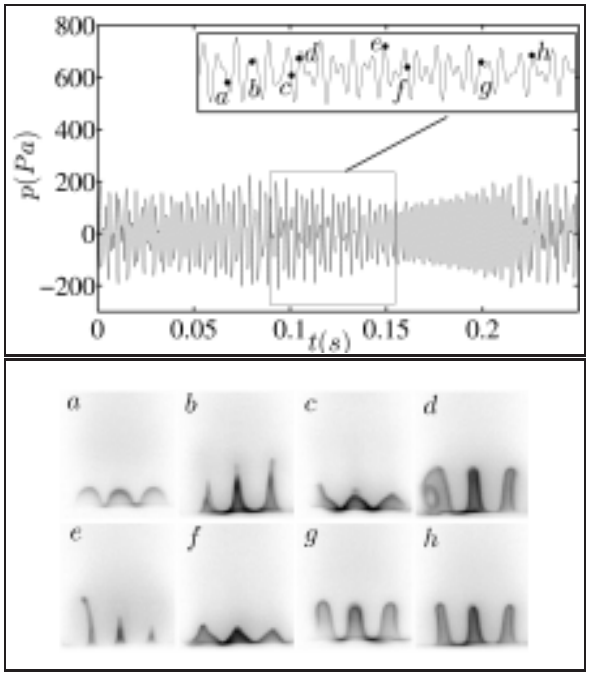

Figure 6.21: Instantaneous flame images for chaotic oscillations. The tagged dots in the pressure time series have corresponding flame images marked by the same lowercase alphabets as used for the tags.

The maximal Lyapunov exponent is a measure of the exponential divergence or convergence of neighboring trajectories of an attractor. A chaotic attractor will have at least one positive Lyapunov exponent. On application of Kantz algorithm (Kantz, 1994) for calculation of Lyapunov exponent for the chaotic attractor obtained here, we obtain a value of 0.16 which indicates that the attractor is chaotic. The route taken by our system to chaotic oscillations is the frequency-locking quasi-periodic route to chaos similar to that observed in the circle map (Hilborn, 2000). As the flame location is changed, several incommensurate frequencies appear in the oscillations which eventually merge to form spectrum with broadband frequency peaks, as seen in Figs. 6.15-VII a(iii) & -VII b(iii). The intersection of this chaotic attractor with the Poincaré plane as shown in Figs. 6.15-VII a(ii) & -VII b(ii) leads to a set of points scattered throughout the plane due to the chaotic nature of oscillations.

Figure 6.21 gives the flame shapes at various phases as marked in the pressure time series data. The chaotic nature of oscillations is reflected in the flame images. We find that the flame exhibits irregular modulations. Chaotic oscillations in the system are accompanied by rolling of the flame surface (image d), lifting-off (images c and g) and elongation (images b and e).

Following this chaotic state, the system jumps back to the stable state at $x_f = 48.5\ cm$. Going in the reverse direction (Fig. 6.14b) all the states discussed above appear again in exactly the reverse order but with a hysteresis in the flame location values where the different bifurcations occur.

6.7 Discussions

In summary, it can be said that thermoacoustic oscillations exhibit a variety of nonlinear phenomena. A simple laboratory combustor running on lean premixed combustion is used to illustrate this point. For a constant equivalence ratio, the system goes from a steady state to limit cycle oscillations through a subcritical Hopf bifurcation, as flame location is varied. This is followed by a second Hopf bifurcation (Neimark-Sacker bifurcation) to a quasi-periodic state. On changing the flame location further, the quasi-periodic state becomes a periodic, frequency-locked state marked by several distinct peaks in the frequency spectrum at rationally related frequencies. Further, the system goes to another quasi-periodic state with sub-harmonic frequency content. This state exists for a long range of control parameter values and is followed by period-2 oscillations. The next bifurcation leads to a chaotic state and eventually the system comes back to the steady state from the chaotic state directly. The complex nonlinear behavior of the system was reflected in the pressure time series, the flame intensity time series and simultaneously in the flame surface modulations in the instantaneous flame images. Nonlinear time series analysis made it possible to look at the oscillations through their phase space representation. This was instrumental in identifying the characteristics of oscillations and differentiating them from each other. A point to note further, is that due to the subcritical nature of the Hopf bifurcation, it is possible that, for different operating conditions, limit cycle oscillation is an unstable state. The self-excited oscillations at the Hopf point can be a period-2 oscillation generated via secondary bifurcation. In fact, when the experiments were performed for different equivalence ratios or flow rates, the self-excited oscillations obtained at the Hopf point were either period-2 or even quasi-periodic oscillations. A possible explanation for the rich nonlinear behavior is as follows. The phenomenon of combustion instability (in the system under study)

is a result of interaction between the flame and the duct acoustic modes. Depending on the flame location, different acoustic modes are excited. As a result, the acoustic fluctuations at the flame location (combination of excited acoustic modes of the duct) varies as the flame location is changed. The nonlinear response of the flames to this acoustic field that is varying with the flame location could lead to the emergence of complex nonlinear oscillations. This complex nonlinear behavior; i.e., bifurcations and different oscillation states, can also be observed if other parameters such as the equivalence ratio or the mean flow rate are chosen as the control parameter.

Thermoacoustic instability, in general, induces high amplitude pressure oscillations within combustion systems. Looking at the results from a practical standpoint, the presence of nonlinear oscillations such as quasi-periodic, frequency-locked and chaotic oscillations, will cause further increase in thermal and mechanical loading to the combustor walls. Thus, leading to premature failure, accelerated crack growth, amplified wear and tear of structural components and higher fatigue loading. All these factors contribute to the reduction in the life span of combustors (Suresh, 1998). Furthermore, limit cycle oscillations consist of a single dominant frequency whereas, other classes of oscillations consist of a range of frequencies, which might include frequencies close to the natural frequency of some of the structural components of the system. As a result, thermoacoustic oscillations can cause resonance in structural components leading to violent vibrations in the system or even structural failure. A controller designed to handle a single frequency or a set of frequencies might fail in the presence of frequencies that have not been considered in the design process. From the results on high speed flame images, it is also seen that along with changes in the frequency content of pressure signals, the flame dynamics drastically changes, giving rise to extreme behavior such as lift-off and flame extinction. Such behavior is also unfavorable for real practical systems.

6.8 Interim Conclusion

The above analysis presents that a simple thermoacoustic system can exhibit a rich variety of dynamics. In addition to limit cycle oscillations, we see states such as, quasi-

periodic, frequency-locked, period-2 and chaos as the bifurcation parameter is varied. It is well known that the flame dynamics plays a crucial role in the phenomenon of thermoacoustic instability. The observed oscillations were investigated in the light of nonlinear dynamics. Changing other parameters or changing the same parameter for different conditions will give a different trend, however, the characteristics of the observed oscillations are expected to remain similar. Nonlinear time series analysis enables us to obtain an understanding of the system dynamics purely through experimental data. The information acquired could be critical in constructing accurate models for thermoacoustic systems and designing effective control strategies.

CHAPTER 7

NONLINEAR COUPLED OSCILLATORS

7.1 Introduction

Investigations on scenarios of transition to chaotic dynamics has a special place in the study of nonlinear systems. It brings together physical systems from a variety of scientific disciplines. In the last few decades, several systems that exhibit common routes to chaos have been identified and studied intensely, both numerically and experimentally, providing evidence in support of the idea of universality in transition scenarios to chaos. Period doubling cascades (Ott, 1993), transition via intermittency (Manneville, 1990) and the Ruelle-Takens route to chaos (Ruelle and Takens, 1971; David *et al.*, 1982) are the most commonly observed routes to chaotic dynamics in nonlinear systems.

From a theoretical point of view, the nonlinear dynamical features of thermoacoustic systems have not been well explored yet. However, due to the significant relevance in many practical applications, a deeper theoretical understanding of thermoacoustic instability is required. In particular, low-dimensional models, that focus on the most significant aspects of the process, are essential to gain insight into the process. In Chapter 6, it was established that thermoacoustic instabilities in the prototypical premixed laminar flame-based Rijke tube system undergoes transition from limit cycle oscillations to chaotic oscillations via the Ruelle-Takens scenario. In an attempt to capture the various nonlinear states of thermoacoustic oscillations and the bifurcation scenario observed in experiments, a low dimensional model of a Rijke-tube system is investigated in this chapter. The results of a numerical bifurcation analysis on the model are in accordance with the experiments, where quasi-periodic transition was observed.

7.2 Low Dimensional Model

A four-dimensional model is derived that captures the complete bifurcation scenario observed experimentally in a thermoacoustic system (Chapter 6). The Rijke tube model has been studied to investigate thermoacoustic instability by several researchers (Balasubramanian and Sujith, 2008; Juniper, 2010; Subramanian *et al.*, 2010) and is considered here as a starting point. A reduction of the high-dimensional phase space to a few relevant modes is made for this specific system to capture the main physical interactions and nonlinearities found in any thermoacoustic system. A Rijke tube is an ideal representation of a thermoacoustic system that can be used for studying the features of thermoacoustic instability. It is a simple straight duct with heat source located at some location such that the heat source is compact with respect to the acoustic length scale. Its dynamics is governed by the linearized dimensionless momentum and energy equations for the acoustic field (Balasubramanian and Sujith, 2008)

$$\frac{\partial u}{\partial t} = -\frac{1}{\gamma M}\frac{\partial p}{\partial x} \tag{7.1}$$

$$\frac{\partial p}{\partial t} = -\gamma M\frac{\partial u}{\partial x} - \zeta \mathbf{p} + K\left[\sqrt{\left|\frac{1}{3}+u(t-\tau)\right|}-\frac{1}{\sqrt{3}}\right]\delta(x-\widetilde{x}_f) \tag{7.2}$$

where u, p, x and t are the dimensionless acoustic velocity, acoustic pressure, position along the axial direction and time, respectively, $\widetilde{x}_f$ is the dimensionless position of the flame, γ the ratio of specific heats of the medium, M the Mach number of the mean flow, K the dimensionless heater power and τ is a time delay [1] that makes explicit the effect of thermal inertia of the heat transfer on the acoustic velocity. ζ is the total amount of damping in the system so that, when we expand the acoustic velocity in Fourier series as $u = \sum_{q=-\infty}^{\infty}\alpha_q e^{iqx}$ we have, from Eqn. (7.1), $p = \sum_{q=-\infty}^{\infty}\frac{i\gamma M}{q}\dot{\alpha}_q e^{iqx}$ and $\zeta\mathbf{p} \equiv \sum_{q=-\infty}^{\infty} 2\zeta_q\omega_q\frac{i\gamma M}{q}\dot{\alpha}_q e^{iqx}$, where ζ_q is the damping coefficient of the mode q and the dot denotes time differentiation. By incorporating these expressions in Eqns. (7.1) and (7.2), a single ordinary differential equation for each mode q is obtained as

$$\ddot{\alpha}_q + a_q\alpha_q + b_q\dot{\alpha}_q = -K\left[\sqrt{\left|1+\sum_q(\alpha_q-\tau\dot{\alpha}_q)f_q\right|}-1\right] \tag{7.3}$$

[1] not to be mistaken as the time-delay for phase space reconstruction

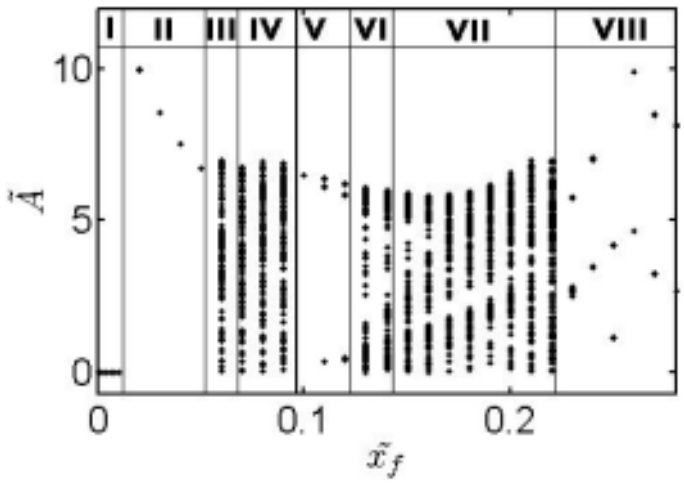

Figure 7.1: Bifurcation plot for the first oscillator. $\widetilde{A}$ is the amplitude of local maxima in the time series of the variable for various flame location $\widetilde{x}_f$. A configuration with both open ends is considered with parameter values, $K = 3$, $a_1 = b_1 = 1/4$ $a_2 = 3/4$ $b_2 = 0.1$ and $\tau = 0.4$ in Eqns. (7.4)-(7.7). The Roman numerals (I-VIII) are used to indicate the different regions in the bifurcation plot. Region I-steady state, II-limit cycle, III-quasi-periodic behavior, IV-chaos, V-period-two oscillation, VI-quasi-periodic behavior, VII-chaos, VIII-period-two oscillation.

where a small time delay approximation $\alpha_q(t-\tau) \approx \alpha_q - \tau\dot{\alpha}_q$ is introduced. Rescalings, $\alpha_q \rightarrow -2i\alpha_q e^{iqx_f}/3$, $K \rightarrow \frac{2K}{\gamma M\sqrt{3}}$ have been made and we have defined $f_q = ie^{2iqx_f}$, $a_q = q^2$ and $b_q = 2\zeta_q\omega_q$. After these transformations, it is observed that the R. H. S. of Eqn. (7.3) is the same for all Fourier modes. Since all modes with short wavelengths are strongly damped, only two dominant modes, q_1, and q_2 are considered. In the following text, labels 1 or 2 refer to either mode respectively. Further defining $x \equiv \alpha_1$, $y \equiv \dot{\alpha}_1$, $s \equiv \alpha_2 - \alpha_1$ and $z \equiv \dot{\alpha}_2 - \dot{\alpha}_1$, the following system of four coupled differential equations is obtained

$$\dot{x} = y \tag{7.4}$$

$$\dot{y} = -a_1 x - b_1 y - K\left[\sqrt{|1 + (x - \tau y)f_1 + (s - \tau z)f_2|} - 1\right] \tag{7.5}$$

$$\dot{s} = z \tag{7.6}$$

$$\dot{z} = -a_2 s - b_2 z + (a_1 - a_2)x + (b_1 - b_2)y \tag{7.7}$$

The parameters f_1 and f_2 will be real valued and will depend on the experimental

boundary conditions (by incorporating both f_q and f_{-q} within f_q). Boundary conditions allow the Fourier coefficients to have certain symmetry properties. For both open ends they are antisymmetrical i.e. $\alpha_q = -\alpha_{-q}$ while for open-close ends they are symmetrical $\alpha_q = \alpha_{-q}$. On substituting these expressions in the Fourier expansion the sum, previously going from $q = -\infty$ to $q = +\infty$ can be reduced to run between $q = 1$ and $+\infty$ (q=0 is excluded). For a Rijke tube with both ends open , we have $f_1 = -\cos(2q_1\widetilde{x}_f) - \cos(2q_2\widetilde{x}_f)$ and $f_2 = -\cos(2q_2\widetilde{x}_f)$. For a closed-open tube, $f_1 = \sin(2q_1\widetilde{x}_f) + \sin(2q_2\widetilde{x}_f)$ and $f_2 = \sin(2q_2\widetilde{x}_f)$. Since the nonlinear dynamical features can be generally described in terms of the parameters f_1 and f_2 and the values of these parameters include all possible boundary conditions through their specific functional relationships to the experimental control parameter $\widetilde{x}_f$, the model given by Eqns. (7.4) to (7.7) is universal for the class of systems that share the same bulk dynamics as the Rijke tube.

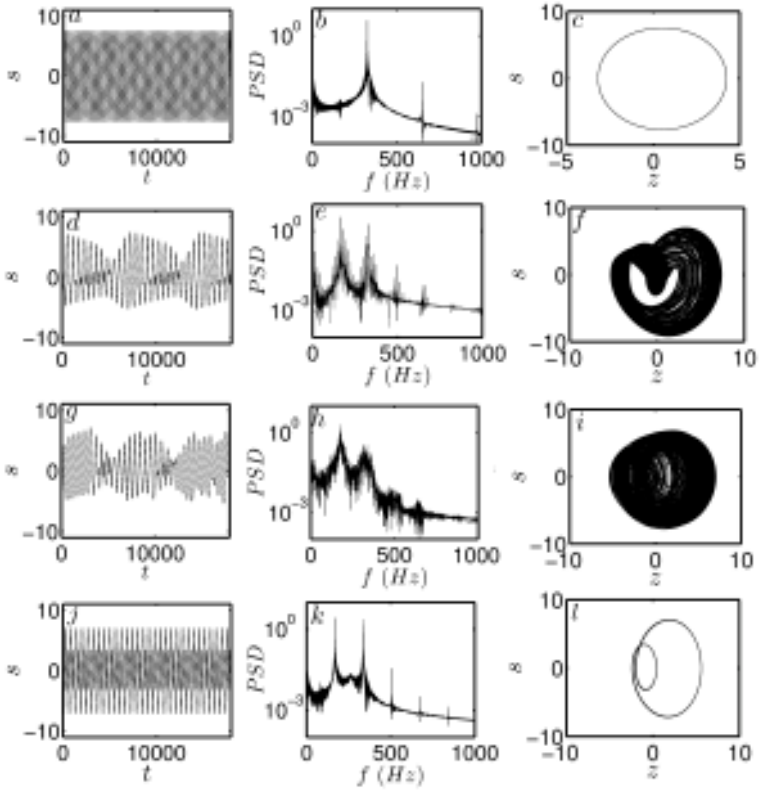

Figure 7.2: a-c: Time series for third oscillator s for limit cycle oscillation, d-f: quasi-periodic oscillation, g-i: chaotic oscillation, j-l:period two. Same parameter values as in Fig. 7.1

$(x^*, y^*, s^*, z^*) = (0, 0, 0, 0)$ is clearly a fixed-point of the system of Eqns. (7.4) to

(7.7). A linear stability analysis shows that it is stable at low $\widetilde{x}_f$ until a Hopf bifurcation occurs, at $f_{1,H} = 2b_1/(K\tau)$. A two-timing method performed on the above model, considering a small coupling of the oscillators and small velocities (the expansion is done around the fixed-point), shows that the bifurcation is subcritical: for a small perturbation around the unstable fixed point ($f_1 > f_{1,H}$) the perturbation grows linearly as $\approx |(x-\tau y)f_1+(s-\tau z)f_2|$. It tends to saturate only when $|(x-\tau y)f_1+(s-\tau z)f_2| >> 1$. In such a situation, the system ends performing a limit cycle of high amplitude. After the Hopf point, the system jumps discontinuously from a state of almost zero amplitude to an oscillatory state with amplitude higher than unity. This limit cycle of high amplitude disappears in a saddle node of periodic orbits when it encounters the unstable limit cycle arising from the Hopf, when $f_1 \lesssim f_{1,H}$.

7.3 Results and Discussions

Equations (7.4)-(7.7) were numerically integrated using MATLAB (R2009a) ode23s function, to obtain asymptotic system dynamics. The bifurcation plot obtained from the model Eqns. (7.4)-(7.7), with the non-dimensional flame location ($\widetilde{x}_f$) as the control parameter, is shown in the Fig. 7.1 where $\widetilde{A}$ is the amplitude of local maxima in the time series of the variable for various flame location $\widetilde{x}_f$. A configuration with both open ends is considered with parameter values, $K = 3$, $a_1 = b_1 = 1/4$ $a_2 = 3/4$ $b_2 = 0.1$ and $\tau = 0.4$ in Eqns. (7.4)-(7.7). Instability appears in the system after a subcritical-Hopf bifurcation of the steady state. At $\widetilde{x}_f = 0.02$, the emergence of limit cycle oscillations is observed. Time series and the frequency spectrum for this state is shown in Figs. 7.2 a and b respectively. As the flame location is varied further, quasi-periodic oscillations arise at $\widetilde{x}_f = 0.06$ as a result of a secondary Hopf-bifurcation. The corresponding time series and frequency spectrum are seen in Figs. 7.2 d and e. Due to the presence of incommensurate frequencies, the trajectory of the attractor makes a dense toroidal structure in the phase space (Fig. 7.2 f). In the Ruelle-Takens route to chaos, the quasi-periodic state is immediately followed by chaotic oscillations. This is also what is observed in our case. The toroidal structure develops distortions and the power spectrum shows the presence of broadband frequency components. This

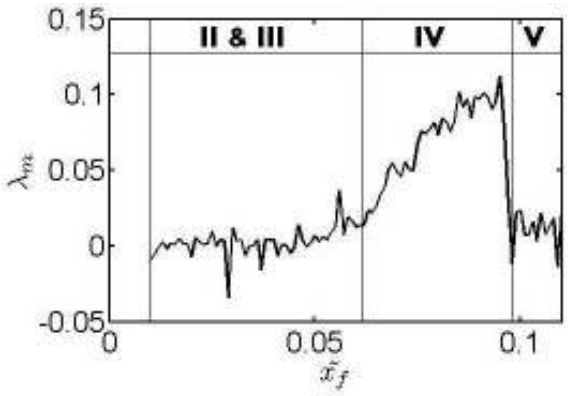

Figure 7.3: Maximum Lyapunov exponent for regions II, III, IV and V in the bifurcation diagram in Fig. 7.1 as a function of the dimensionless flame location $\widetilde{x}_f$. A transition from quasi-periodic behavior in region III to chaotic behavior, with a positive Lyapunov exponent, in region IV is observed. In region V, stable period-two oscillations are found and the Lyapunov exponent decays again to zero.

transition occurs at $\widetilde{x}_f = 0.07$. The phase space trajectories can be seen in Fig. 7.2 i.

The chaotic state is followed by periodic oscillations at $\widetilde{x}_f = 0.1$. This is a period-two oscillation as seen in Figs. 7.2 j, k and l, the corresponding time series, frequency spectrum and phase space trajectories. The period-2 region is again followed by another chaotic regime. The bifurcation diagram Fig. 7.1 summarizes the different transitions displayed by the thermoacoustic model. In other parameter regimes (results not shown) we found frequency-locked states, as also observed in the experiments (refer Chapter 6). A sequence of periodic and aperiodic oscillations and the appearance of two bands of chaotic oscillations has also been observed in a different physical context in the triatomic molecule by Tran *et al.* (1990). It is to be noted that, while the model in Tran *et al.* (1990) requires six equations, which are first order in time, our model requires only four, since it involves only two nonlinearly coupled oscillators.

In Fig. 7.3, the maximum Lyapunov exponent, calculated using the algorithm proposed by Sprott (2003), is shown for the first transition into chaos in the bifurcation diagram in Fig. 7.1. On the oscillatory regime with stable limit cycles or quasi-periodic behavior, the maximum Lyapunov exponent is zero indicating marginal stability. However, in region IV of the bifurcation diagram, a positive Lyapunov exponent proves the existence of chaotic behavior in such regime, a state that is reached from quasi-periodicity in Region III through the Ruelle-Takens route to chaos. This behavior is

also found in the experiments (Chapter 6). The model reproduces qualitatively all dynamical behavior found in the experiments as well as the whole bifurcation scenario.

It is to be noted that, since the frequency of the oscillations is not an experimental control parameter, the system cannot be externally tuned to have tori with frequencies arbitrarily close to the golden mean ratio on the quasi-periodic regime. The oscillations are intrinsic to the system, and although their frequency can be quantitatively estimated close to the fixed point at (0,0,0,0), the effective frequencies of the oscillators are significantly affected by the high amplitude of the limit cycles past the subcritical Hopf point. These limit cycles are highly non-harmonic because of the specific form of the nonlinearity and the transitions into chaos cannot be generally modeled in these situations by the circle map, since in the latter the coupling between the oscillators is harmonic.

This four-variable model can qualitatively describes the nonlinear dynamical behavior and routes to chaos found in experiments on the thermoacoustic instability. The model consists of two nonlinearly coupled oscillators, the first of them containing a square root nonlinearity that reflects the effect of the heat transfer on the acoustic field, and the second one being simply a linearly forced and damped oscillator. Further refinements of the model might include additional linearly forced oscillators like the second oscillator. It is remarkable that all effects of the nonlinearity can be accounted for in only one oscillator, which forces linearly all the others. This oscillator, containing the nonlinear term, is responsible for the main subcritical Hopf bifurcation structure found theoretically and in the experiments (Chapter 6). Because of its simplistic nature, the model also opens the possibility of devising systematic mechanisms for the control of the thermoacoustic instability, a concerning problem in many engines.

CHAPTER 8

CONCLUSIONS

The most important aspect of thermoacoustic instability that needs to be understood is the nonlinear interaction of the acoustic field with combustion and other processes active in the combustion zone. Previous studies have shown the existence of dynamics such as quasi-periodicity and chaos. The root of such nonlinear behavior and therefore, the inherent nonlinear nature of thermoacoustic instabilities however remains unclear.

The basis of this investigation is to conduct a deeper investigation of self-excited instabilities from the point of view of dynamical systems theory. The self-excited oscillations are studied through measurements of acoustic pressure within the duct, chemiluminescence and flame imaging. In particular, phase space based analysis is performed on the time series data of acoustic pressure and chemiluminescence. The information that can be derived from the results of this investigation indicates that nonlinearities involved in the thermo-acoustic coupling tend to conform to the universal behavior of general nonlinear systems that has been established through extensive numerical, analytical and experimental studies on different nonlinear systems. The most striking similarity is in the bifurcation scenarios that characterize transition from steady state to chaotic oscillations. These results are obtained on the most simple thermoacoustic system involving combustion, the laminar premixed flame driven Rijke tube. This suggests that the complex nonlinear states obtained in the bifurcation analysis are a result of inherent thermoacoustic interactions and not a manifestation of other complexities such as turbulence (in the base flow or the flame). It is to be noted however that, large scale hydrodynamic structure do play an important role as is inferred through modulations in the flame during different oscillatory states.

The investigation was first performed on a single flame based Rijke tube type system operating at a lean equivalence ratio. It was observed that limit cycle oscillations appear in the system as a result of a subcritical Hopf bifurcation. As the flame location is further varied, another bifurcation takes place leading to the emergence of quasi-periodic

oscillations through a secondary Hopf bifurcation. This is seen in the acoustic pressure time trace as well as in the power spectrum. The phase space structure formed by these oscillations resembles a toroidal structure. As the flame location is further varied, the smooth structure of the toroidal attractor as seen in the reconstructed phase space ruptures and eventually leads to burst oscillations. The dynamics is similar to what is referred to as intermittency in the theory of dynamical systems, where the dynamical behavior of nonlinear systems exhibits random transitions between stable oscillations and chaotic bursts. The chaotic bursts were found to be similar to the dynamical behavior of intermittency using return maps. Further, through recurrence analysis, intermittency was identified as a type-II intermittency. The intermittent state is followed by flame blowout. This observation suggests a connection between the phenomenon of thermoacoustic instability and the process of flame blowout. The bifurcation scenario clarifies how this connection becomes apparent. According to the bifurcation theory, once limit cycle undergoes transition to quasi-periodic oscillations, the system can undergo further transitions to chaos. In such a transition, intermittency is one of the standard intermediate states. However, as intermittency develops, the stabilization of the flame is repeatedly disturbed. At a certain point, prior to a transition to complete chaos, burst oscillations cause flame blowout to occur.

The issue of flame blowout continues to exist as a unsolved problem. This study provides a lead that could be further investigated to achieve a certain level of understanding of the phenomenon from the dynamical systems perspective. An inference is made directly from the investigations that intermittency can be seen as a precursor to flame blowout. In addition, results of flame imaging during the intermittent state, prior to blowout, indicate that inclusion of hydrodynamics is essential to model system dynamics. The strength of the hydrodynamic coupling varies from one oscillation state to another. For instance, hydrodynamic interactions play a dominating role during burst oscillations and the effect can be observed even in instantaneous line of sight flame images. This statement is a hypothesis based on flame imaging and needs further investigation. But it can clearly be stated that a complete exclusion of hydrodynamics will not capture full system dynamics.

The case of multiple flame configuration has also been investigated, again in the

frame work of dynamical systems theory through analysis of the phase space representation of the system and the bifurcation behavior. A variety of attractors - periodic, quasi-periodic and chaotic states, were observed in the system as the control parameter was changed. A route to chaos for thermoacoustic oscillations is established experimentally for the first time in a thermoacoustic system. It has been shown experimentally that as the location of the combustion source is gradually varied, self-excited periodic thermoacoustic oscillations undergo transition to chaos via the Ruelle-Takens scenario and the frequency-locking route to chaos. Modulations of the flame surface area were found to differ significantly from one oscillatory state to the other. During quasi-periodic and chaotic states, interaction of individual flames with each other was observed. These observations reveal new aspects of thermoacoustic oscillations.

In the last section of this investigation, a coupled oscillator model has been constructed to reproduce theoretically the nonlinear dynamical behavior and routes to chaos found in experiments on the thermoacoustic instability. The model consisted of two nonlinearly coupled oscillators. The first oscillator consisted of a square root nonlinearity used to model the effect of the heat release rate on the acoustic field. The second one was simply a linearly forced and damped oscillator. All the effects of the nonlinearity can be accounted for in only one oscillator, which forces the other oscillators linearly. This oscillator, containing the nonlinear term, is responsible for the subcritical Hopf bifurcation structure found theoretically and in the experiments. The coupled oscillator model was also found to capture the Ruelle-Takens bifurcation scenario and the associated nonlinear oscillatory states found experimentally.

Information on the nonlinear aspects of thermoacoustic instability reported in this thesis are quite critical for obtaining accurate models for thermoacoustic instability and designing effective control techniques. Nonlinear time series analysis enables us to obtain an understanding of the system dynamics purely from experimental data. Findings reported in this thesis has significant implications. Practical combustion systems are highly susceptible to frequencies corresponding to the natural modes of structural components, which can set the system to resonance and can lead to catastrophic failure. Such structural resonance is more likely to happen during quasi-periodic, mode-locked, chaotic and intermittent oscillations because of broadband spectral content. Addition-

ally, these aperiodic behavior are associated with variable amplitude, which will cause a higher fatigue loading to the structures compared to limit cycle oscillations and hence can reduce the performance and life span of the system.

CHAPTER 9

DIRECTIONS FOR FUTURE WORK

The main aspect that needs further investigation is the flow field interacting with the flame during thermoacoustic instability. Results have shown that hydrodynamics has a dominant role to play during the various nonlinear self-excited states. More insight into the phenomenon can be obtained by the identification of coherent structures in the flow that directly affect flame dynamics. Simultaneously, changes in the flow field in response to acoustic oscillations in the system during different nonlinear states needs characterization. Instantaneous flow field determination, for instance through high-speed Particle Image Velocimetry, will be required towards this end.

Secondly, to asses the universality of the results obtained and to asses the applicability of the inferences made to general thermoacoustic systems, similar investigations need to be conducted on more thermoacoustic systems, including other simple configurations such as the electrically heated Rijke tube, diffusion flame, V-flame and flat-flame systems. Such investigations accompanied with numerical and analytical investigations on nonlinear self-excited states, particularly with the incorporation of flame kinematics formulation in the presence of multiple frequencies and the effect of coherent flow structures.

Of equal importance is to investigate industrial systems with the application of dynamical systems theory and nonlinear time series analysis. Furthermore, the effect of nonlinear oscillations such as quasi-periodic, frequency locked and chaotic oscillations on structural components of combustion systems will be quite different when compared to limit cycle oscillations. Therefore, the effect of such highly nonlinear behavior in industrial systems should be evaluated. Such behavior of thermoacoustic instability could enhance crack growth which would eventually decrease the life span of the system. This may be unacceptable in gas turbines systems, where maximizing operating hours and minimizing maintenance is important.

The scenario of flame blowout in the single flame system investigated here opens up a new approach to looking at the phenomenon of flame blowout. Thermoacoustic instability was found to be associated with flame blowout and intermittency was found to be a precursor to flame blowout. Further investigation on these aspects of flame blowout is expected to yield new results and understanding. It is certain that flame stretch and strain effects become particularly important prior to flame blowout. The pinch-off behavior of the flame during quasi-periodic oscillations causes nonlinearities that are currently not accounted for in laminar flame response modeling. Investigations are required to evaluate the effect of features such as flame pinch-off and subsequent cusp formation. The strong participation of hydrodynamics in the process of repeated flame blowout has been hypothesized here. Analysis to ascertain the specific role of hydrodynamics in the process of thermoacoustic oscillations is essential.

The simple model presented in Chapter 7 is powerful enough to reproduce results obtained experimentally in Chapter 6. This model can be investigated and developed further by incorporating the effects of critical factors such as the temperature distribution within the duct. Numerical continuation analysis can be performed on the system of equations to understand the physics behind nonlinear phenomenon such as hysteresis.

APPENDIX A

INVESTIGATION OF SUBCRITICAL INSTABILITY IN DUCTED PREMIXED FLAMES

An experimental investigation of the bistable region of instability in a thermoacoustic system comprising of ducted, premixed laminar flames has been performed. The stability diagram of the system is obtained and the bistable region for a range of flame locations at different fuel-air mixture equivalence ratios is identified. Subsequently, threshold amplitudes for triggering instability in the system using externally introduced sinusoidal acoustic forcing, is obtained. It is observed that depending on how close the system is to the Hopf point and the nature of oscillations at the Hopf point, the triggered oscillations can exhibit different dynamical behavior.

The transition of a thermoacoustic system from steady equilibrium state (fixed point) to an oscillatory state, on variation of operating conditions occurs in two ways - through a supercritical Hopf bifurcation or a subcritical Hopf bifurcation (Lieuwen, 2002). In the first scenario, there exists a clear demarcation between steady and oscillatory states with respect to the bifurcation or control parameter. The transition from the stable to oscillatory state and vice versa is gradual and occurs exactly at the same parameter value. On the other hand, in the case of a subcritical Hopf bifurcation, as we vary the control parameter, at the critical (Hopf) point, the system jumps from steady equilibrium state to a high amplitude oscillation. While going in the reverse direction, transition back to the steady state does not take place at the Hopf point; the control parameter value needs to be changed further, till the fold point (Strogatz, 1994) to restore the steady non-oscillating state of the system. Thus, hysteresis in the system behavior is a manifestation of subcritical Hopf bifurcation (Lieuwen, 2002; Strogatz, 1994). This region of hysteresis is called the subcritical zone or the bistable zone. This bistable zone as we infer from the discussion alone, has two possible states - the steady state that exists when the zone is approached from a stable state and the oscillatory state that exists

when the zone is approached from an initially unstable state. At any operating condition, within the bistable zone, it is possible to 'trigger' the system from a stable state to the corresponding oscillatory state, through the introduction of finite amplitude perturbations. This phenomenon is known as triggering instability in the combustion instability parlance (Wicker *et al.*, 1996; Blomshield *et al.*, 1997; Lieuwen, 2002). Triggering instability is a concern because the subcritical region, where it occurs, is linearly stable but nonlinearly unstable; i.e. small amplitudes of perturbations will not cause transition but finite amplitudes might trigger instability. Hence, the classical stability analysis and the linear flame transfer function cannot predict triggering instability. In recent investigations, Noiray *et al.* (2008); Boudy *et al.* (2011), have reported, both experimentally and theoretically that using the nonlinear describing function, it is possible to predict various nonlinear characteristics of thermoacoustic systems such as triggering instability, mode switching and hysteresis. Previous studies reveal that thermoacoustic systems often exhibit subcritical Hopf bifurcation (Lieuwen and Banaszuk, 2005; Wicker *et al.*, 1996; Moeck *et al.*, 2008). Blomshield *et al.* (1997)reported observation of triggering instability during full scale tactical motor stability tests.

In this study, we investigate the bistable region of a simple laminar ducted premixed flame. The flame location with respect to the duct is used as the bifurcation parameter. We identify the bistable regions of the system for different fuel-air mixture ratios. Self-sustained oscillations are triggered in the system, within the bistable regions, through resonant forcing of the system. The triggering of self-sustained oscillations at different flame locations and fuel-air mixture ratios is then discussed. For a single equivalence ratio, we find that the amplitude required for triggering is dependent on the value of the control parameter - the flame location. The variation of triggering amplitude with respect to flame location is discussed. Finally, we discuss the phenomena of triggering instability within the framework of dynamical systems theory. We observe that attractors other than the limit cycle oscillations exist in the bistable zone. This has a bearing on the overall dynamics of the system in this zone. Based on the results, we support the conjecture that, an analogy could be drawn between triggering instability and bypass transition in hydrodynamic flows.

A.1 Experimental Setup

The bifurcation analysis is conducted on a premixed combustor, as depicted in Fig. A.1. A multipoint injection burner, similar to the configuration used by Matsui (1981) for flame transfer function measurements of premixed, laminar flames, is employed in this study. A similar burner configuration has also been used recently by Noiray *et al.* (2008) and Boudy *et al.* (2011) for nonlinear flame transfer measurements. The premixed burner has seven conical LPG (Liquefied Petroleum Gas) air premixed flames (A) anchored on a $18\ mm$ thick copper block. The top view of the burner is given on the top right of Fig. A.1. In preliminary experiments, it was observed that the onset of instability causes flame blowout. In order to facilitate investigation, a fine wire mesh is used to stabilize the flames. The burner tube (C) is $800\ mm$ long with an inner diameter of $14\ mm$ and thickness of $1.5\ mm$. The burner is connected to a decoupler (D) as shown, which is in turn connected to a premixing chamber (E) for enhanced mixing of the fuel and air. The burner is enclosed in a glass duct (B), $800\ mm$ long, closed at the bottom. This glass duct acts as the combustion chamber. During the experiments, the acoustic modes of the duct get coupled with the heat release rate fluctuations leading to self-excited oscillations. The volumetric fuel flow rate (V_f) is maintained at $64\ ccm$ and $72\ ccm$ and the volumetric air flow rate (V_a) at $3.7\ lpm$, measured using rotameters with an accuracy of 2%. The corresponding uncertainty in the equivalence ratio is estimated to be around 2.8%. For the results on bifurcation analysis, reported in this thesis, two cases, with the equivalence ratio, ϕ, at 0.50 and 0.57, have been studied.

Three pressure microphones (model:103B02, PCB piezotronics make), P1 , P2 and P3, flush mounted on the walls of the glass duct, as shown in Fig. A.1, were installed to monitor the unsteady pressure oscillations. The results reported here are based on pressure time series ($p(t)$) obtained from the microphone P1, which is mounted at a distance of $20\ cm$ from the top. A 16-bit analog to digital conversion card (NI-6143) was used for data acquisition which has a resolution of $0.15\ mV$ taking the input voltage range as $\pm 5V$. The uncertainty in pressure microphone measurement is 0.14 *Pa*. Two sub-woofers, driven by an amplifier connected to a function generator, are installed outside the duct, as shown in Fig. A.1, for generating acoustic signals. A microphone (P4) is mounted close to the sub-woofers to monitor the generated acoustic signals. The inten-

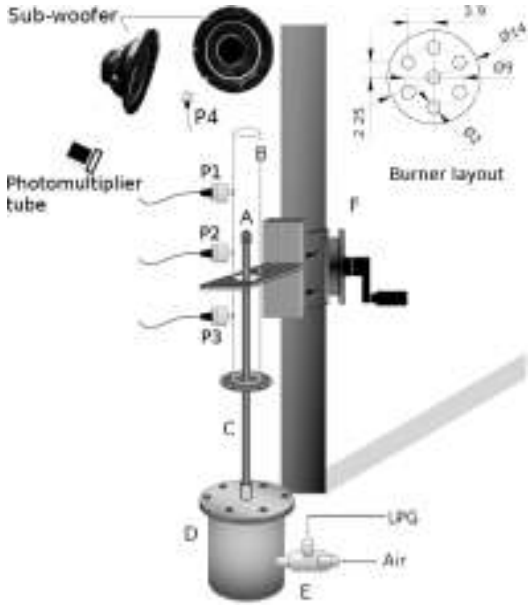

Figure A.1: Schematic of the setup, A-multiple flames, B-open-closed glass duct, C-burner tube, D-decoupler, E-LPG-Air premixer, F-Traverse, P1, P2, P3 & P4-pressure microphones. Two subwoofers , oriented towards the duct open end are mounted outside the duct for external excitation. Top view of the burner is given at the top right corner of the figure. All dimensions in mm.

sity fluctuations ($I(t)$), which are proportional to the heat release rate oscillations in the flame, were detected simultaneously with pressure oscillations using a photomultiplier tube (model no. H5784, Hamamatsu make) equipped with a *CH** filter (bandwidth $10\ nm$, centered at $431.4\ nm$). The flame location was measured using a ruler with least count $1\ mm$.

A.2 Results and Discussions

We focus here primarily on triggering instability and how the threshold amplitude changes with respect to the control parameter within the bistable region and the dynamics of triggered oscillations. It is possible to trigger instabilities in a thermoacoustic system by introducing a perturbation, in the bistable region, with a large enough perturbation. The perturbation (or the initial condition) given to the system governs the system evolution. However, unfortunately, in experiments, it is often quite difficult to introduce well-determined and controlled initial conditions. In this present investigation, we force

the system using sinusoidal acoustic forcing at the observed frequency of self-excited limit cycle oscillations at Hopf point of our system ($f = 563.4\ Hz$). This frequency is close to the second harmonic of a quarter-wave tube with length corresponding to the length of the glass duct used in the experiments.

In subcritical Hopf bifurcation, at the Hopf point, the stable equilibrium fixed point attractor losses its stability and a new branch - an unstable limit cycle is born. This branch is turned backwards and exists before the Hopf point, hence, the term subcritical bifurcation (Strogatz, 1994). A saddle-node bifurcation (Strogatz, 1994; Moon, 2004) of the unstable limit cycle creates a stable limit cycle branch. This branch can undergo further bifurcations on changing the control parameter gradually, as reported in Chapter 6. Beyond the Hopf point, all trajectories originating near the fixed point attractor spiral out and settle on the nearest attractor (Hilborn, 2000). Hence, we have three attractors in the subcritical zone, a fixed point, a limit cycle and an unstable limit cycle.

In order to identify the bistable region of the system, a stability map of the system is first constructed. The volumetric air flow rate (V_a) is fixed at $3.7\ lpm$. Stability of the system is then assessed for all flame location values, and volumetric fuel flow rates (V_f) in the range $56\ ccm - 80\ ccm$. This corresponds to a lean fuel-air mixture. The range is chosen to maintain well-stabilized conical-shaped flames. The stability diagram of the system is given in Fig. A.2. At each fuel-air mixture ratio, the flame location is gradually varied for both increasing and decreasing directions with respect to the open end of the duct. The system is identified as stable if self-sustained oscillations in pressure and intensity measurements are absent. On the other hand, the presence of such oscillations indicates instability. The dark grey shaded region in Fig. A.2 marks the linearly unstable regions, where the system is unconditionally unstable. As this region is approached from an initially stable state, oscillations arise spontaneously as the value of the flame location crosses the boundary of this region. The point at which this jump in the behavior of the system is observed is the linear stability boundary for the system corresponding to the particular operating condition (the Hopf point Strogatz, 1994). The light-shaded region is linearly stable, but nonlinearly unstable, as the system is unstable if approached from an unstable state and stable is approached from a stable state. This region, is known as the bistable region as two possible equilibrium states exist - the

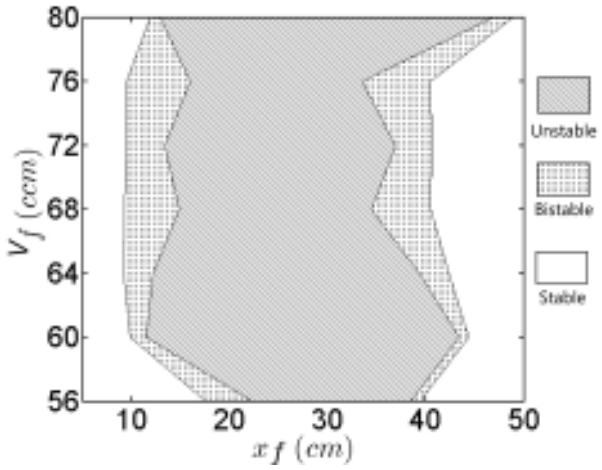

Figure A.2: Stability diagram of the system for an air flow rate ($V_a = 3.7\ LPM$). Flame location x_f measured from the open end of the duct. Shaded region is unstable irrespective of the state it is approached from. Dotted region corresponds to the bistable or subcritical zone. Other flame locations are stable. System remains stable beyond the range of flame location values shown in the plot.

stable state with no oscillations and an oscillating state which we call unstable. In present study we conduct experimental analysis of this region and discuss the results from a dynamical systems point of view.

It should be noted that the boundaries drawn are extremely sensitive to changes in the operating parameters, the magnitude of noise in the system and any changes in the system configuration. The aim of the present investigation is to study the system behavior in the bistable region. Establishing the sensitivity of the stability boundaries to noise and constructing a full stability diagram for all possible fuel-air combinations will be a topic of future investigations.

Experiments are performed first at $V_f = 64\ ccm$. At a flame location in the bistable region, $5\ mm$ from the Hopf point, we introduce acoustic forcing to the system ($f = 563.4\ Hz$), using sub-woofers mounted outside as shown in Fig. A.1. This forcing excites a single acoustic duct mode and also the flame surface area oscillations. The system evolution is reported in terms of reconstructed phase portraits (Abarbanel *et al.*, 1993) from pressure (from microphone P1, Fig. A.1) and intensity measurements. A phase portrait is extremely helpful in understanding the evolution of the dynamical system and the embedding theorem (Takens, 1981) enables one to reconstruct the phase portrait from data acquired experimentally. We will discuss briefly about phase space

reconstruction from time series data.

Since, the acoustic forcing is applied with frequency same one of the duct acoustic modes (the second harmonic), due to resonance, the pressure amplitude of oscillations within the duct are observed to grow. After a predetermined duration of time, the forcing is stopped and the system evolves on its own. The dynamics of the system then depends on the control parameter value and the amplitude gained by the oscillations by the end of the forcing. If a threshold amplitude is crossed in this process, self-sustained oscillations are set up in the system, otherwise, resonant growth is followed by a decay in the amplitude of oscillations.

To understand subcritical Hopf bifurcation and transition from stable equilibrium state to oscillatory state within the subcritical zone, we will introduce concepts from the dynamical systems theory. From the reconstructed phase space, Fig. A.3a, it is seen that the reconstructed trajectories of the system evolve from a steady equilibrium state (fixed point), as marked in Fig. A.3, and spirals out towards the inner black loop due to resonant amplification. The inner loop corresponds to the obtained threshold amplitude of oscillations that system needs to cross in order to get triggered. Forcing is discontinued at the time corresponding to the time taken by the trajectories to reach the inner loop. The system evolves on this threshold loop for a while before spiralling out again towards the self-sustained limit cycle state - the outer black loop in Figs. A.3a & b. If forcing is ceased earlier, or if it is continued for a longer time, oscillations will decay to the steady state or immediately grow exponentially to the self-sustained state. The same behavior is seen in the phase portrait reconstructed from flame intensity time series (Fig. A.3b).

In the case just discussed, the bistable region was found to be limited to $5\ mm$ (Fig. A.2). This restricts the number of flame locations that can be investigated for triggering. To overcome this limitation, we perform experiments with a different set of operating conditions ($V_a = 3.7\ lpm, V_f = 72\ ccm$). The bistable region for this set of operating conditions is wider with respect to the parameter space, allowing us to observe the differences in triggering amplitudes at different flame locations. In addition, self-sustained instabilities that emerge in the system at the Hopf point are period-2 oscillations instead of limit cycle oscillations. The time period of oscillation, for the case

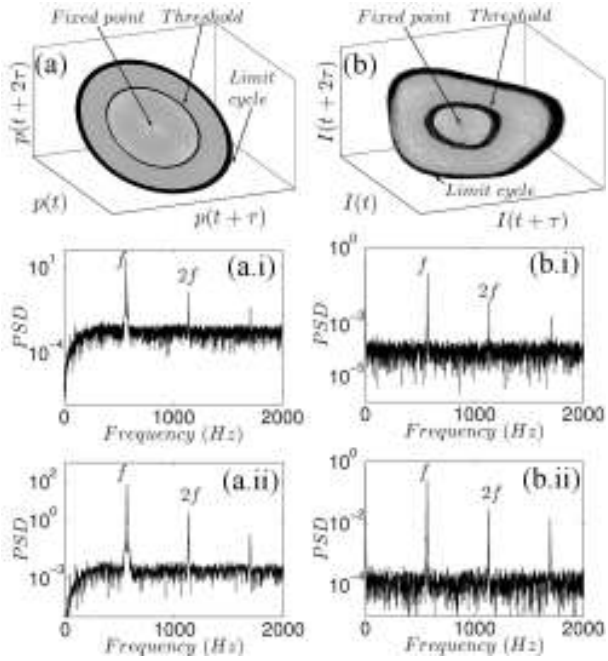

Figure A.3: Triggering to limit cycle oscillations. Figures a, a.i and a.ii correspond to phase portrait, power spectra after forcing is stopped and power spectra for self-sustained oscillations from pressure time series. Figures b, b.i and b.ii similarly are obtained from flame intensity (*CH**) time series.

Table A.1: Threshold amplitudes for triggering as given in Fig. A.5. The threshold amplitude is stated as the percentage of self-sustained oscillation amplitude.

Image	Flame Location (x_f)	Threshold amplitude (%)
a	10.4 cm	46.0
b	11.4 cm	30.8
c	11.9 cm	25.6
d	12.1 cm	12.1

of a period-2 oscillation is doubled when compared to limit cycle oscillations (hence, the name period-2). The Fourier spectrum, correspondingly, contains a subharmonic frequency and in the phase space representation, the attractor will be a doubled looped structure. This period-2 oscillation is a result of a period-doubling bifurcation that must have occurred in the parameter space prior to the Hopf point. Further analysis of the bistable region is required to illustrate the system dynamics within this region.

Similar experiments as discussed above are conducted in the bistable region for $V_f = 72\ ccm$ at four different flame locations in the bistable region. The threshold amplitudes are obtained for each flame location along with the amplitude of triggered

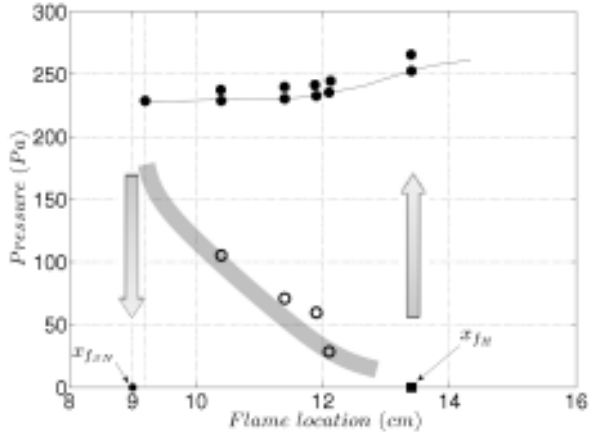

Figure A.4: Bistable region for $V_a = 3.7\ lpm$ and $V_f = 72\ ccm$. Filled circles indicate the amplitude of self-sustained oscillations. Double dots indicate period-2 oscillations. Empty circle represent threshold amplitudes required for triggering. Filled rectangle marks the hopf point. Hand drawn curves connect the experimentally obtained point. Arrows indicate jump in the system behavior.

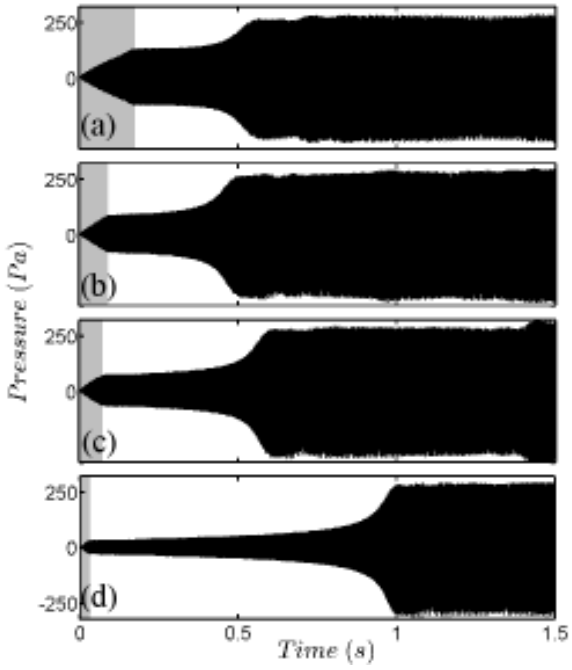

Figure A.5: Pressure time series for triggering instability via resonant forcing at different flame locations (Refer Table A.1). Shaded regions correspond to the duration of forcing.

oscillations. This information when plotted gives us Fig. A.4. As the control parameter (the flame location) is varied, self-sustained oscillations spontaneously arise at the point marked by a filled rectangular marker, x_{f_H} = 13.6 cm, the Hopf point, from a set of 20 readings, the standard deviation in the Hopf point location was found to be $0.46\ mm$. In the reverse direction, system jumps to steady non-oscillatory state at flame location, $x_f = x_{f_{SN}}$. This flame location is the point where the saddle-node bifurcation of the unstable limit cycle branch must have occurred. These two points mark the extremities of the bistable region. The arrows indicate a jump in the system behavior. Empty circles in the figure denote the threshold amplitudes obtained at different flame locations and filled circles represent the amplitude of triggered self-sustained oscillations, the two filled circles for each flame location represents the local maxima of the measured pressure time series.

Table A.1 gives the threshold amplitudes as a percentage of the triggered oscillations. In Fig. A.4, hand drawn curves have been drawn connecting the experimentally obtained points to get an idea of the trend followed by triggering amplitude using resonant forcing. Since, the triggering amplitude cannot be pinpointed exactly, a band has been drawn instead of a sharp line. Furthermore, the triggering amplitude inherently depends on the type of forcing or disturbance given to the system (Wicker *et al.*, 1996).

Time traces from pressure microphone P1 (see Fig. A.1) corresponding to triggering at the four flame locations is given in Fig. A.5a-d. The grey shaded region in the figure corresponds to the time duration for which sinusoidal resonant forcing is provided. The amplitude of pressure oscillations remains constant for a few cycles and grows exponentially towards period-2 oscillations. Reconstructed phase portraits and power spectra corresponding to Fig. A.5c are given in Fig. A.7. The period-2 nature of triggered oscillations is evident from the power spectra of pressure and intensity time series (Fig. A.7a.ii & b.ii) which contains the dominant frequency f and its subharmonic $f/2$. In the phase portraits (Fig. A.7a & b) three outer loops are seen. This is because the system first goes to limit cycle oscillations (single loop) and immediately transitions to period-2 oscillations (refer Fig. A.6). The frequency component of the signal in Fig. A.7a.i & b.i again indicates that system dynamics fills more than two dimensions.

The dynamical properties of a nonlinear system and changes in the dynamics as a

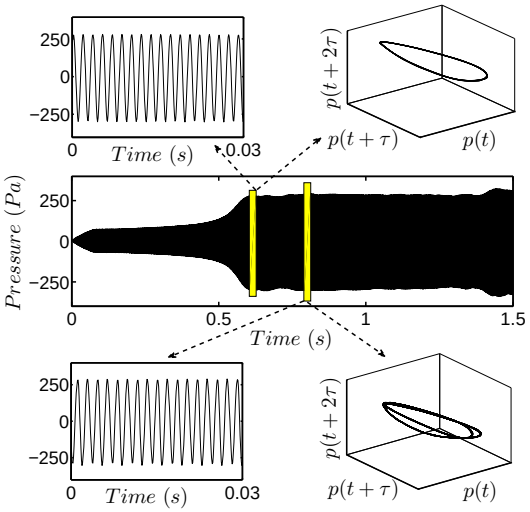

Figure A.6: Detailed analysis of time series showed in Fig. A.5c. Oscillations first get triggered to a limit cycle state and then immediately goes to a period-2 state. a, b represent the time series and phase portrait of the limit cycle state and c, d are obtained from a period-2 state of the triggered oscillations. The thin horizontal lines in figures a and c pass through the local maxima and minima of the signal. For a period-2 state three lines are given indicating one local maxima lines and two local minima values are possible.

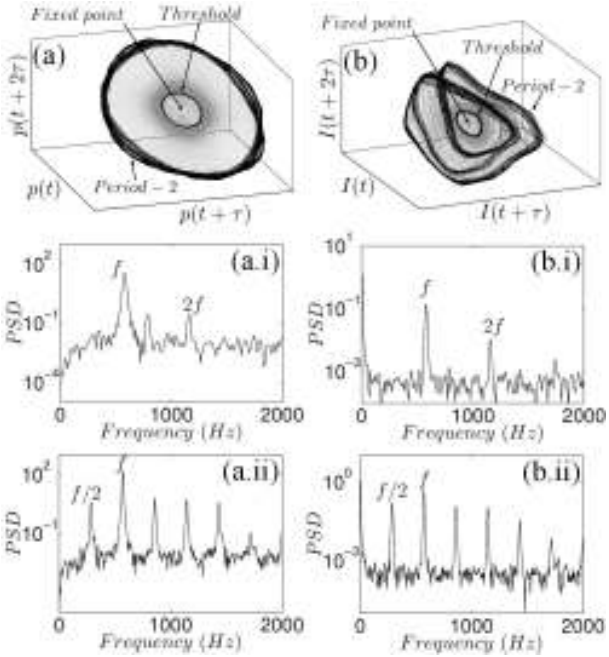

Figure A.7: Triggering to period-2 oscillations. Figures a, a.i and a.ii correspond to phase portrait, power spectra after forcing is stopped and power spectra for self-sustained oscillations from pressure time series. Figures b, b.i and b.ii similarly are obtained from flame intensity time series.

result of bifurcations can be studied in a vector space formed by the state variables of the system (Moon, 2004) - the phase space. A system with n degrees of freedom can be represented in an n-dimensional phase space constructed by the state variables . The phase space is filled by trajectories that denote the evolution of the system starting from a point in the phase space - the initial condition in terms of state variables. Every point in the phase space is a possible initial condition. Embedded in this phase space are sets of points called attractors. Trajectories are attracted towards these attractors and eventually evolve on them, once transients have died. Hence, there exists a set of points in the phase space such that trajectories originating from those points settle on one of the attractors present in the phase space. This set forms the basin of attraction for that particular attractor (Moon, 2004). Figure A.8 illustrates the concept of attractors and their basin of attraction in a 3-dimensional phase space. It can be seen that the evolution depends on the direction in which disturbance has been given and the amplitude. If the given disturbance is such that the system has entered the vicinity of the dark region of the Fig. A.8, then the system eventually will settle to the attractor A2 and if the disturbance is such that instead of falling in the dark region it falls in the grey region then it eventually settles to the attractor A1. In a real system, there could be other attractors embedded in the phase space. The dark patch in the Fig. A.8 is the basin of attraction of the attractor A2 and the grey is the basin of attraction for A1. The boundary which separates the basins of attraction is called basin boundary. The Fig. A.4 is the obtained result of the present study which explains that there is existence of more than two attractors in the subcritical zone.

Phase space representation of results as discussed in this section reveals the interesting dynamics in the bistable region. The extent of the bistable region is highly dependent on the system and the operating conditions. Additionally, the stability boundaries are strongly affected by the presence of noise and other disturbances in the system. Having said that, it is still possible to study the general properties of the bistable region in thermoacoustic systems. For the model thermoacoustic setup discussed here, we observe that for two different operating equivalence ratios, the self-excited oscillations at the Hopf point exhibit two different dynamics - limit cycle and period-2 oscillations. The limit cycle is a result of a subcritical Hopf bifurcation and the period-2 oscillation results from a standard period doubling bifurcation (Hilborn, 2000; Strogatz, 1994).

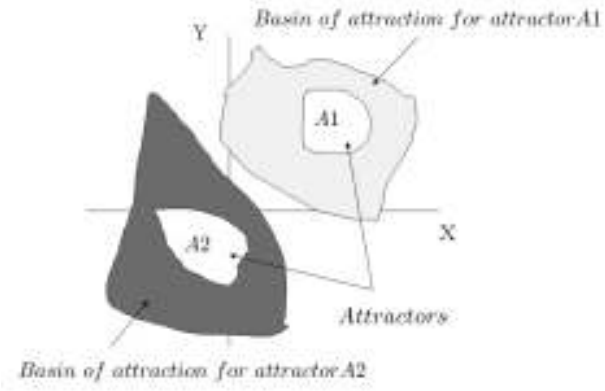

Figure A.8: A sketch of basin of attraction in phase space, A1 and A2 are different attractors, they are surrounded by their own basin of attraction, the line bounding the each basin of attraction is called separatrix. Adapted from Hilborn (2000)

.

For the same system as discussed here, it is possible that the system undergoes further bifurcations to chaotic oscillations as reported in Chapter 6. In practical systems with a higher degrees of freedom and several control parameters, it is expected that such behavior will be more significant and complex.

Another approach of looking at the results is through the idea of basins of attraction. The phase space of the dynamical system as explained above has regions which attract the system dynamics - the attractors, each having its own basin of attraction and a basin boundary. For the results reported here, the system has basins of attraction belonging to three stable attractors namely, the fixed point, limit cycle oscillation and period-2 oscillation. Depending on the operating conditions and amplitude of oscillations present, the system goes to one of the attractors. Again, larger and more complex systems can be expected to have a more complicated phase space structure. This has direct bearing to the implementation of control approaches and the safe operating range of thermoacoustic systems.

Although the structure of the phase space is responsible for the asymptotic states assumed by the system, the transition scenario from a fixed point to another attractor, within the bistable region, is observed to be same for the two different cases seen here. On introduction of the acoustic forcing, the oscillation amplitude grows and depending on the amplitude level at the time forcing is ceased, system goes to a self-excited state

or back to the fixed point state. A special case occurs when the amplitude is just at the threshold level. The oscillations then continue at the same amplitude level for a certain time, before growing towards one of the stable attractors (limit cycle or period-2, in the cases presented here).

An analogy could be drawn between the observations in the obtained results and the scenario of bypass transition to turbulence observed in hydrodynamic flows (Drazin, 1992). For hydrodynamic flows, the basins of attraction of the chaotic attractor, corresponding to turbulence and the fixed point attractor, corresponding to the laminar state are separated by a basin boundary. Similarly, the oscillatory limit cycle state and the fixed point steady state are separated here by an unstable limit cycle. The unstable limit cycle lies on the surface of the basin boundary and is like a separatrix which separates the two basins of attraction (Duguet *et al.*, 2008). If initial perturbations take the system across the basin boundary, into the basin of attraction of the stable limit cycle oscillations, system evolves to the self-sustained oscillatory state. If the initial condition falls within the basin of attraction of the stable fixed point state, oscillations decay to zero. A similar explanation has been given by Juniper (2010) for the occurrence of triggering instability in thermoacoustic systems. In the subcritical region, thermoacoustic systems have two competing attractors - the fixed point and the self-sustained oscillatory state, separated by an $N-1$- dimensional basin boundary surface, where N is the number of degrees of freedom of the system.

The characteristics of the disturbance introduced to the system within the bistable region determines the threshold amplitudes required for triggering in addition to deciding the attractor that attracts the system dynamics. This is in accordance with the above discussion on the basin of attraction. Wicker *et al.* (1996) had discussed their numerical analysis on triggering instability in rocket motors with a similar conclusion. This inherent property of dependence on the type of disturbance could be because of the complex structure of the basin boundary. If the basin boundary is a hypersurface enclosing a finite region in the phase space created out of state variables and containing the fixed point attractor, the direction and magnitude of the initial condition vector will determine if the system is taken out of the basin boundary of the fixed point. Depending on the structure of the basin boundary, certain directions might be more favourable (in terms

of amplitude required for transition) and hence, a lower magnitude of perturbation will be required when compared to initial conditions in other directions.

In this study, the system is forced using a single frequency acoustic excitation. Equivalently, the phase space representation (Fig. A.3 and Fig. A.7) shows the evolution to be localised on a plane (a dimensionality of two). Through several experiments we have determined the amplitude which is just enough for the system to evolve to self-sustained oscillations - either a limit cycle or a period-2 oscillation. The frequency of forcing was chosen as the second harmonic of the duct since it was found to be most effective in establishing interaction between flame oscillations and acoustics of the duct. The point where forcing is ceased is the initial condition from where the system evolves on its own. Before getting attracted towards the limit cycle or period-2 oscillation, oscillations stay at a constant amplitude for a certain interval of time (oscillations at the threshold or the inner loops in Fig. A.3 a & b and Fig. A.7 a & b). The superharmonics observed in the power spectrum while the oscillation is at the threshold amplitude indicate that the dimensionality of the system during that time interval is higher than two. This state corresponds to an unstable attractor towards which the system is initially attracted before going towards a stable attractor. Additionally, the fact that this unstable attractor has a dimension higher than two indicates that the basin boundary is a structure more complicated than a simple loop.

A.3 Conclusions

In the present study, experimental investigation of the bistable region in a simple laminar ducted premixed flames, with respect to the flame location has been conducted. Resonant acoustic forcing is used to drive oscillations in the system. The evolution of the system after the external forcing is discontinued is recorded in terms of pressure and heat release rate through flame intensity time series data. In the bistable region for our system, it was observed that instability could be triggered in the system, which is linearly stable, if oscillations are forced beyond certain threshold amplitude. Two cases with different equivalence ratios were chosen for experiments. In the first case, we found that limit cycle oscillations emerged in the system as the control parameter

crossed the Hopf point. The triggered oscillations also were limit cycles oscillations. Whereas, in the second case, the self-sustained oscillations at the Hopf point and the triggered oscillations in the bistable region were period-2 oscillations. The threshold amplitudes for triggering thermoacoustic oscillations via resonant acoustic forcing is determined for the latter case for different flame locations and a bifurcation plot for the bistable region is constructed.

This study, if seen from a dynamical systems perspective, probes into the subcritical zone through a specific section in the phase plane which is determined by the sinusoidal acoustic forcing provided. This forcing takes the system towards the unstable limit cycle which lies on the basin boundary between the fixed point attractor and the stable limit cycle attractor. From the phase space and power spectrum, it is clear that the phase space trajectories evolve on a surface which is closely, but not exactly aligned with the unstable limit cycle loop. In the bistable region as the flame location is changed, the extent of the unstable limit cycle loop changes. The shape and extent of the corresponding basin boundary is also expected to change as the flame location is varied. The basin boundary could be a complex structure, but the unstable limit cycle is a loop on that basin boundary. Investigation in the bistable region by using different shapes of perturbations will help to explore the overall structure of the basin boundary. These observations of the bistable zone could aid in improving currently available techniques for prediction of thermoacoustic instabilities.

APPENDIX B

Algorithms

Algorithm B.0.1: AVERAGE MUTUAL INFORMATION(τ)

comment: Calculating the average mutual information, for a given time-delay

Input time series (T1)

Specify time-lag, τ

Create time-lagged time series (T2), using T1 and τ

Divide the amplitude range of T1 (or T2) into N bins

$L = length(T1) = length(T2)$

Initialize: $AMI = 0$

for $i \leftarrow 1$ **to** N

do
- **for** $j \leftarrow 1$ **to** N
- **do**
  - $A =$ (Count #[All x in T1 such that x $\in$ (i^{th} bin)])
  - $B =$ (Count #[All y in T2 such that y $\in$ (j^{th} bin)])
  - $AB =$ (Count #[All x in T1, y in T2 such that x $\in$ (i^{th} bin) AND y $\in$ (j^{th} bin) simultaneously])
  - $Pa = A/(L - \tau)$
  - $Pb = B/(L - \tau)$
  - $Pab = AB/(L - \tau)$
  - $AMI = AMI + Pab \times \log_2(Pab/(Pa \times Pb))$

Algorithm B.0.2: FALSE NEAREST NEIGHBORS(d, τ)

comment: Calculating percentage of false nearest neighbors

Input time series (T)

Specify time-delay, τ

Specify dimension to be evaluated, *d*

$D =$ points in *d*-dimensional reconstructed phase space

$D1 =$ points in (*d*+1)-dimensional reconstructed phase space

$L = length(D)$

$\Theta =$ threshold to identify false neighbors†

Initialize: $FNN = 0$

for $i \leftarrow 1$ **to** L

do
- $X_D(i) =$ Current point in D
- $Y_D(i) =$ Nearest neighbor to $X_D(i)$ in D
- $\Delta_D(i) = ||X_D(i) - Y_D(i)||$
- $X_{D+1}(i) = X_D(i)$ in D1
- $Y_{D+1}(i) = Y_D(i)$ in D1
- $\Delta_{D+1}(i) = ||X_{D+1}(i) - Y_{D+1}(i)||$
- $\Delta = |\Delta_D(i) - \Delta_{D+1}(i)|$
- **if** $\Delta > \Theta$
  - **then**
    - $(X_D(i), Y_D(i))$ is a false nearest neighbor pair
    - $FNN = FNN + 1$

Calculate the percentage of false nearest neighbors

The dimension, *d* at which the percentage of false nearest neighbors goes to 0 is the optimum dimension for phase space reconstruction.

† Recommendations for optimum thresholds can be found in Nayfeh and Balachandran (2004); Moon (2004).

Algorithm B.0.3: CORRELATION DIMENSION(d, τ)

comment: Calculating the correlation dimension of a reconstructed attractor

Input time series (T)

Specify time-delay, τ

$D =$ points in *d*-dimensional reconstructed phase space

$L = length(D)$

$R_{min}, R_{max} =$ minimum and maximum radius (r) to check for a scaling in the correlation integral C†

Initialize: $C(r) = 0$

for $n \leftarrow 1$ **to** L

do
- **for** $r \leftarrow R_{min}$ **to** R_{max}
  - **do**
    - $X(n) =$ Current point in D
    - $X_i(n) =$ Other points in D
    - $N(n, r) = H(r - |X(n) - X_i(n)|),\ H$ here is the Heaviside function
    - $C(r) = C(r) + N(n, r)$

$C(r) = C(r)/L^2$

Within the scaling region, $C(r) \propto r^{\nu}$, where ν gives the correlation dimension. Scaling between the correlation integral and r will exist for a small r, compared to the attractor size.

† R_{min} and R_{max} will depend on the size of the recontructed attractor.

Algorithm B.0.4: MAXIMAL LYAPUNOV EXPONENT(d, τ)

comment: Calculating the maximal Lyapunov exponent in a reconstructed attractor

Input time series (T)

Specify time-delay, τ

Define a neighborhood size, $\epsilon^{\dagger}$

$\Delta n_{min}, \Delta n_{max} =$ range of time-steps to be considered for evaluating S

$D =$ points in *d*-dimensional reconstructed phase space

$L = length(D)$

Initialize: $S(\Delta n) = 0$

for $i \leftarrow 1$ **to** L

do { **for** $\Delta n \leftarrow \Delta n_{min}$ **to** Δn_{min}

do { $X_{i+\Delta n} =$ Current point in D shifted in time by Δn

$X^{j}_{i+\Delta n} =$ Points within ϵ neighborhood of X_i, shifted by Δn

$D(i, \Delta n) = \sum_{j} |X_{i+\Delta n} - X^{j}_{i+\Delta n}|$

$D(i, \Delta n) = D(i, \Delta n)/\epsilon$

$$S(\Delta n) = \frac{1}{L} \sum_{i} \ln D(i, \Delta n)$$

For a chaotic system, $S(\Delta n)$ will vary linearly with Δn in a certain intermidiate range of Δn values. The slope of this linear curve gives the maximal Lyapunov exponent.

† Size of the neighborhood, ϵ, should be chosen with consideration to several factors such as the amount of noise in the data and the total number of points considered. For a detailed discussion, see Kantz (1994)

REFERENCES

1. **Abarbanel, H. D. I.**, *Analysis of Observed Chaotic Data*. Springer-Verlag New York, Inc., 1996.

2. **Abarbanel, H. D. I.**, **R. Brown**, **J. J. Sidorowich**, and **L. S. Tsimring** (1993). The analysis of observed chaotic data in physical systems. *Reviews of Modern Physics*, **65**, 1331–1392.

3. **Almela, P. R.**, **D. Fanaca**, **C. Hirsch**, **T. Sattelmayer**, and **B. Schuermans** (2010). Determination and scaling of thermoacoustic characteristics of premixed flames. *International Journal of Spray and Combustion Dynamics*, **2**(2), 169–198.

4. **Ananthkrishnan, N.**, **S. Deo**, and **F. E. C. Culick** (2005). Reduced-order modeling and dynamics of nonlinear acoustic waves in a combustion chamber. *Combustion Science and Technology*, **177**(2), 221–248.

5. **André, S. P. N.**, **B. H. S. Bruno**, and **G. Lino** (2009). Parameter identification for a low order network model of combustion instabilities. *International Journal of Spray and Combustion Dynamics*, **1**(1), 113–142.

6. **Baillot, F.**, **D. Durox**, and **R. Prudḥomme** (1992). Experimental and theoretical study of a premixed vibrating flame. *Combustion and Flame*, **88**, 149–168.

7. **Balasubramanian, K.** and **R. I. Sujith** (2008). Thermoacoustic instability in a Rijke tube: non-normality and nonlinearity. *Physics of Fluids*, **20**, 61–67.

8. **Batiste, O.**, **E. Knobloch**, **I. Mercader**, and **M. Net** (2001). Simulations of oscillatory binary fluid convection in large aspect ratio containers. *Physical Review E*, **65**, 016303.

9. **Becker, H. A.** and **T. A. Massaro** (1968). Vortex evolution in a round jet. *Journal of Fluid Mechanics*, **31**, 435–448.

10. **Bérge, P.**, **M. Dubois**, **P. Manneville**, and **Y. Pomeau** (1980). Intermittency in Rayleigh-Bénard convection. *Journal de Physique Letters*, **41**, 341–345.

11. **Birbaud, A. L.**, **D. Durox**, and **S. Candel** (2006). Upstream flow dynamics of a laminar premixed conical flame submitted to acoustic modulations. *Combustion and Flame*, **146**(3), 541–552.

12. **Blomshield, F. S.**, **J. E. Crump**, **H. B. Mathes**, **R. A. Stalnaker**, and **M. W. Beckstead** (1997). Stability testing of full-scale tactical motors. *Journal of Propulsion and Power*, **13**(3), 349–366.

13. **Bloxsidge, G. J.**, **A. P. Dowling**, **N. Hooper**, and **P. J. Langhorne** (1988). Reheat buzz: an acoustically coupled combustion instability .2. theory. *Journal of Fluid Mechanics*, **193**, 445–473.

14. **Bondar, M. L.** (2007). *Acoustically perturbed Bunsen flames: modelling, analytical investigations and numerical simulations*. Ph.D. thesis, Technische Universiteit Eindhoven, Eindhoven, The Netherlands.

15. **Boudy, F.**, **D. Durox**, **T. Schuller**, and **S. Candel** (2011). Nonlinear mode triggering in a multiple flame combustor. *Proceedings of the Combustion Institute*, **33**, 1121 – 1128.

16. **Bourehla, A.** and **F. Baillot** (1998). Appearance and stability of a laminar conical premixed flame subjected to an acoustic perturbation. *Combustion and Flame*, **114**, 303–318.

17. **Boyer, L.** and **J. Quinard** (1990). On the dynamics of anchored flames. *Combustion and Flame*, **82**(1), 51–65.

18. **Brandstäter, A.**, **J. Swift**, **H. L. Swinney**, **A. Wolf**, **J. D. Farmer**, **E. Jen**, and **P. J. Crutchfield** (1983). Low-dimensional chaos in a hydrodynamic system. *Physical Review Letter*, **51**, 1442–1445.

19. **Broomhead, D. S.** and **G. P. King** (1986). Extracting qualitative dynamics from experimental data. *Physica D: Nonlinear Phenomena*, **20**, 217–236.

20. **Burnley, V. S.** and **F. E. C. Culick** (2000). Influence of random excitations of acoustic instabilities in combustion chambers. *AIAA Journal*, **38**, 1403–1410.

21. **Candel, S.** (2002). Combustion dynamics and control: progress and challenges. *Proceedings of the Combustion Institute*, **29**(1), 1–28.

22. **Cho, J. H.** (2005). Laminar premixed flame response to equivalence ratio oscillations. *Combustion and Flame*, **140**, 116–129.

23. **Clavin, P.** (1985). Dynamic behavior of premixed flame fronts in laminar and turbulent flows. *Progress in Energy and Combustion Science*, **11**(1), 1–59. ISSN 0360-1285.

24. **Crocco, L.** and **S. Cheng** (1956). Theory of combustion instability in liquid propellant rocket motors. *Technical Report Rep 0429886, RTO AGARDorgraph. Butterworths London*.

25. **Crocco, L.** and **C. E. Mitchell** (1969). Nonlinear periodic oscillations in rocket motors with distributed combustion. *Combustion Science and Technology*, **1**, 147–169.

26. **Culick, F. E. C.** (1970). Stability of longitudinal oscillations with pressure and velocity coupling in a solid propellant rocket. *Combustion Science and Technology*, **2**(4), 179–201.

27. **Culick, F. E. C.**, Some recent results for nonlinear acoustics in combustion instabilities. *In AIAA, Aeroacoustics Conference, 13th, Tallahassee, FL, October 22-24*. 1990.

28. **Culick, F. E. C.** (2006). Unsteady motions in combustion chambers for propulsion systems. *Technical Report AG-AVT-039, RTO AGARDorgraph.*.

29. **David, R.**, **S. Ostlund**, **J. Sethna**, and **E. D. Siggia** (1982). Universal transition from quasiperiodicity to chaos in dissipative systems. *Physical Review Letter*, **49**, 132–135.

30. **Dowling, A. P.** (1997). Nonlinear self-excited oscillations of a ducted flame. *Journal of Fluid Mechanics*, **346**, 271–290.

31. **Dowling, A. P.** (1999). A kinematic model of a ducted flame. *Journal of Fluid Mechanics*, **394**, 51–72.

32. **Dowling, A. P.** and **A. S. Morgans** (2005). Feedback control of combustion oscillations. *Annual Review of Fluid Mechanics*, **37**, 151–182.

33. **Dowling, A. P.** and **S. R. Stow** (2003). Acoustic analysis of gas turbine combustors. *Journal of Propulsion and Power*, **19**, 751–764.

34. **Dowling, A. P.** and **J. E. F. Williams**, *Sound and Sources of Sound*. Ellis Horwood Ltd, 1983.

35. **Drazin, P. G.**, *Nonlinear Systems*. Cambridge University Press, 1992.

36. **Ducruix, S.**, **T. Schuller**, **D. Daniel**, and **S. Candel**, *Combustion Instabilities in Gas Turbine Engines: Operational Experience, Fundamental Mechanisms, and Modeling.*, chapter Combustion Instability Mechanisms in Premixed Combustors. Progress in Astronautics and Aeronautics, AIAA, Editor: Lieuwen, T. C. and Yang, V., 2005, 179–210.

37. **Duguet, Y.**, **A. P. Willis**, and **R. R. Kerswell** (2008). Transition in pipe flow: the saddle structure on the boundary of turbulence. *Journal of Fluid Mechanics*, **613**, 255–274.

38. **Durox, D.**, **F. Baillot**, **G. Searby**, and **L. Boyer** (1997). On the shape of flames under strong acoustic forcing: a mean flow controlled by an oscillating flow. *Journal of Fluid Mechanics*, **35**, 295–310.

39. **Eckmann, J. P.**, **S. O. Kamphorts**, and **R. Ruelle** (1987). Recurrence plots of dynamical systems. *Europhysics Letters*, **4**, 973–977.

40. **Feigenbaum, M. J.** (1978). Quantitative universality for a class of nonlinear transformations. *Journal of Statistical Physics*, **19**, 25–52. ISSN 0022-4715.

41. **Fleifil, M.**, **A. M. Annaswamy**, **Z. A. Ghoneim**, and **A. F. Ghoniem** (1996). Response of a laminar premixed flame to flow oscillations: a kinematic model and thermoacoustic instability results. *Combustion and Flame*, **106**, 487–510.

42. **Fraser, M., Andrew** and **H. L. Swinney** (1986). Independent coordinates for strange attractors from mutual information. *Physical Review A*, **33**, 1134–1140.

43. **George, J. K.** and **R. I. Sujith** (2011). On Chu's disturbance energy. *Journal of sound and vibration*, **330**, 5280–5291.

44. **Gollub, J. P.** and **S. V. Benson** (1980). Many routes to turbulent convection. *Journal of Fluid Mechanics*, **100**, 449–470.

45. **Gotoda, H.**, **H. Nikimoto**, **T. Miyano**, and **S. Tachibana** (2011). Dynamic properties of combustion instability in a lean premixed gas turbine combustor. *Chaos*, **21**(1), 013124.

46. **Grassberger, P.** and **I. Procaccia** (1983). Characterization of strange attractors. *Physical Review Letter*, **50**(5), 346–349.

47. **Hemchandra, S.** (2010). Recent advances in flame response prediction for combustion instability modelling. *V European Conference on Computational Fluid Dynamics*.

48. **Hilborn, R. C.**, *Chaos and Nonlinear Dynamics: An Introduction for Scientists and Engineers*. Oxford University Press, 2000.

49. **Jahnke, C. C.** and **F. E. C. Culick** (1994). An application of dynamical systems theory to nonlinear combustion instabilities. *Journal of Propulsion and Power*, **10**, 508–517.

50. **Jegadeesan, V.** and **R. I. Sujith** (2012). Experimental investigation of noise induced triggering in thermoacoustic system. *Proceedings of the Combustion Institute*, **34**.

51. **Juniper, M. P.** (2010). Triggering in the horizontal Rijke tube: non-normality, transient growth and bypass transition. *Journal of Fluid Mechanics*, **667**, 272–308.

52. **Kantz, H.** (1994). A robust method to estimate the maximal Lyapunov exponent of a time series. *Physics Letters A*, **185**, 77–87.

53. **Kantz, H.** and **T. Schreiber**, *Nonlinear Time Series Analysis.*. Cambridge Press, 2003.

54. **Karimi, N.**, **J. S. H. M. Brear**, and **J. P. Monty** (2009). Linear and nonlinear forced response of conical, ducted, laminar, premixed flames. *Combustion and Flame*, **156**, 2201–2212.

55. **Keanini, R. G.**, **K. Yu**, and **J. W. Daily** (1989). Evidence of a strange attractor in ramjet combustion. *AIAA paper 89-0624*, 117–132.

56. **Kennel, M. B.**, **R. Brown**, and **H. D. I. Abarbanel** (1992). Determining embedding dimension for phase space reconstruction using a geometrical construction. *Physical Review A*, **45**, 3403–3411.

57. **Kerstein, A. R.**, **W. T. Ashurst**, and **F. A. Williams** (1988). Field equation for interface propagation in an unsteady homogeneous flow field. *Physical Review A*, **37**, 2728–2731.

58. **Kim, K. T.** and **S. Hochgreb** (2012). Measurements of triggering and transient growth in a model lean premixed gas turbine combustor. *Combustion and Flame*, **159**(3), 1215–1227.

59. **Kitano, M.**, **T. Yabuzaki**, and **T. Ogawa** (1983). Chaos and period-doubling bifurcations in a simple acoustic system. *Physical Review Letter*, **50**, 713–716.

60. **Klimaszewska, K.** and **J. J. Zebrowski** (2009). Detection of the type of intermittency using characteristic patterns in recurrence plots. *Physical Review E*, **80**, 026214.

61. **Knoop, P.**, **F. E. C. Culick**, and **E. E. Zukoski** (1997). Nonlinear self-excited oscillations of a ducted flame. *Combustion Science and Technology*, **123**, 363–376.

62. **Krebs, W.**, **G. Walz**, and **S. Hoffmann** (1999). Thermoacoustic analysis of annular combustor. *AIAA Paper No. AIAA 99-1971*.

63. **Kurz, R.** and **K. Brun** (2007). Gas turbine tutorial: maintenance and operating practices effects on degradation and life. *Proceeding of the Thirty Sixth Turbomachinery Symposium*, 173–185.

64. **Langhorne, P. J.** (1988). Reheat buzz: an acoustically coupled combustion instability. Part 1. Experiment. *Journal of Fluid Mechanics*, **193**, 417–443.

65. **Le Conte, J. M. D.** (1858). On the influence of musical sounds on the flame of a jet of coal gas. *Philosophical Magazine Series*, **4**, 235–239.

66. **Lei, S.** and **A. Turan** (2009). Nonlinear/chaotic behavior in thermoacoustic instability. *Combustion Theory and Modelling*, **13**(3), 541–557.

67. **Levine, J. N.** and **J. D. Baum** (1983). A numerical study of nonlinear instability phefnomena in solid rocket motors. *AIAA Journal*, **21**, 557–564.

68. **Libchaber, A.**, **C. Laroche**, and **S. Fauve** (1982). Period doubling cascade in mercury, a quantitative measurement. *Journal of Physique Letters*, **43**, 211–216.

69. **Liepmann, D.** and **M. Gharib** (1992). The role of streamwise vorticity in the near field entrainment of round jets. *Journal of Fluid Mechanics*, **245**(643).

70. **Lieuwen, T.** and **A. Banaszuk** (2005). Background noise effects on combustion instability. *Journal of Propulsion and Power*, **21**(1), 25–31.

71. **Lieuwen, T.** and **Y. Neumeier** (2002). Nonlinear pressure-heat release transfer function measurements in a premixed combustor. *Proceedings of the Combustion Institute*, **29**(1), 99–105.

72. **Lieuwen, T.**, **Y. Neumeier**, and **B. T. Zinn** (1998). The role of unmixedness and chemical kinetics in driving combustion instabilities in lean premixed combustors. *Combustion Science and Technology*, **135**, 193–211.

73. **Lieuwen, T.**, **H. Torres**, **C. Johnson**, and **B. T. Zinn** (2001). A mechanism of combustion instability in lean premixed gas turbine combustors. *Journal of Engineering for Gas Turbines and Power*, **123**(1), 182–189.

74. **Lieuwen, T. C.** (2002). Experimental investigation of limit cycle oscillations in an unstable gas turbine combustor. *Journal of Propulsion and Power*, **18**, 61–67.

75. **Lieuwen, T. C.** (2003). Modeling premixed combustion acoustic wave interactions: A review. *Journal of Propulsion and Power*, **19**, 765–781.

76. **Ma, Y.**, **W. K. van Moorhem**, and **R. W. Shorthill** (1991). Experimental investigation of velocity coupling in combustion instability. *Journal of Propulsion and Power*, **7**, 692–699.

77. **Macquisten, M.** (1995). Combustion oscillations in a twin-stream afterburner. *Journal of Sound and Vibration*, **188**(4), 545–560.

78. **Manneville, P.**, *Dissipative Structures and Weak Turbulence*. Academic Press, INC, 1990.

79. **Mariappan, S.**, **P. J. Schmid**, and **R. I. Sujith**, Role of transient growth in subcritical transition to thermoacoustic instability in a horizontal Rijke tube. *In 16th AIAA/CEAS Aeroacoustics Conference. AIAA 2010-3857, Stockholm, June 7-9*. 2010.

80. **Mariappan, S.** and **R. I. Sujith** (2010). Thermoacoustic instability in a solid rocket motor: non-normality and nonlinear instabilities. *Journal of Fluid Mechanics*, **653**, 1–33.

81. **Mariappan, S.** and **R. I. Sujith** (2011). Modeling nonlinear thermoacoustic instability in an electrically heated rijke tube. *Journal of Fluid Mechanics*, **680**, 511–533.

82. **Mariappan, S.**, **R. I. Sujith**, and **P. J. Schmid**, Non-normality of thermoacoustic interactions: an experimental investigation. *In 47th AIAA/ASME/SAE/ASEE Joint Propulsion Conference, July 31- August 3*. 2011.

83. **Marwan, N.** (2003). *Encounters with neighbours - current developments of concepts based on recurrence plots and their applications*. Ph.D. thesis, University of Potsdam.

84. **Marwan, N.**, **M. Carmenromano**, **M. Thiel**, and **J. Kurths** (2007). Recurrence plots for the analysis of complex systems. *Physics Reports*, **438**, 237–329.

85. **Matsui, Y.** (1981). An experimental study on pyro acoustic amplification of premixed laminar flames. *Combustion and Flame*, **43**, 199–209.

86. **Matveev, I.** (2003). *Thermo-acoustic instabilities in the Rijke tube: experiments and modeling*. Ph.D. thesis, CalTech, Pasadena, CA.

87. **McManus, K.**, **T. Poinsot**, and **S. Candel** (1993). A review of active control of combustion instabilities. *Progress in Energy and Combustion Science*, **19**, 1–29.

88. **Merk, H. J.** (1956). Analysis of heat-driven oscillations of gas flows I general considerations. *Applied Scientific Research*, **6**, 317–335.

89. **Moeck, J.** and **C. O. Paschereit** (2012). Nonlinear interactions of multiple linearly unstable thermoacoustic modes. *International Journal of Spray and Combustion Dynamics*, **4**(1), 1–28.

90. **Moeck, J. P.**, **M. R. Bothien**, **S. Schimek**, **A. Lacarelle**, and **C. O. Paschereit** (2008). Subcritical thermoacoustic instabilities in a premixed combustor. *14th AIAA/CEAS Aeroacoustics Conference*, 1–18.

91. **Moon, F. C.**, *Nonlinear Chaotic and Fractal Dynamics: An Introduction for Applied Scientists and Engineers*. Wiley-VCH Verlag GmbH & Co. KGaA, Weinheim, 2004.

92. **Murganandam, T. M.** and **J. M. Seitzman** (Tuscon, Arizon, 10-13 July, 2005). Characterization of extinction events near blowout in swirl dump combustors. *41st AIAA/ASME/SAE/ASEE Joint Propulsion Conference & Exhibit*.

93. **Nair, S.** and **T. C. Lieuwen** (2005). Acoustic detection of lean blowout in premixed flames. *Journal of Propulsion and Power*, **21**, 32–39.

94. **Nair, V.**, **S. Sunetra**, and **R. I. Sujith** (2010). Uncertainty quantification of subcritical bifurcation in a Rijke tube. *16th AIAA/CEAS Aeroacoustics Conference, Stockholm*.

95. **Nayfeh, A. H.** and **B. Balachandran**, *Applied Nonlinear Dynamics: Analytical, Computational, and Experimental Methods*. Wiley-VCH Verlag GmbH & Co. KGaA, Weinheim, 2004.

96. **Nicoud, F.** and **T. Poinsot** (2005). Thermoacoustic instabilities: should the Rayleigh criterion be extended to include entropy changes. *Combustion and Flame*, **142**, 153–159.

97. **Noiray, N.**, **D. Durox**, **T. Schuller**, and **S. Candel** (2008). A unified framework for nonlinear combustion instability analysis based on the flame describing function. *Journal of Fluid Mechanics*, **615**, 139–167.

98. **Okamoto, H.**, **N. Tanaka**, and **M. Naito** (1998). Intermittencies and related phenomena in the oxidation of formaldehyde at a constant current. *The Journal of Physical Chemistry A*, **102**(38), 7353–7361.

99. **Ott, E.**, *Chaos in Dynamical Systems*. Cambridge University Press, New York, 1993.

100. **Packard, N. H.**, **J. P. Crutchfield**, **J. D. Farmer**, and **R. S. Shaw** (1980). Geometry from a time series. *Physical Review Letter*, **45**, 712–716.

101. **Palies, P.**, **D. Durox**, **T. Schuller**, and **S. Candel** (2011). Experimental study on the effect of swirler geometry and swirl number on flame describing functions. *Combustion Science and Technology*, **183**(7), 704–717.

102. **Pankiewitz, C.** and **T. Sattelmayer** (2003). Time domain simulation of combustion instabilities in annular combustors. *Journal of Engineering for Gas Turbines and Power*, **125**, 677–685.

103. **Paschereit, C. O.**, **E. J. Gutmark**, and **W. Weisenstein** (1998). Structure and control of thermoacoustic instabilities in a gas-turbine combustor. *Combustion Science and Technology*, **138**, 213–32.

104. **Paschereit, C. O.**, **D. Oster**, **T. A. Long**, **H. E. Fiedler**, and **I. Wygnaski** (1992). Vortex evolution in a round jet. *Experiments in Fluids*, **12**(189).

105. **Paschereit, C. O.** and **W. Polifke** (1998). Investigation of thermoacoustic characteristics of a lean premixed gas turbine burner. *ASME Turbo Expo,Paper 98-GT-582, June*.

106. **Paschereit, C. O.**, **B. Schuermans**, **V. Bellucci**, and **P. Flohr**, *Combustion Instabilities in Gas Turbine Engines: Operational Experience, Fundamental Mechanisms, and Modeling*, chapter Chapter 15: Implementation of Instability Prediction in Design: ALSTOM Approaches. Progress in Astronautics and Aeronautics, AIAA, Editor: Lieuwen, T. C. and Yang, V., 2005, 445–478.

107. **Paschereit, C. O.**, **B. Schuermans**, **W. Polifke**, and **O. Mattson** (1999). Measurement of trasfer matrices and source terms of premixed flames. *ASME Turbo Expo, Indianapolis, IN, June*.

108. **Peracchio, A. A.** and **W. M. Proscia** (1999). Nonlinear heat-release/acoustic model for thermoacoustic instability in lean premixed combustors. *Journal of Engineering for Gas Turbines and Power*, **121**(3), 415–421.

109. **Perry, L.** and **J. R. Blackshear** (1993). Driving standing wave by heat addition. *Fourth International Symposium on Combustion. The Williams and Wilkins Company, Baltimore*, 553.

110. **Platt, N.**, **E. A. Spiegel**, and **C. Tresser** (1993). The intermittent solar cycle. *Geophysical & Astrophysical Fluid Dynamics*, **73**(1-4), 147–161.

111. **Plavnik, G.**, Pulse combustion technology. *In 14th North American Waste to Energy Conference May 1-3, 2006, Tampa, Florida USA NAWTEC14-3195*. 2006.

112. **Poinsot, T.** and **D. Veynante**, *Theoretical and Numerical Combustion*. R. T. Edwards, Inc., 2005.

113. **Polifke, W.**, **A. Poncet**, **C. O. Paschereit**, and **K. Döbbeling** (2001). Reconstruction of acoustic transfer matrices by instationary computational fluid dynamics. *Journal of Sound and Vibrations*, **245**, 483–510.

114. **Pomeau, Y.** and **P. Manneville** (1980). Intermittent transition to turbulence in dissipative dynamical systems. *Communications in Mathematical Physics*, **74**, 189–197.

115. **Pomeau, Y.**, **J. C. Roux**, **A. Rossi**, **S. Bachelart**, and **C. Vidal** (1981). Intermittent behaviour in the Belousov-Zhabotinsky reaction. *Journal de Physique Letters*, **42**(13), 271–273.

116. **Powell, E. A.** and **B. Zinn** (1969). Solution of linear combustion instability problems using the galerkin method. *Israel Journal of Technology*, **7**, 79–89.

117. **Preetham** (2007). *Modeling the response of premixed flames to flow disturbances*. Ph.D. thesis, Aerospace Engineering Georgia Institute of Technology.

118. **Preetham**, **H. Santosh**, and **T. C. Lieuwen** (2008). Dynamics of laminar premixed flames forced by harmonic velocity disturbances. *Journal of Propulsion and Power*, **24**, 1390–1402.

119. **Putnam, A. A.**, *Combustion Driven Oscillations in Industry*. American Elsevier New York, 1971.

120. **Rayleigh, J. S. W.** (1878). The explanation of certain acoustic phenomena. *Nature*, **18**, 319–321.

121. **Richards, G. A.** and **M. C. Janus** (1998). Characterization of oscillations during premix gas turbine combustion. *ASME Journal of Engineering for Gas Turbines and Power*, **120**, 294–302.

122. **Richards, G. A.**, **M. C. Janus**, and **E. H. Robey** (1999). Control of flame oscillations with equivalence ratio modulation. *Journal of Propulsion and Power*, **15**, 232–40.

123. **Rienstra, S. W.** and **A. Hirschberg**, *An Introduction to Acoustics*. Technische Universiteit Eindhoven, Netherlands, IWDE 92-06 edition, 2004.

124. **Roux, J.**, **A. Rossi**, **S. Bachelart**, and **C. Vidal** (1981). Experimental observations of complex dynamical behavior during a chemical reaction. *Physica D: Nonlinear Phenomena*, **2**(2), 395–403.

125. **Ruelle, D.** and **F. Takens** (1971). On the nature of turbulence. *Communication in Mathematical Physics*, **20**(3), 167–192.

126. **Santosh, H.**, Direct numerical simulation study of premixed flame response to fuel-air ratio oscillations. *In ASME Turbo Expo 2011 June 6-10, 2011, Vancouver, British Columbia, Canada, paper number GT2011-45590*. 2011.

127. **Schadow, K. C.** and **E. Gutmark** (1992). Combustion instability related to vortex shedding in dump combustors and their passive control. *Progress in Energy and Combustion Science*, **18**(2), 117–132.

128. **Schuermans, B.**, **V. Bellucci**, **G. Felix**, **M. Francois**, **F. Peter**, and **C. O. Paschereit**, A detailed analysis of thermoacoustic interaction mechanisms in a turbulent premixed flame. *In ASME Turbo Expo 2004 Power for Land, Sea, and Air June 14-17, Vienna, Austria*. 2004.

129. **Schuermans, B.**, **W. Polifke**, and **C. O. Paschereit** (2000). Prediction of acoustic pressure spectra in gas turbines based on measured transfer matrices. *ASME Turbo Expo 00, Munich, Germany, May*.

130. **Schuller, T.**, **S. Ducruix**, **D. Durox**, and **S. Candel** (2002). Modeling tools for the prediction of premixed flame transfer functions. *Proceedings of the Combustion Institute*, **29**, 107–113.

131. **Schuller, T.**, **D. Durox**, and **S. Candel** (2003). A unified model for the prediction of laminar flame transfer functions comparisons between conical and v-flame dynamics. *Combustion and Flame*, **134**, 21–34.

132. **Shanbhogue, S. J.**, **S. Husain**, and **T. Lieuwen** (2009). Lean blowoff of bluff body stabilized flames: Scaling and dynamics. *Progress in Energy and Combustion Science*, **35**(1), 98 – 120. ISSN 0360-1285.

133. **Shashvat, P.** (2007). *Lean Blowout Mitigation in Swirl Stabilized Premixed Flames*. PhD Thesis, Georgia Institute of Technology.

134. **Sprott, J. C.**, *Chaos and Time-Series Analysis*. Oxford University Press, 2003.

135. **Sreekrishna, H.**, **H. Santosh**, and **T. C. Lieuwen** (2010). Premixed flame response to equivalence ratio perturbations. *Combustion Theory and Modelling*, **5**, 681–714.

136. **Sterling, J. D.** (1993). Nonlinear analysis and modelling of combustion instabilities in a laboratory combustor. *Combustion Science and Technology*, **89**(1), 167–179.

137. **Sterling, J. D.** and **E. E. Zukoski** (1991). Nonlinear dynamics of laboratory combustor pressure oscillations. *Combustion Science and Technology*, **77**, 225–238.

138. **Stöhr, M.**, **I. Boxx**, **C. Carter**, and **W. Meier** (2011). Dynamics of lean blowout of a swirl-stabilized flame in a gas turbine model combustor. *Proceedings of the Combustion Institute*, **33**, 2953–2960.

139. **Strogatz, S. H.**, *Nonlinear Dynamics and Chaos: With Applications To Physics, Biology, Chemistry and Engineering*. Westview Press, 1994.

140. **Subramanian, P.**, **S. Mariappan**, **P. Wahi**, and **R. I. Sujith** (2010). Bifurcation analysis of thermoacoustic instability in a horizontal Rijke tube. *International Journal of Spray and Combustion Dynamics*, **2**(4), 325–356.

141. **Subramanian, P.** and **R. I. Sujith** (2011). Non-normality and internal flame dynamics in premixed flame-acoustic interaction. *Journal of Fluid Mechanics*, **679**, 315–342.

142. **Suresh, S.**, *Fatigue of Materials*. Cambridge University Press, 1998.

143. **Swinney, H. L.** (1983). Observations of order and chaos in nonlinear systems. *Physica 7D*, 3–15.

144. **Takens, F.**, *Dynamical Systems and Turbulence*, chapter Detecting strange attractors in turbulence. Springer Berlin / Heidelberg, 1981, 366–381.

145. **Tran, P. X.**, **D. W. Brenner**, and **C. T. White** (1990). Complex route to chaos in velocity driven atoms. *Physical Review Letter*, **65**, 3219–3222.

146. **Tyndall, J.** (1857). Lxiii. on the sounds produced by the combustion of gases in tubes. *Philosophical Magazine Series 4*, **13**(89), 473–479.

147. **Venkataraman, K. K.** (2000). *An investigation of the acoustic instability mechanisms in lean premixed dump combustors*. Ph.D. thesis, The University of Pennsylvania.

148. **Wang, H. Y.**, **C. K. Law**, and **T. Lieuwen** (2009). Linear response of stretch-affected premixed flames to flow oscillations. *Combustion and Flame*, **156**, 889–895.

149. **Waugh, I. C.** and **M. P. Juniper** (2011). Triggering in a thermoacoustic system with stochastic noise. *International Journal of Spray and Combustion Dynamics*, **3**(3), 225–242.

150. **Wicker, J. M.**, **W. D. Greene**, **S. Kim**, and **V. Yang** (1996). Triggering of longitudinal combustion instabilities in rocket motors: Nonlinear combustion response. *Journal of Propulsion and Power*, **12**, 1148–1158.

151. **Williams, F. A.**, *Combustion Theory*. The Benjamin/Cummings Publishing Company, 1985, 2 edition.

152. **Yazaki, T.**, **S. Takashima**, and **F. Mizutani** (1987). Complex quasiperiodic and chaotic states observed in thermally induced oscillations of gas columns. *Physical Review Letter*, **58**, 1108–1111.

153. **Zbilut, J. P.** and **C. L. J. Webber** (1992). Embeddings and delays as derived from quantification of recurrence plots. *Physics Letters A*, **171**, 199–203.

154. **Zinn, B. T.** and **T. C. Lieuwen**, *Combustion instabilities in gas turbine engines: operational experience, fundamental mechanisms, and modeling.*, chapter Combustion Instabilities: Basic concepts. Progress in Astronautics and Aeronautics, AIAA, Editor Lieuwen, T. C. and Yang, V., 2005, 3–26.

155. **Zou, Y.** (2007). *Exploring recurrences in quasi-periodic systems*. Ph.D. thesis, University of Potsdam.

LIST OF PAPERS BASED ON THESIS

Papers in Refereed Journals

1. **Kabiraj, L., R. I. Sujith,** and **P. Wahi** (2012). Investigating dynamics of combustion driven oscillations leading to lean blowout. *Fluid Dynamic Research,* **44** (pp. 12).

2. **Kabiraj, L., R. I. Sujith,** and **P. Wahi** (2012). Bifurcations of self-excited ducted laminar premixed flames. *Journal of Engineering for Gas Turbines and Power,* **134** (3).

3. **Kabiraj, L., A. Saurabh, P. Wahi** and **R. I. Sujith** (2012). Route to chaos for combustion instability in ducted laminar premixed flames. *Chaos,* **22** 023129.

4. **Kabiraj, L.,** and **R. I. Sujith**. Nonlinear self-excited thermoacoustic oscillations, intermittency and flame blowout. *Journal of Fluid mechanics* (under revision).

Papers in Conferences

1. **Kabiraj, L.,** and **R. I. Sujith**. Bifurcation analysis and observation of intermittency in combustion-driven thermoacoustic oscillations. AIAA 50^{th} AIAA Aerospace Sciences Meeting Including the New Horizons Forum and Aerospace Exposition, AIAA 2012-1136965, Nashville, January 9-12, 2012.

2. **Kabiraj, L.,** and **R. I. Sujith**. Dynamics of thermoacoustic oscillations leading to lean flame blowout. ASME Turbo Expo Copenhagen, GT2012-68696, Denmark June 11-15, 2012.

3. **Kabiraj, L., R. I. Sujith** and **P. Wahi**. Nonlinear self-excited oscillations in a thermoacoustic system. 4^{th} International Symposium Bifurcations and Instabilities in Fluid Dynamics, Barcelona, July 18-21, 2011.

4. **Kabiraj, L.,** and **R. I. Sujith**. Investigation of subcritical instability in ducted premixed flames, Proceedings of the ASME Turbo Expo 2011: Power for Land, Sea, and Air, GT2011-46155, Vancouver, Canada June 5-10, 2011.

5. **Kabiraj, L., R. I. Sujith,** and **P. Wahi**. Experimental studies of bifurcations leading to chaos in a laboratory scale thermoacoustic system, Proceedings of the ASME Turbo Expo 2011: Power for Land, Sea, and Air, GT2011-46149, Vancouver, Canada June 5-10, 2011.

6. **Kabiraj, L., A. Saurabh, P. Wahi** and **R. I. Sujith**. Experimental study of thermoacoustic instability in ducted premixed flames: periodic, quasi-periodic and

chaotic oscillations, n^3l-International Summer School and Workshop on Non-Normal and Nonlinear Effects in Aero- and Thermoacoustics, Munich, May 17-21, 2010.

7. **Kabiraj, L., A. Saurabh, P. Wahi** and **R. I. Sujith**. The nature of combustion driven oscillations in a premixed laboratory combustor. 8^{th} Asia Pacific Conference on Combustion, ASPACC2010, Hyderabad, December 10-13, India, 2010.